2014

Utilization of Carbon Nanofibers Grown on Glass Microballoons (NMBs) in Point-of-Care Diagnostic Devices

Emmanuel Gikunoo
Louisiana State University and Agricultural and Mechanical College

UTILIZATION OF CARBON NANOFIBERS GROWN ON GLASS MICROBALLOONS (NMBs) IN POINT-OF-CARE DIAGNOSTIC DEVICES

A Dissertation

Submitted to the Graduate Faculty of the
Louisiana State University and
Agricultural and Mechanical College
in partial fulfillment of the
requirements for the degree of
Doctor of Philosophy

in

The Department of Mechanical and Industrial Engineering

by
Emmanuel Gikunoo
B.Sc., Kwame Nkrumah University of Science and Technology, 1999
M.Sc., University of Saskatchewan, 2005
December 2014

To my lovely kids

Nathan and Chloe

ACKNOWLEDGEMENTS

It is with humility and appreciation that I wish to acknowledge the great minds that have brought me this far in my academic journey. My sincere appreciation goes to my advisor, Dr. Eyassu Woldesenbet, for his thoughtful insights, mentorship and advice throughout this research. Special thanks also go to my dissertation committee members, Dr. Ying Wang, Dr. Ram Devireddy, and Dr. Evgueni E. Nesterov for their useful suggestions. Technical assistance provided by Dr. Matthew Brown at the LSU Socolofsky Microscopy Center is gratefully acknowledged.

I am equally grateful to my mentors and colleagues at the Next Generation Composites Crest Center, Southern University and A & M College, especially Dr. Patrick Mensah, Dr. Yoonyoung Jin, Dr. Adeyabeba Abera, Dr. Ali Ghamsari, Dr. Ephraim Zegeye, Dr. Fareed Dawan, and Jude Mgbanwunne whose contributions and encouragements have taken me this far. Without them this journey would not have come to a successful end. To my best friends and motivators, Dr. Anthony Andrew and Dr. Patrick Feglo, thanks for bringing me this far. You have and continue to be my source of encouragement.

Words cannot express my sincerest appreciation to my wife, kids, mum, dad, and siblings. Your immense support, love and sacrifices are endless. To my auntie, Victoria Tetteh and her kids, your help and sacrifices have brought me this far. I would also like to thank the Ghanaian community at LSU: Julius Codjoe and family, Godfrey Mills, William Armah, Wisdom Wardy, Owen Boaitey, Emmanuel Kyereh, and Nutifafa Adotey, the support and candid pieces of advice we share are greatly appreciated.

Finally, to everyone that has been part of my life along this journey, may God richly bless you.

TABLE OF CONTENTS

ACKNOWLEDGEMENTS iii

LIST OF TABLES vii

LIST OF FIGURES viii

ABSTRACT xi

CHAPTER 1
INTRODUCTION 1
1.1 Motivation 1
1.1.1 Point-of-Care (POC) Diagnostic Devices 1
1.1.2 Carbon Nanofibers 3
1.1.3 Carbon Nanofibers Grown on Glass Microballoons (NMBs) 4
1.2 Research Objectives 6
1.3 Outline of Dissertation 7

CHAPTER 2
FABRICATION AND SURFACE FUNCTIONALIZATION OF CARBON NANOFIBERS GROWN ON GLASS MICROBALLOONS 8
2.1 Introduction 8
2.2 Structure of CNF 11
2.3 Surface Functionalization of CNFs 14
2.4 Experimental Procedures 18
2.4.1 Catalyst Coating of Glass Microballoons 18
2.4.2 CNF Growth 19
2.4.3 Surface Functionalization of CNF 20
2.4.4 Characterization 21
2.5 Results and Discussions 22
2.5.1 Catalyst Layer Formation 22
2.5.2 CNF Growth 25
2.5.3 Surface Functionalization Results 27
2.6 Summary 32

CHAPTER 3
IMMUNOASSAY ON GLASS SLIDE USING CARBON NANOFIBERS GROWN ON GLASS MICROBALLOONS (NMBs) 34
3.1 Introduction 34
3.2 Antibodies as Recognition Elements 37
3.3 Binding of Antibodies to Carbon Nanofibers 40
3.4 Blocking as a Means of Preventing Non-Specific Binding 42
3.5 Detection Principle 44
3.5.1 Biomolecule – NMBs Conjugation 44
3.5.2 NMBs Immobilization on Glass Slide 45

3.6 Experimental Procedures 46
3.6.1 Blocking 47
3.6.2 Functionalization of NMBs with EDC/Sulfo-NHS 47
3.6.3 Biomolecule – NMBs Conjugation 47
3.6.4 Preparation of Immunosensor 49
3.6.5 Imaging 51
3.6.6 Electrical Measurements 51
3.7 Results and Discussion 52
3.7.1 EDC/Sulfo-NHS Functionalized NMBs 52
3.7.2 Non-Specific Binding 53
3.7.3 Conjugation of Biomolecules to NMBs 56
3.7.4 Immunosensor 60
3.8 Summary 65

CHAPTER 4
ULTRA-LOW IMMUNOASSAY DETECTION OF MALARIA AND PREGNANCY IN HUMANS 67
4.1 Introduction 67
4.2 Malaria 70
4.3 Diagnosis of Malaria 72
4.3.1 Microscopy 73
4.3.2 Molecular 74
4.3.3 Serology 75
4.3.4 Antigen Detection 75
4.4 Pregnancy 77
4.5 Diagnosis of Pregnancy 78
4.6 Experimental Procedures 79
4.6.1 Reagents and Materials 79
4.6.2 NMB-*Plasmodium* Species Conjugation 79
4.6.3 Preparation of Glass Substrate 80
4.6.4 Characterization 81
4.7 Results and Discussion 81
4.7.1 Principle of Disease Detection 81
4.7.2 Detection Limit of *Pf*HRP-2 Assay 82
4.7.3 Selectivity of the *Pf*HRP-2 Detection Assay 87
4.7.4 Selectivity of the hCG Detection Assay 90
4.8 Summary 92

CHAPTER 5
CONCLUSIONS AND FUTURE WORK 94
5.1 Conclusions 94
5.1.1 Surface Functionalization of NMBs 94
5.1.2 Conjugation of Biological Species to NMBs 95
5.1.3 Pathogen Detection on Immunochromatographic Device 96
5.2 Future Work 97
5.2.1 Pathogen Detection in Microfluidic Device 97

5.2.2 Design and Optimization of Microfluidic Device 98
5.2.3 Clinical Trials using Microfluidic Device 99

REFERENCES 99

APPENDIX: PERMISSION TO USE COPYRIGHTED MATERIAL 117

VITA 119

LIST OF TABLES

Table 4.1 Summary of the percent area of the capture zone covered with NMBs for varying *Pf*HRP-2 concentrations……84

Table 4.2 Summary of the measured resistance values of the capture zone for varying *Pf*HRP-2 concentrations……87

Table 4.3 Summary of the percent area of the capture zone covered with NMBs for varying *Pv*MSP-1 concentrations……90

Table 4.4 Summary of the measured resistivity values of the capture zone for varying *Pv*MSP-1 concentrations……90

Table 4.5 Summary of the percent area of the capture zone covered with NMBs for varying hCG concentrations……91

Table 4.6 Summary of the measured resistance values of the capture zone for varying hCG concentrations……92

LIST OF FIGURES

Figure 1.1 CNTs grown on (a) hollow nickel microsphere [37], (b) ceramic beads [38] and (c) alumina microparticle [39]. 5

Figure 2.1 Schematics of the different structures of CNFs [40]. 11

Figure 2.2 Schematic of the CVD system. 20

Figure 2.3 Flow mechanism of electroless nickel deposition on glass microballoon. 23

Figure 2.4 Images of as-received microballoons, microballoons after electroless nickel deposition, and carbon nanofiber grown on nickel coated microballoons. 23

Figure 2.5 (a) SEM micrograph of nickel coated MBs and (b) typical optical micrograph of a layer of nickel coated MBs formed on silicon wafer [102]..... 24

Figure 2.6 FTIR spectra of (a) as received MB and (b) nickel coated MB. 24

Figure 2.7 (a), (b) SEM micrographs of as-fabricated NMBs at different magnifications. 26

Figure 2.8 Raman spectra of as-fabricated CNFs [102]. 26

Figure 2.9 The modification process of CNFs by HNO_3 treatment. Carbonaceous fragments are represented by red wavy lines. Similar processes are found elsewhere [88]. 28

Figure 2.10 SEM micrographs of (a) air oxidized, (b) HNO_3 oxidized, (c) HNO_3/H_2SO_4, and (d) fractured and peeled off CNFs from acidic oxidization of MBs. 29

Figure 2.11 Dispersion of NMBs in PBS after modification with HNO_3, HNO_3/H_2SO_4, and air (from left to right). All solutions have 1 mg/ml concentration of NMBs and at times (a) just dispersed, (b) 2 minutes, and (c) 10 minutes. 31

Figure 2.12 FTIR Spectra of as-fabricated and the different types of surface oxidized samples used in the research. 32

Figure 3.1 Schematic structure of IgG [134]..... 39

Figure 3.2 Reaction of the carboxylate functional group with a primary amine containing molecule, in the presence of EDC and sulfo-NHS [139]. 41

Figure 3.3 Schematic of the processing stages of a sandwich immunoassay protocol. 44

Figure 3.4 Schematic of the capture procedure of NMBs on glass slide. (a) NMBs, (b) secondary anti-IgG conjugated NMBs, (c) primary IgG immobilized on glass slide, (d) anti-IgG locked by immobilized primary IgG, (e) immobilized NMBs on slide, and (f) signal detection setup..... 45

Figure 3.5 Schematic of increasing anti-IgG concentrations on NMBs network at the capture zone. 46

Figure 3.6 FTIR spectra of EDC/Sulfo NHS treated NMBs. 53

Figure 3.7 Dispersion of NMBs in PEG solution at times (a) just dispersed, (b) 10 minutes, and (c) 20 minutes. 54

Figure 3.8 Fluorescence micrographs of anti-IgG-FITC bound to NMBs (a) without PEG and (b) with PEG. (c) Fluorescence micrograph of PEG treated NMBs initially conjugated with excess anti-IgG followed by treatment with anti-IgG-FITC. 55

Figure 3.9 FTIR spectra of PEG modified EDC/Sulfo NHS treated NMBs. 56

Figure 3.10 Fluorescence micrographs of NMBs conjugated with IgG and further treated with (a) 0.01 ng/ml, (b) 1 ng/ml, and (c) 10 ng/ml of anti-IgG-FITC. 58

Figure 3.11 Fluorescence micrographs of NMBs conjugated with anti-IgG and further treated with (a) 0.01 ng/ml, (b) 1 ng/ml, and (c) 10 ng/ml of IgG-FITC. 58

Figure 3.12 Fluorescence micrographs of NMBs conjugated with IgG. The NMBs were then treated with varying anti-IgG concentrations followed by anti-IgG-FITC (a) 0.01 ng/ml, (b) 1 ng/ml, and (c) 50 ng/ml of anti-IgG. 59

Figure 3.13. Fluorescence micrograph showing sandwich conjugation of IgG/anti-IgG/ IgG-FITC on NMBs. 60

Figure 3.14 NMBs immobilized on glass substrate using the sandwich format for IgG and anti-IgG biomolecules. 62

Figure 3.15 Optical micrographs showing NMBs captured on glass slides in a sandwich assay format with (a) 1, (b) 5, (c) 10, and (d) 50 ng/ml of anti-IgG concentrations. 62

Figure 3.16 Variation of percent area of the capture zone covered with NMBs against anti-IgG concentrations. 63

Figure 3.17 Variation of the resistance of the capture zone with anti-IgG concentration for immobilized NMBs and CNTs. 64

Figure 4.1 Global distribution of malaria endemicity [170]. 68

Figure 4.2 The life cycle of the malaria parasite [167]. 71

Figure 4.3 (a) Schematic illustration of the sandwich immunochromatographic set-up used to detect *Pf*HRP-2 and (b) Illustration of the two different types of signal generation from the immunosensor. The yellow cable is used for electrical measurements. 83

Figure 4.4 Optical micrographs showing NMBs captured on glass slides in a sandwich assay format with (a) 0.025, (b) 0.1, (c) 1, and (d) 10 ng/ml concentrations of *Pf*HRP-2. 84

Figure 4.5 (a) Variation of percent area of the capture zone covered with NMBs against *Pf*HRP-2 concentrations and (b) Variation of the resistivity of the capture zone with immobilized *Pf*HRP-2 concentration. The error bars in both graphs each shows the variation of five concentration points. 85

Figure 4.6 Glass slides showing (a) visual signal obtained at the first capture zone from the detection of *Pf*HRP-2 in PBS solution, (b) signal observed at the second capture zone from the detection of *Pv*MSP-1 in solution, and (c) signals obtained at the *Pf*HRP-2 and *Pv*MSP-1 capture zones from a mixed *Pf*HRP-2 and *Pv*MSP-1 solution. 88

Figure 4.7 (a) Variation of percent area of the capture zone covered with NMBs against *Pv*MSP-1 concentrations and (b) Variation of the resistivity of the capture zone with immobilized *Pv*MSP-1 concentration. 89

Figure 4.8 (a) Variation of percent area of the capture zone covered with NMBs against hCG concentrations and (b) Variation of the resistivity of the capture zone with immobilized hCG concentration. 91

ABSTRACT

The use of point-of-care (POC) diagnostic systems holds great promise for the early detection of various diseases. However, detection limits for commercially available POC systems have not been able to meet the lower cutoffs offered by the specialized laboratory testing methods. Research into the use of carbon nanofibers (CNFs) grown on glass microballoons in POC devices was studied.

The growth of several millions of the CNFs on each microballoon (NMBs) presented a large surface area with high probability of capturing minute concentrations of biospecies. Functionalization of the NMBs with the carboxyl group needed for biospecies conjugation was achieved by air oxidation. This oxidation process makes our process environmental friendly to other downstream processes. Primary IgG was immobilized on glass slides. An immunochromatographic device was developed using a sandwich assay protocol to detect varying concentrations of immobilized anti-IgG on the slides. Covalent conjugated NMBs with secondary IgG were used in generating both visual and electrical signals. False signals were prevented by coating both the antibody immobilized slides and NMBs with surfactants. A lower visual detection limit of 0.010 ng/ml and faster detection (~ 1 min) were achieved for the IgG/anti-IgG detection.

This promising result led to the modification of the immunochromatographic device for the detection of malaria infection and pregnancy. *Plasmodium falciparum* histidine rich protein-2 (*Pf*HRP-2) and *Plasmodium vivax* merozoites surface protein-1 (*Pv*MSP-1) antigen were used for malaria testing. Human chorionic gonadotropin (hCG) was also used for pregnancy testing. The approach made it possible to detect *Pf*HRP-2 and *Pv*MSP-1 in PBS over their linear range of 0.01

– 10 ng/ml. The ultrasensitive approach resulted in detecting as low as 0.025 ng/ml of *Pf*HRP-2 and 0.025 ng/ml of *Pv*MSP-1in PBS using visual signal within only one minute of testing. The approach is highly selective and specific in identifying *Pf*HRP-2 from a mixed solution of *Pf*HRP-2 and *Pv*MSP-1. A visual detection limit of 0.050 ng/ml of hCG in PBS was also obtained for the pregnancy antigen. Thus, the highly reactive, rapid, selective and signal amplification capabilities of NMBs is a promising tool for use in POCs for the early diagnosis of malaria and pregnancy.

CHAPTER 1
INTRODUCTION

1.1 Motivation

The advancement in technology is continuously changing the way the world operates. Improvements in disease detection devices are no exceptions. Research of incorporating carbon nanosized particles in disease detection devices has been growing. Carbon nanofibers (CNFs) with their high aspect ratios and large surface areas have been reported to provide numerous binding sites for biological entities [1-3]. Several millions of these CNFs can be grown on a glass microballoon (NMBs) thereby providing extensive areas for binding with bio species. The NMBs conjugated with secondary antibody will therefore have a significantly higher probability of capturing antigens in solution. Exploiting this advantage can lead to the discovery of a different generation of rapid detection kits (RDTs). These kits will have the advantages of being sensitive to minute protein concentrations and the ability to sense biomolecules in real time.

1.1.1 Point-of-Care (POC) Diagnostic Devices

Biosensors are devices that use specific biochemical reactions mediated by isolated enzymes, immunosystems, tissues, organelles or whole cells to detect chemical compounds usually by electrical, thermal or optical signals [4]. These sensors detect, transmit and record information regarding physiological, chemical and biological compounds of a living environment with the help of a specific biological recognition element. The ability of a biosensor to function effectively depends on its sample handling, bio-recognition, transduction and signal interpretation efficiencies. Biosensors are designed to analyze minute volumes of analyte in solution, usually a drop of blood. Bio-recognition is achieved when the biomolecule recognizes the target analyte. The transducer converts the recognition event into measurable signals generated in the form of

electrical, optical, thermal, chemical, mechanical or magnetic outputs [5-10]. Biomolecules currently being used are antibodies [6], enzymes [5, 7], deoxyribonucleic acid (DNA) [11], and whole cells [12].

There is an increasing demand for inexpensive and reliable sensors for use in doctor's offices, emergency and operating rooms. Ultimately, patients themselves should reliably be able to use biosensors in the monitoring of a clinical condition, such as diabetes and malaria. Currently, the major biosensor market is mainly found in highly developed countries. However, most of the top deadly diseases, such as malaria, diarrhea and tuberculosis, are found in developing countries where access to disease detection in some areas is greatly limited. These diseases require highly specialized equipment and personnel in their diagnostics. Producing biosensors for use in detecting these deadly diseases, and making them widely available and affordable, will help in detection at early stages leading to less mortality of patients.

POC test kits are gaining increasing popularity in the world [13]. Their need in low-resource settings are striking. These kits are used in lieu of diagnostic testing in hospital laboratories, because conventional services may be too distant, prohibitively costly, or in mostly cases unavailable. Gains have started to be obtained by healthcare professionals in rapidly obtaining common laboratory results either at or near patient's bedside or in their offices. Benefits from their use will include the improvement in decision making and triage, reduction in operating times, reduction in emergency room visits, reduction in number of outpatient clinic visits, reduction in number of hospitalization, and ensuring optimal use of health professionals.

Rapid detection kits (RDT) are based on immunoassays methods that are able to directly identify the presence of microorganism in a sample. These rely on the specific binding of an antigen to its antibody. This method combines the specificity of antibodies which are usually immobilized on solid supports, like polystyrene tubes or microtiter plates, with the sensitivity of conjugated enzymes [14]. However, an incubation period of a few minutes is necessary prior to the interpretation of the biochemical reactions. Examples of some of these RDT are the Clearblue pregnancy kits [15] which has 3 minutes incubation time and BinaxNow Malaria kit [16] with 10 minutes incubation period. Although these immunoassay kits are rapid, real time sensing devices are the ultimate goal for all biosensing devices, hence the need for incorporation of instant labels. Also, their mechanism is based on fluorescent emission which requires the use of specific dyes for labeling of samples [14]. False alarms sometimes result due to the use of these dyes leading to inconclusive or wrong diagnostics. The use of alternate labeling agents, such as Carbon Nanofibers, in RDT will lead to improvements in their outputs.

1.1.2 Carbon Nanofibers

The existence of carbon nanostructures dates back to the 19th century [17, 18]. However, it was in the early 1980s that unprecedented research began in the area of carbon nanostructures [19-23]. This led to a rapid increase in the numbers of discovered carbon nanostructures. The fullerenes, nanotubes, carbon toroidal structures, nanocones, and the helicoidal tubes [19-23] are examples of those discovered few years thereafter. The fibrous nanostructures, carbon nanotubes (CNTs) and CNFs, have ordered arrangements with high aspect ratio, ultra-light weight, biocompatibility, high reactivity, high mechanical strength, high thermal conductivity, metallic or semi-metallic behavior, and very high surface area which can be exploited in biosensing devices [24].

Rolled graphene sheets, hexagonally arranged sp^2 bonded carbon atoms, are the building block of the carbon nanofibers. In CNFs, these graphene sheets are stacked at an angle to the fiber axis whiles the CNTs have the sheets running parallel to the fiber axis [25]. CNFs therefore have relatively larger diameters, up to 500 nm, and up to a few millimeters in length. The overwhelming research in CNTs after its discovery by Iijima [20] attracted and continues to draw interest in several scientific fields such as chemistry, physics, biology, medicine, biochemistry and electronics. However, CNFs have some advantages over CNTs in microfluidic applications due to their larger inner diameter and the presence of graphene edge planes, which are ledges of carbon that protrude from the surface at regular intervals [26]. The fibrous carbon nanostructures are also known to be highly reactive at their end caps and the defect regions on their sidewalls [27]. These sites, when exploited for chemically immobilizing biological species in biosensing applications, will lead to the fabrication of highly sensitive devices. Price and his colleagues reported the bonding of bone cells with CNFs due to the protrusion of these ledges of carbon in the CNFs structure [26]. These numerous plane terminations of CNFs, unlike the passive graphene surfaces of CNTs, can be modified easily and applied in biosensing applications [3].

1.1.3 Carbon Nanofibers Grown on Glass Microballoons (NMBs)

Research in the potential use of CNTs and CNFs based nano-devices for ultrasensitive sensing is widely being pursued with several demonstrations confirming the exciting possibilities ahead [28-32]. Smaller and lightweight sensors with higher sensitivity and ability to sense in real time will revolutionize the way detections are made. However, utilization of carbon nanofibers in sensing devices pose challenges. Though they lead to improvements in the sensitivity of these devices, their reliability is questionable. This comes to light when attempting detection of multiple

molecules in a sample. A large range of signal fluctuations has been encountered due to statistical reasons [33]. The ability to organize these fibers into well-defined spatial orientations will improve their reliability leading to their potential use in various applications.

Chemical modification combined with self-assembly of individual CNTs/CNFs [34, 35] and a multistep chemical vapor deposition (CVD) process [36] are some methods being used to construct carbon nanofiber superstructures. Employing a direct and relatively simple method of enabling the position of CNFs on the surface of other useful three dimensional structures could help grow CNFs forest for applications in biosensing devices. Hollow nickel microspheres [37], ceramic beads [38], and alumina microparticles [39] are examples of some of the three dimensional structures on which these fibrous nanostructures have been synthesized. Figure 1.1 shows some of these superstructures.

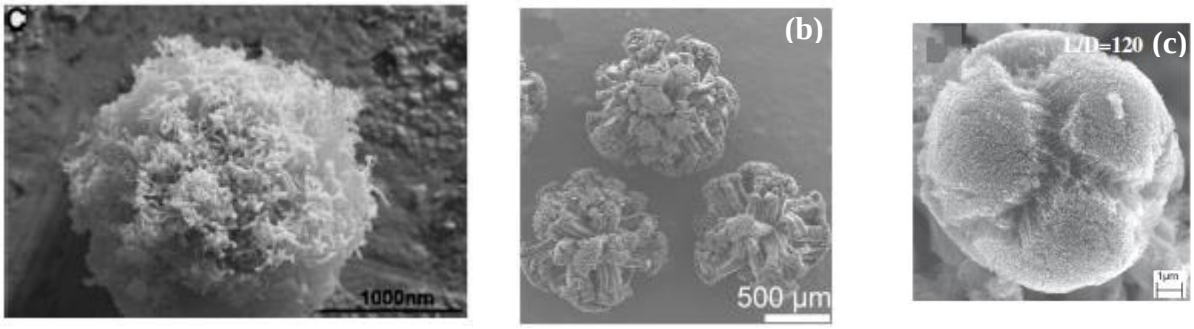

Figure 1.1 CNTs grown on (a) hollow nickel microsphere [37], (b) ceramic beads [38] and (c) alumina microparticle [39].

Catalyst coated hollow glass microballoons made from soda-lime borosilicate glass also has a potential of being used in growing vertically aligned CNFs using the CVD route. Growing these CNFs on glass microballoons (NMBs) has the potential of being utilized in point-of-care diagnostic devices. These immunosensor devices may provide high reliability, ultra-low detection

limits, improved sensitivity, easy handling of labeling materials, and ability to quantify the level of infection. Their use could lead to medical results being made available quicker to the patient and the care team allowing immediate clinical management decisions to be made.

1.2 Research Objectives

The ability to provide immediate diagnosis to patients has been an area of study in the sensing community for some time now. Various rapid detection kits have evolved over time. The pregnancy test kit which analyzes urine samples in a minimum of 3 minutes and the malaria rapid test kits which have a minimum detection time of 10 minutes are a few of POC kits commercially available. More sensitive and real time detection can be achieved if NMBs are incorporated into these devices.

This study proposes the development of a POC testing kit for microorganisms in which NMBs are used as label. Successful growth of several CNFs on a glass microsphere will increase the probability of capture of antigens thereby improving the reliability of the CNFs for electrical and optical detection. This will be the first attempt in fabricating instant diagnostics POC devices with ultra-low detection limit, high sensitivity and selective detection of minute concentrations of multiple disease causing antigens simultaneously. Plasmodium falciparum, Plasmodium vivax, and human chorionic gonadotropin will be used as markers for the study. Visual observation and electrical measurement will be employed for signal detection. Quantification of varying marker concentrations will be obtained from electrical measurements.

1.3 Outline of Dissertation

This dissertation contains six chapters. Chapter 1 presents the motivation and objectives of this research. It also introduces POC devices, CNFs, and CNFs grown on 3D structures. Chapter 2 describes the relevant structures and surface functionalization protocols for CNFs. Experimental procedures and results for fabricating and functionalizing the surface of CNFs are also presented. Chapter 3 introduces antibodies, their binding to CNFs, and modes of preventing nonspecific binding in CNFs. Studies on the conjugation of immunoglobulin G (IgG) and anti-IgG to NMBs and their use as a platform in immobilizing the conjugated NMBs on glass slides are reported. Chapter 4 introduces malaria and the various methods of diagnosing the disease. Pregnancy, a clinical condition is also introduced and its diagnostic methods briefly outlined. An immunochromatographic sensor is proposed that incorporates NMBs to selectively and sensitively detect ultra-low concentrations of malaria and pregnancy antigens in solution. Results and discussions from the sensor are presented. Finally, Chapter 5 summarizes the results obtained from the study and proposes further work.

CHAPTER 2
FABRICATION AND SURFACE FUNCTIONALIZATION OF CARBON NANOFIBERS GROWN ON GLASS MICROBALLOONS

2.1 Introduction

The study and applications of carbon nanostructures have grown since the reported discovery of CNTs by Iijima in 1991 [20]. Although CNTs and CNFs are synthesized using similar setups, their major difference results from the angle of inclination of the rolled graphene sheets. While CNTs are rolled up in a cylindrical form with their plane parallel to the fiber axis, CNFs have their graphene layers inclined with respect to their fibril axis [40]. These differences in inclination are as a result of differences in fabrication temperatures. Hence CNFs are relatively larger in diameter, up to 500 nm, compared to the CNTs. Benefits of using CNFs over CNTs include relatively easier synthesis methods and ease in their dispersion and functionalization. Other properties of these materials have been reported to be similar by several authors [25, 40-43] although better controllability of the location and size of CNFs compared with CNTs have also been reported [44].

Arc discharge, laser ablation and chemical vapor deposition (CVD) remain the most widely used techniques in fabricating CNTs/CNFs due to their ability to synthesis large quantities of the CNTs/CNFs. The discovery of CNTs by Iijima was made possible by the arc-discharge evaporation method [20]. Since then, several researchers have employed modified methods of this process in their approach [45-47]. Even though this method has the advantage of being a simple process that produces CNTs/CNFs with excellent crystallinity, its products do suffer from low purity [46, 48]. The laser ablation method requires complex and expensive equipment and give a limited yield as well [48]. Purification and separation of products from both the arc-discharge and laser ablation techniques have negative impact on subsequent use of the CNTs/CNFs. The CVD

process is much more amenable to scale-up allowing the fabrication of relatively large amount of nanofibers with the least cost. CVDs also enable synthesis to be achieved under relatively mild conditions, giving more control over the growth process. This has allowed the growth of aligned and ordered CNT/CNF structures in a controllable manner on various surfaces [37, 39, 49, 50].

Various structures obtained from the CVD synthesis of CNFs have been proposed. However, the ability to control and tailor the structure of CNFs demonstrated by Rodriquez et al. [51] is the adopted one by most researchers. It involves the creation of a faceted catalyst particle on which the carbon feedstock decomposes on certain surfaces with carbon precipitation occurring on the remaining surfaces of the catalyst [51, 52]. The conditions of growth favors the formation of graphene sheets which grow parallel to the surface of the faceted catalyst particle which in turn determines the angle between the planes and the fibril axis [53]. Under different conditions of gases and catalyst compositions, and temperature, the faceted catalysts undergo surface reconstruction forming unique geometrical shapes which drive the formation of the different CNFs structures [51, 54, 55]. The use of acetylene and hydrogen gas mixtures, fabrication temperatures around 600 °C, and nickel and its alloys as catalysts, have been reported to favor the formation of the herringbone structure [51, 52]. The presence of excess hydrogen have been reported to favor the termination of the large number of dangling bonds at the edges of the stacked graphene platelets, whereas the more stable form of the carbon filament with closed tubular graphene sheets and without dangling bonds are favored without hydrogen termination [25, 56].

The fabricated CNFs appear as powders resembling soot. The individual nanofibers are generally combined into aggregates which can often be seen even by the naked eye. They have extraordinary

thermal, optical, mechanical and electrical properties. The exploitation of their extraordinary electrical and optical properties can be achieved commercially if the nanofibers are applied as carbon nanofiber superstructures. This will eliminate the signal fluctuations associated with measurements from individual fiber strands and also improve their visibility due to the cluster of nanofibers produced. The well-known techniques for consolidating metallic and ceramic particles, pressing and sintering, cannot be applied to CNFs. As a result, other methods are being used to produce forests of CNTs/CNFs on three dimensional substrates [37-39, 49, 50, 57].

Successful grafting of CNTs/CNFs forests on the surfaces of spherical substrates have been achieved by different researches [37-39, 49, 50, 57]. These spheres provide added advantages in that they can be stacked easily while still providing much larger outer surfaces than conventional flat wafers while they also have the best fluidity among all shapes of solid particles. Xiang et al. [50] successfully used a large-scale production technique to fabricate aligned CNT arrays on ceramic spheres comprising of SiO_2, Al_2O_3, and ZrO_2. They reported being able to use their product in constructing a conducting matrix in a polymer as well as in electromagnetic shielding applications. Multi-scale hybrid structures of multi-walled CNTs and micrometric alumina particles have also been produced using chemical vapor deposition process with promising application in advanced multifunctional composite materials [39]. CNFs on glass microballoons (NMBs) have been fabricated by the author in the laboratory and NMBs' use in syntactic foams [58] and thin film conductive nanocomposites and sensors [59] have been reported by colleagues.

2.2 Structure of CNF

The building blocks of both CNF and CNT are the graphene layers. The angle of inclination of these layers with respect to the fibril axis differentiates the CNFs from the CNTs. While the CNTs have parallel orientation to the fiber axis making them cylindrical, the CNFs are inclined at varying angles to the fibril axis. The different inclination angles have led to the discovery of different CNF structures. The various identifiable structures of CNFs are shown in Figure 2.1. The chemical nature of the catalyst, the conditions of its pretreatment, the composition and flow rate of the gas mixture, the duration of the synthesis are properties related to the structure of the CNFs [60-63]. The electrical and optical properties are also largely dependent on their structures [40, 64, 65].

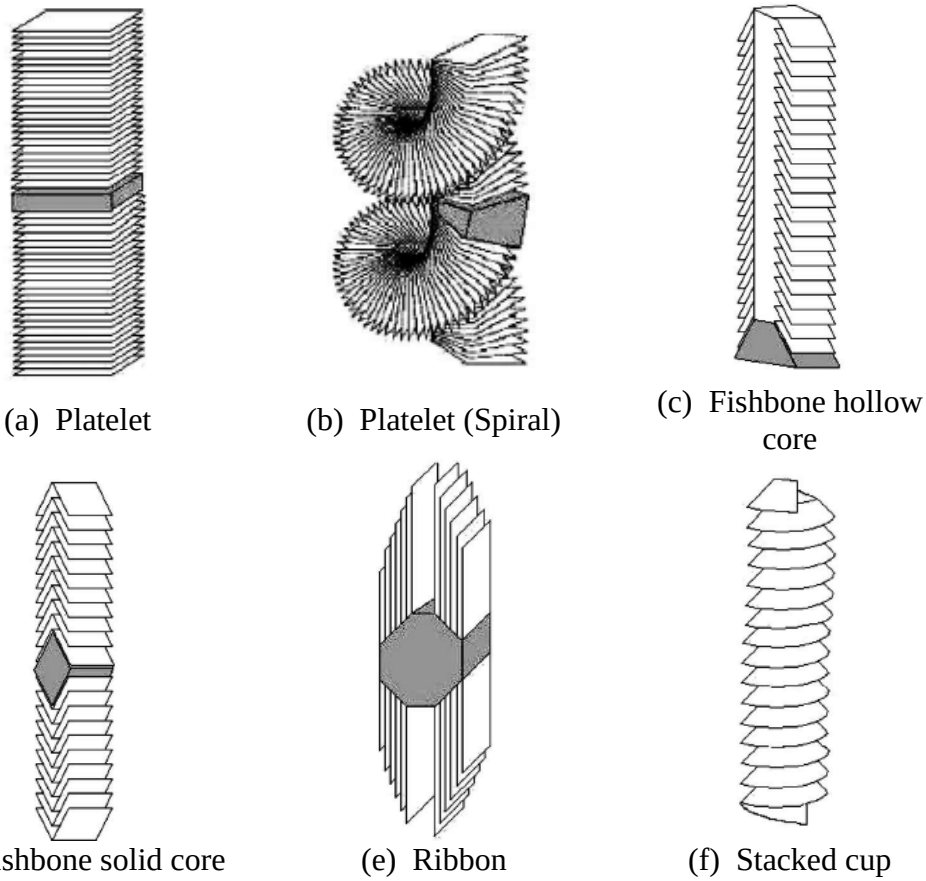

(a) Platelet (b) Platelet (Spiral) (c) Fishbone hollow core

(d) Fishbone solid core (e) Ribbon (f) Stacked cup

Figure 2.1 Schematics of the different structures of CNFs [40].

Platelet CNFs have the graphene layers perpendicular to the fiber axis {Figure 2.1(a)} and with fibril widths up to about 100 nm [40]. Platelets do contain non-negligible amounts of hydrogen or other heteroatoms for the stabilization of their structure. The catalyst used is usually located in the mid portion of the fiber resulting in bidirectional fibers [51, 66]. Coiled structures of these platelets have also been reported [67, 68]. CNF structures produced with the graphene layers inclined at angles less than 90° to the fiber axis have been identified as fishbone. The inclined angle has been reported to depend, among other parameters, on the presence of hydrogen in the feedstock [56]. The resulting structures are either hollow core {Figure 2.1(c)} [69] or solid cores {Figure 2.1(d)} [51]. The structure of ribbon CNFs and multi-walled carbon nanotubes (MWCNTs) bear striking resemblance. The ribbon CNFs {Figure 2.1(e)} comprise of straight unrolled graphene layers running parallel to the fiber axis [51]. The cylindrical cross-sections of the MWCNT enables their distinction to be made. The last identified structure, stacked cup CNFs, is made up of a spiral graphene layer along the fibril axis. They have been reported to have a circular cross-section with a huge hollow space [70]. This structure is favored by the use of a molten catalyst [40].

Despite distinct differences in the internal structures of CNFs and CNTs, the term CNTs are more often used to classify CNFs as well since they can display similar morphology to MWCNTs; however, their physical and chemical properties are quite different. While CNTs are reported to display ballistic electron transport [71] and diamond like tensile strength [41] along their axis, CNFs have proven their robustness as individual, freestanding structures with higher chemical reactivity and electron transport across their sidewalls. Their high chemical reactivity makes them candidate materials for applications such as biosensing which requires selective functionalization

and attachment of biological molecules while their outstanding electron transport ability is exploited in their use in electrochemical applications.

The graphene sheet is a flat monolayer of carbon atoms packed tightly into a two dimensional and crystallizes in a honeycomb lattice. Carbon has an outer shell containing the $2s^2 2p^2$ orbitals and the hexagonal lattice arrangement of the carbon atoms in graphene allows the formation of two penetrating sub-lattices, which is a result of its sp^2 hybridization [72]. The four valence carbon electrons only bonds to three other carbon atoms leaving an unoccupied $2p_z$ orbital perpendicular to the plane of the graphene sheet of the valence atomic bonds. Stable sigma bonds between the three nearest carbon atoms are formed in the planar orbitals with the remaining free $2p_z$ orbitals overlapping between neighboring carbon atoms to form weak pie bonds. These out of plane pie bonds are responsible for the excellent electrical properties of the graphene sheets, and hence the good conductivities of various CNF structures. The conduction electrons can travel large distances without being scattered, that's up to 25000 cm^2 per volt-second, which is only 300 times less than the speed of light [73]. The 2.3% cloudiness on the honeycomb graphene surface leaving over 97% visual transmission rate gives graphene, and hence CNFs, their extraordinary optical properties [74].

The structural configuration of CNFs and their high surface area-to-volume ratios therefore allows the confinement of the free pi electrons around the circumference and length of the CNFs. The presence of strong covalent and pi bonds and the ability to selectively attach functional groups makes these structures ideal for use in a wide range of applications such as in biosensors, composite materials, electronic devices, and field emission displays.

2.3 Surface Functionalization of CNFs

All known methods of synthesizing of carbon nanostructures have been reported to generate some amount of amorphous carbon and catalyst nanoparticles as impurities in the final product [45-50]. Hence contamination and their poor solubility in aqueous media have been their major obstacle to their use in biosensors and other applications. The various techniques, for the purification of the "as fabricated" carbon nanostructures involve their manipulation into a useful state which consist of extensive mechanical and chemical processing. These processes change the surfaces of the carbon nanostructures and more often creates isolated point defects or vacancies, topological defects, and sp^2-sp^3 hybridization defects in the hexagon graphene framework. The absence of carbon atoms from their original positions as a result of incomplete bonding during synthesis results in the introduction of point defects in the structure. The topographical defects are created as a result of pentagon and heptagon carbon lattice formation along the carbon nanostructure walls. Stone-Wales defects, 2 pentagons and 2 heptagons, have a unique characteristic in adsorption of hydrogen and other foreign atoms and this has a potential in applications such as biosensing and energy storage. The interaction between the adsorbing hydrogen and carbon atoms during the synthesis process also leads to the generation of the hybridization defects [75]. Purification techniques leads to the production of cleaner materials as well as the introduction of functional groups which makes it easier for further processing of the carbon nanostructures. They however, results in partial loss of structure and material as well as increased number of defects on their surfaces.

The presence of van der Waals forces in these carbon nanostructures is also responsible for the agglomeration of the individual strands in various aqueous media. Due to their smaller sizes, these

van der Waals forces are stronger in carbon nanostructures, requiring the use of functionalization techniques to aid and maintain dispersion. With all the carbon nanostructures, the CNFs are less affected by the van der Waals forces and tend to stay dispersed for longer periods of time. Controlling the surface chemistry of these CNFs is therefore critical to defining their functionality. Their surface charge, hydrophobicity, and chemical reactivity can be and have been altered through both covalent and non-covalent modifications [62, 76-78].

Covalent, or chemical attachment of functional groups takes advantage of the higher reactivity of carbon atoms at defect sidewalls and the end caps of carbon nanostructures to carry out a series of reaction steps. Only a smaller fraction undergoes the functionalization compared to the non-covalent type. The direct covalent sidewall functionalization is associated with a change of hybridization from the sp^2 to sp^3 losing p-conjugation system on the graphene layer in the process. Molecules with higher chemical reactivity are used due to the inert nature of the sidewalls [79].

The use of xanthates in the functionalization process has been reported to offer the advantages of easy processing and versatility towards applications in a multitude of domains [80]. Use of other molecules such as elemental fluorine in the functionalization of the carbon nanoparticles have resulted in weaker C-F bonds which provides substitution sites for additional functionalization [81]. Successful replacement of the fluorine atoms by amino, alkyl and hydroxyl groups have been achieved [82]. Other methods of sidewall functionalization, including cycloaddition [83], gas-phase azide [84], and silylation [85] have also been successfully employed.

Functionalization of the defect sites and end caps are achieved by oxidative damage to the nanostructure framework by strong acids and oxidants which results in the formation of carboxyl acid, ketone, alcohol and ester groups at the sites attacked by the acid. These functional groups serve to tether many different types of chemical moieties onto the ends and defect sites of these nanostructures. Treatments of carbon nanostructures with strong acids such as HNO_3, H_2SO_4 or a mixture of them [86-88], or with strong oxidants such as $KMnO_4$ [89], ozone [90], reactive plasma [91] tend to open up these structures with the introduction of the functional groups. These functional groups have rich chemistry and have been used for further chemical reactions in applications such as biosensing, silanation, and esterification [79, 85, 86].

Covalent functionalization introduces several polar and non-polar functional groups onto the carbon nanostructures making them soluble in various organic and inorganic solvents. Two major drawbacks are however associated with these methods. First, ultrasonication and centrifugation associated with these methods leads to the creation of large number of defects on the sidewalls, and in some cases, fragmentation of the nanostructures into smaller pieces. These damaging effects lead to severe degradation in the mechanical properties and the disruption of π electron system. Electrical and thermal properties of the structure is subsequently reduced since the defect sites tend to scatter the conducting electrons and phonons [92]. The other major drawback is the effect of the concentrated acids and strong oxidants on downstream processes. These chemicals are environmentally unfriendly and may affect the further applications in biosensing and other acid sensitive use.

An alternative method of tuning the interfacial properties of the hydrophobic carbon nanostructures is through the use of non-covalent functionalization. The use of ionic surfactants such as sodium dodecyl sulfate (SDS), which is widely used in household products such as shampoo and shaving foam, has been found to be of great value in solubilizing CNTs. The ionic surfactants operate by transferring a charge to the surfaces of the CNTs. The CNTs are then dispersed by electrostatic forces with the behavior of the dispersion showing a strong dependence on pH [93]. Non-ionic surfactants, such as triton X-series, have also been used to solubilize CNTs in water [94]. These non-ionic surfactants operate using a combination of hydrogen bonding and/or steric dispersion forces. At high concentrations, these surfactants form micelles, with the CNTs held in the hydrophobic core of the micelles [93].

The use of relatively small molecules containing planar groups that irreversibly adsorb to the nanostructure surfaces by π-stacking forces have also been used. Chen et al. [95] used a planar pyrenyl group to non-covalently functionalize the surface of SWCNT. This formed the van der Waals bonds and a 'tail' consisting of succinimidyl ester group. Finally, helically wrapping the tubes with linear polymers such as polyvinylpyrrolidone (PVP) and polyethylene glycols (PEG) have also been successfully used. Zhang et al. [96] used PVP to modify the surface of MWCNTs. They reported a straightforward and efficient method for dispersing the MWCNTs in water and a variety of organic solvents with the solvents being kept for up to 2 months without the MWCNT precipitating out. The use of PEG in non-covalently modifying the surface of carbon nanostructures have also been reported to improve water solubility and long blood circulation [97].

2.4 Experimental Procedures

2.4.1 Catalyst Coating of Glass Microballoons

Glass microballoons (MBs), the three dimensional microstructure on which the carbon nanofibers were synthesized was purchased from 3M Corporation, USA. They are chemically stable lightweight/high strength hollow glass spheres with a soda-lime-borosilicate composition and a true density of 0.22 g/cm^3. Their diameters range between 5 to 75 µm with their surface amendable to treatment with a variety of functional coatings [98]. Electroless deposition (ELD) of nickel on the glass microballoons was achieved using the three stage functionalization, activation and deposition technique [99]. 3-aminopropyltrimethosxysilane (APTMS), sodium hypophosphite ($NaH_2PO_2.H_2O$), nickel (II) chloride hexahydrate ($NiCl_2.6H_2O$), and ammonium chloride (NH_4Cl) were purchased from Alfa Aesar Chemicals, MA, USA; palladium (II) chloride ($PdCl_2$) from Strem Chemicals, Inc., USA; sodium citrate dihydrate ($Na_3C_6H_5O_7.2H_2O$) from Mallinckrodt Chemicals, Inc.; and ammonium hydroxide solution (NH_4OH) obtained from BDH Aristar were used in the ELD process. Temperatures for all processes not stated were carried out at 25 °C. The steps used for Ni deposition are explained in detail below:

- Functionalization

Glass microballoons (about 10g) were cleaned repeatedly with acetone, isopropyl alcohol, and ethanol respectively. The microballoons were filtered from each of the solvents using a vacuum assisted set-up. The washed microballoons were then dispersed in 700 ml of ethanol.

The washed microballoon/ethanol solution was placed on a combined hot-plate magnetic-stirrer device and vigorously agitated. 1.4 ml of APTMS was added to the suspension and the stirring

was allowed to proceed for 2 hours. The functionalized microballoons were washed twice with ethanol and filtered using the vacuum assisted set-up.

- Activation

The functionalized microballoons were transferred to a 700 ml ethanol solution containing 0.14 g of $PdCl_2$. The mixture stirred and left to react for 2 hours at room temperature. The activated microballoons were then thoroughly cleaned by washing twice with ethanol and deionized water. 420 ml of deionized water was then added.

- Deposition

The electroless solution was prepared by dissolving 4.2 g of $NiCl_2$.6H2O, 1.39 g of $NaH_2PO_2.H_2O$, 7.0 g of $Na_3C_6H_5O_7.2H_2O$, and 6.96 g of NH_4Cl in 140 ml of deionized water. The pH of the solution was adjusted to 8.30 by adding sufficient amount of NH_4OH. This solution was introduced into the 420 ml activated microballoons solution and the temperature raised to 90 °C. It was vigorously stirred and the reaction left to proceed for 15 minutes.

2.4.2 CNF Growth

An OTF-1200X-80-II-F3LV dual zone tube CVD furnace was used for the CNF growth. This process of growth was first reported by Lee et al. [100] and a schematic of the setup is shown in Figure 2.2. 20 mg of Ni coated microballoons was uniformly spread on two 40 cm^2 silicon wafers. The wafers were placed in the second heating zone of the furnace. The temperatures of the CVD zones were set at 850 °C and 650 °C respectively and the furnace programmed to reach these temperatures in 40 minutes. An inert atmosphere was maintained in the furnace by flowing 160

sccm of Ar gas throughout the fabrication process. The growth was carried out in 15 minutes by flowing a mixture of 100 sccm of H_2, 30 sccm of C_2H_2, and 350 sccm of Ar through a deionized water maintained at 60 °C. After the growth process, the temperatures in the two chambers were programmed to attain 100 °C in 50 minutes. All gas tank pressures were maintained at 5 psi.

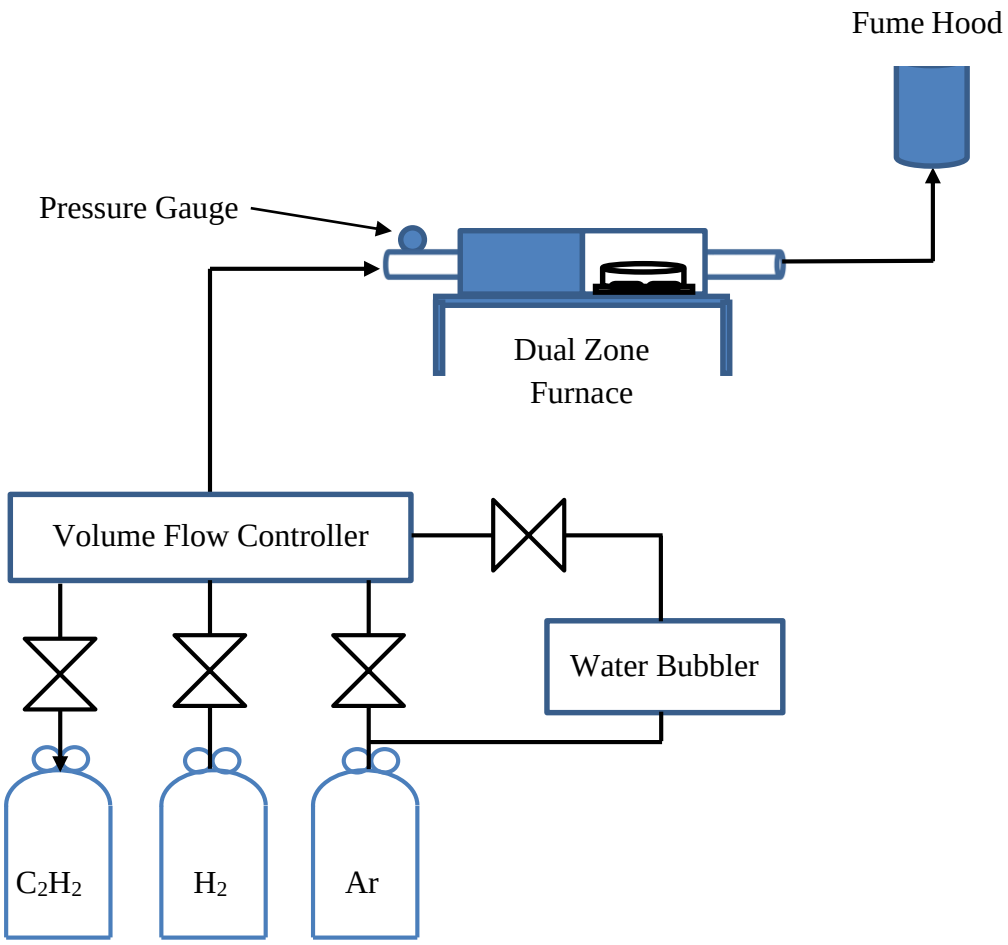

Figure 2.2 Schematic of the CVD system.

2.4.3 Surface Functionalization of CNF

Nitric acid (68% v/v) (HNO_3) obtained from Macron Chemicals and H_2SO_4 (98% v/v) from Fisher Scientific were used for the acid functional process. As fabricated NMBs was used for the surface modification studies. The carboxyl groups were grafted onto the surface of the as-fabricated NMBs

following modifications of two different acidic processes reported by Osorio et al. [101] and Liang et al. [88]. The first method involved the treatment with nitric acid where 2 mg of NMBs was refluxed with 2 ml concentrated HNO_3 for 24 hours. The second procedure involved the treatment 10 mg of NMBs with 8 ml 1:3 volume concentrated solution of HNO_3/H_2SO_4 also for 24 hours. The resulting NMBs solutions were filtered and washed using distilled water. Both filtrates were suspended in 8 M NaoH, obtained from Macron Chemicals, for 24 hours and then filtered. To neutralize the filtrates, they were rinsed with dilute HCl, obtained from Macron Chemicals, filtered, washed with an excess of distilled water, and then left to dry.

A third and simpler method used to graft carboxyl groups onto the surface of the CNF was conducted in the reaction chamber of the CVD equipment. 20 mg of NMBs was heated to 400 °C in dry air for 30 minutes after which it was allowed to cool.

2.4.4 Characterization

Scanning electron microscopy (SEM) was carried out to observe the morphology of the four different NMBS samples. These are the as fabricated, HNO_3 treated, HNO_3/H_2SO_4 treated and air oxidized samples. Characterization was performed using an FEI Quanta 3D FEG Dual Beam FIB/SEM with an xT Microscope Control Software. Images were recorded with an accelerating voltage of 5 kV by placing samples on a double sided copper tape and attaching it to a stand.

The Nicolet 6700 with OMNIC software was used for the Fourier transformed infrared spectroscopy (FTIR) characterization to determine the successful carboxyl functionalization of the CNFs. Samples were loaded onto an ATR sample holder for analyses. The surface chemical

bonding and structure of all four samples analyzed were obtained in the frequency range of 600 – 4000 cm^{-1}.

The Renishaw 2000 Micro-Raman was used for the Raman studies of the as-fabricated CNF. The presence of defective graphitic sheets was obtained in the frequency range of 1000 – 2500 cm^{-1}.

2.5 Results and Discussions

2.5.1 Catalyst Layer Formation

The three stage flow mechanism employed for the ELD process is shown in Figure 2.3. The functionalization stage introduces the amine group onto the surface of the MBs which is subsequently activated by the adsorption of Pd(II). The final deposition results in a color change of the glass spheres due to the uniform layer of nickel coating deposited on the glass surface. Figure 2.4 shows images of MB, nickel coated MB, and NMBs. Figure 2.5 shows an SEM micrograph of the nickel coated MB and a typical optical micrograph of the nickel coated MBs formed on silicon wafer [102]. The FTIR spectra of as-received MBs and ELD nickel coated MBs are shown in Figure 2.6. Similar spectra were obtained for both samples. The spectra composed mainly of the broad absorption bands at ~700 – 1000 cm^{-1} corresponding to the S-O stretching vibrations. The bands at ~1405 corresponds to the O-H bends respectively [103]. The peaks at ~2364 cm^{-1} can be associated with the O-H stretch from strongly hydrogen-bonded –COOH [104]. The nickel coating therefore did not contribute any functional groups to the surface since they only acted as nucleation sites for the growth of the CNF.

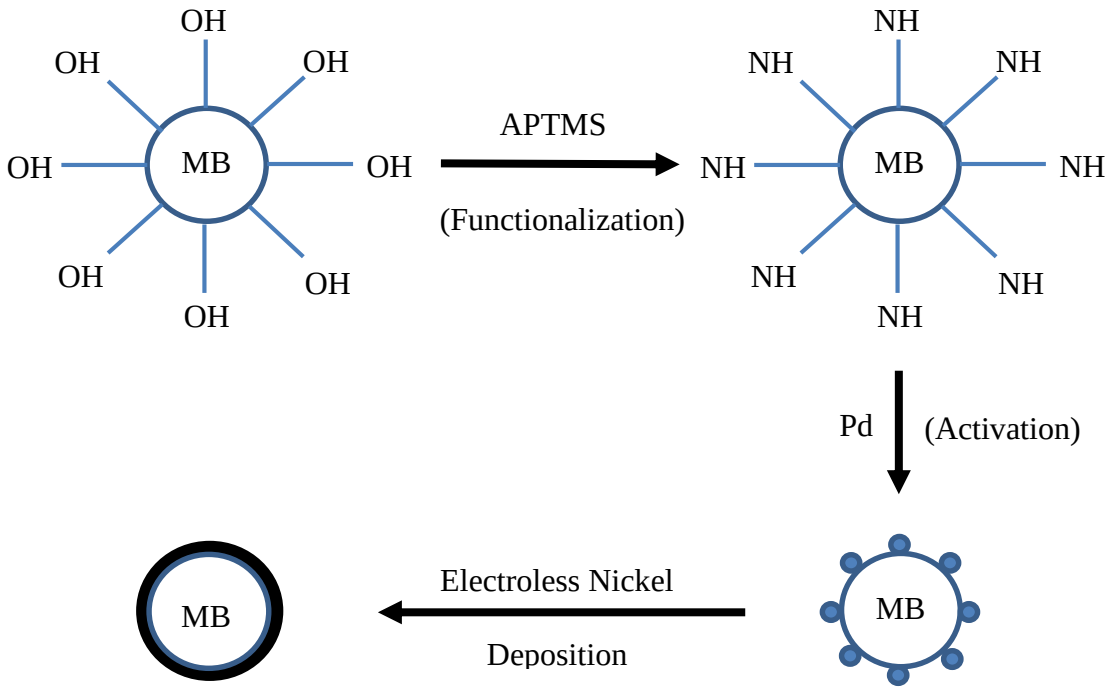

Figure 2.3 Flow mechanism of electroless nickel deposition on glass microballoon.

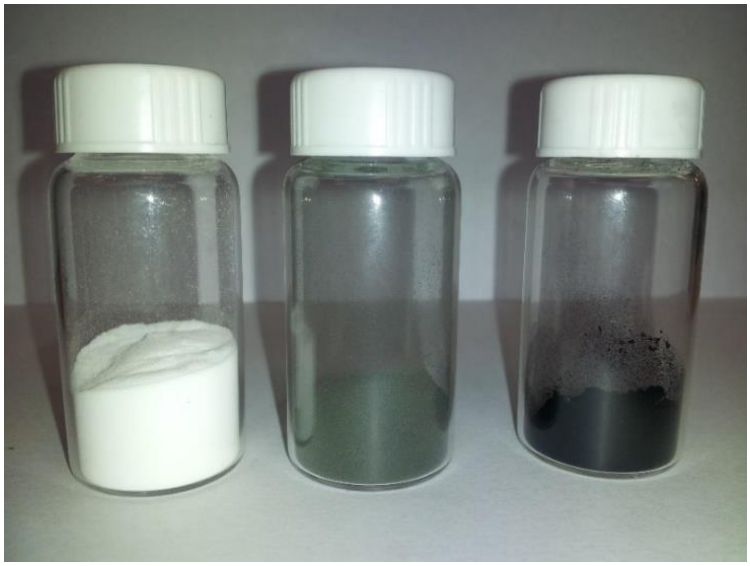

Figure 2.4 Images of as-received microballoons, microballoons after electroless nickel deposition, and carbon nanofiber grown on nickel coated microballoons.

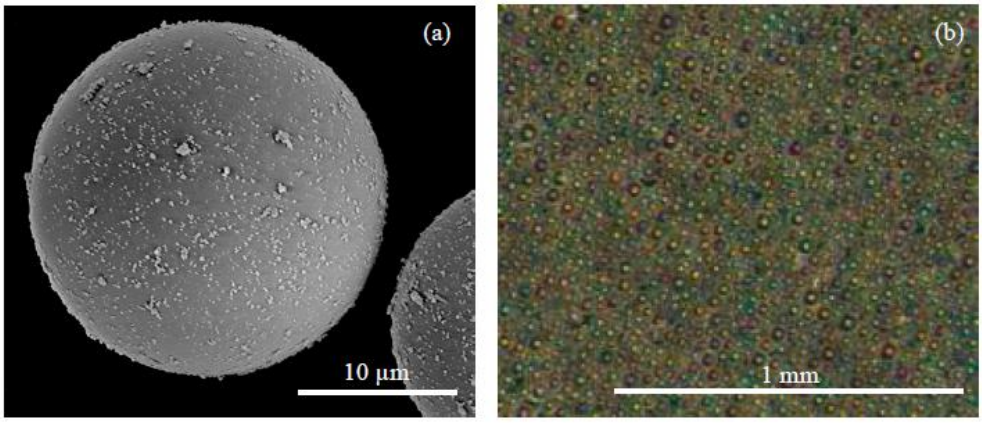

Figure 2.5 (a) SEM micrograph of nickel coated MBs and (b) typical optical micrograph of a layer of nickel coated MBs formed on silicon wafer [102].

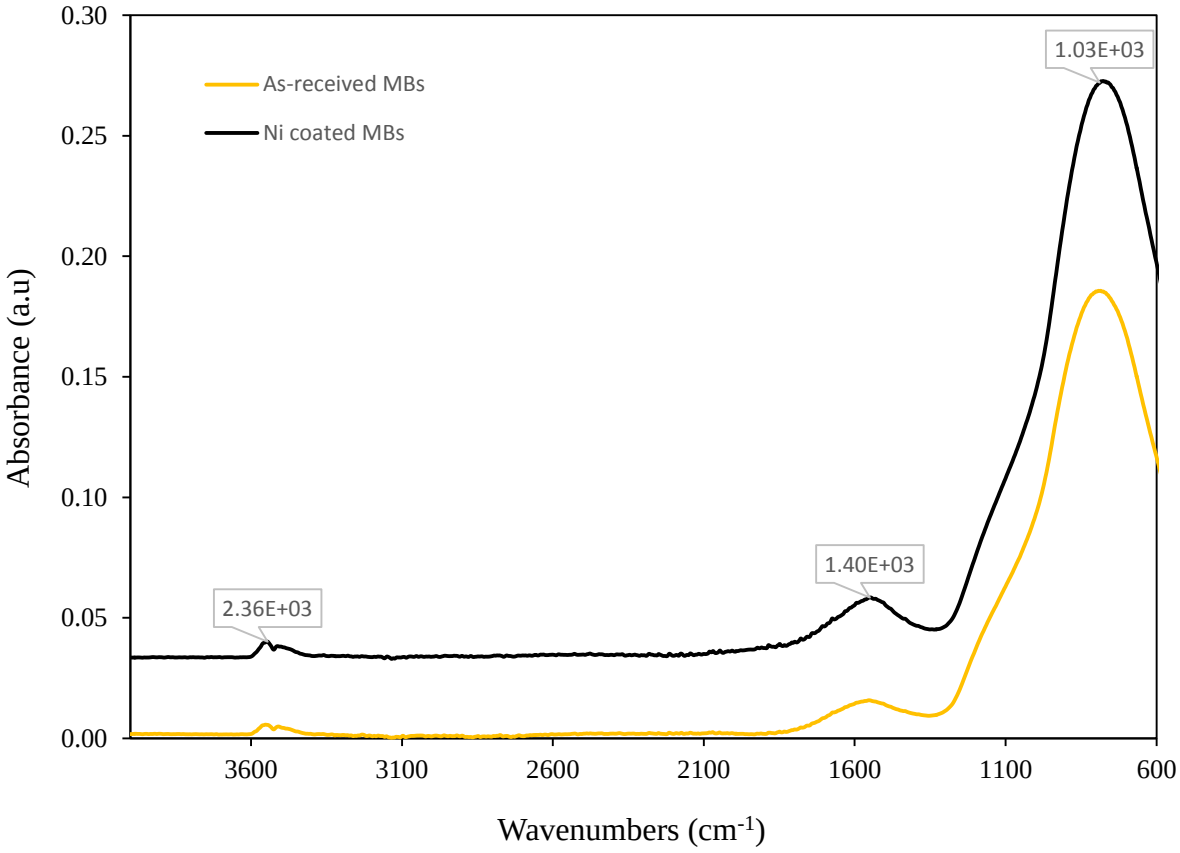

Figure 2.6 FTIR spectra of (a) as received MB and (b) nickel coated MB.

Nonmetallic substrates like glass microballoons lack the catalytic properties required for CNF growth as well as forming a strong bond with the CNF synthesized on their surfaces. This is

achieved by coating the surface of our glass microballoons with nickel. The presence of hydroxyl groups on the surface of glass makes them easily amenable to surface modification. These silanol functional groups, Si-OH, bonds strongly with amino groups, such as APTMS, to form the stable siloxane bond, Si-O-Si as a result of the partial protonation of the APTMS. This has been reported to uniformly coat the surface of the glass while the amine group protrudes outwards serving as active sites on the glass surface for binding with other molecules [105, 106]. However, these amine groups have low affinity for nickel hence the use of Pd (II) as catalyst. This is reduced by the presence of $H_2PO_2^-$ to form Pd which is strongly bonded to underlying siloxane layer. These Pd particles act as seeds for the nickel deposition process resulting in the almost uniform nickel coating of the surface of the MB.

2.5.2 CNF Growth

Figure 2.7 shows the SEM micrographs of CNFs grown on the MB at two different magnifications. The nickel layer formed on the MB acted as nucleation sites and growth for the CNFs. This ensured that the CNFs are connected to the MB along their axial direction, which is essential in building efficient charge and load transfer interfaces. The micron dimension of the spheres also allows the uniform and randomly oriented growth of several CNFs on each MB as shown in Figure 2.7. Average CNF diameters of 40 nm with high CNF density on each MB were fabricated using this process. Figure 2.8 shows the Raman spectra of the as fabricated CNFs [102]. Defective graphitic sheets are always present in fabricated CNFs and this was confirmed by the D-band observed at 1325 cm^{-1} in the Raman spectra.

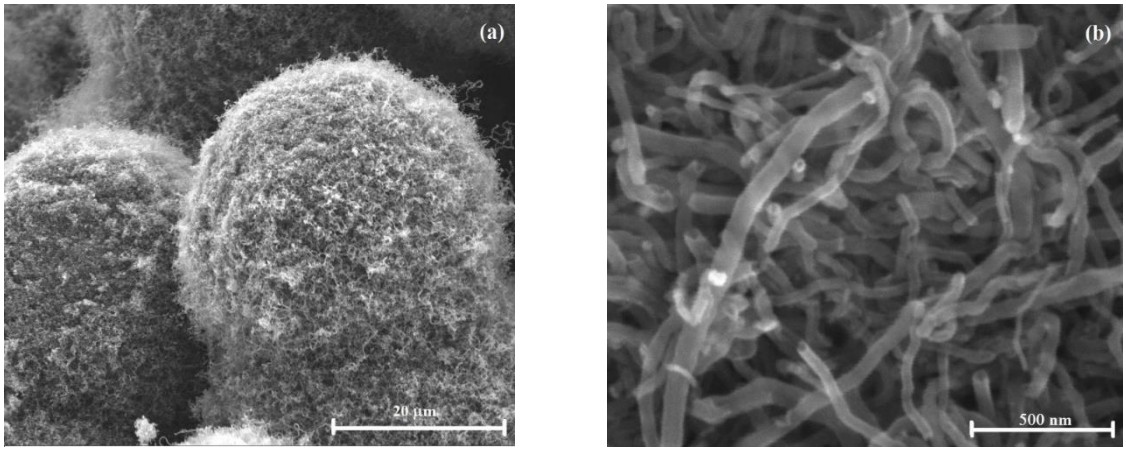

Figure 2.7 (a), (b) SEM micrographs of as-fabricated NMBs at different magnifications.

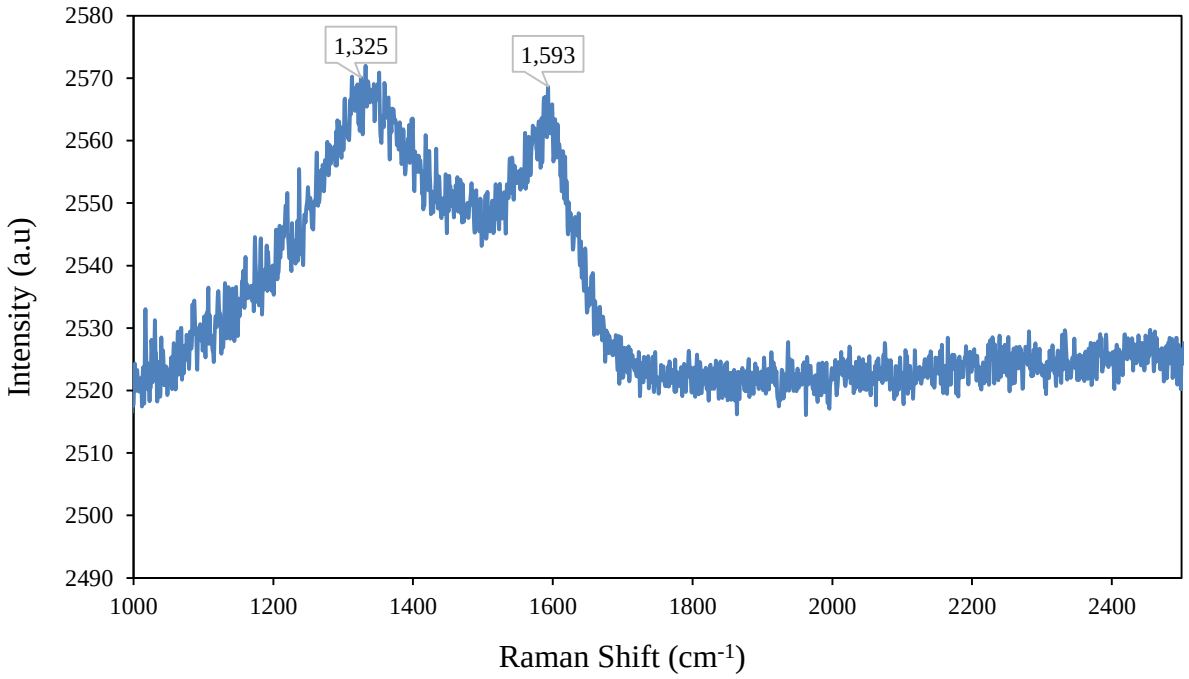

Figure 2.8 Raman spectra of as-fabricated CNFs [102].

Gases such as methane, acetylene, xylene, ethylene, and carbon monoxide have all been used in the fabrication of CNFs with varying advantages of each of these carbon sources [107]. The use of C_2H_2 as the source of carbon for the growth was chosen due to its higher decomposition rates even at the 650 °C used in fabrication. C_2H_2 also can be used in the absence of NH_3 as NH_3 have

been reported to suppress the CNF growth due to its enhanced etching effect [107]. The use of hydrogen influenced the decomposition of the nickel precursors and C_2H_2, avoided the formation of amorphous carbon on the surface of the nickel catalyst and also acted as a carrier gas. The use of water vapor, a weak oxidizer, selectively removed amorphous carbon deposits thereby preventing the coating of the catalyst particles and hence improving the CNF growth. Argon gas acted as the major carrier gas in the system while maintaining a neutral environment in the chamber [108].

From the fabrication parameters, the length of the CNFs, evident in Figure 2.4 (b), curved with irregular wave shapes due to the surrounding neighboring particles as the CNF length increased. This is consistent with the report published by Zhang et al. regarding the increase of the branched length of CNF with growth time progressively in a quasi linear manner [49]. This type of structure, compared to the vertically aligned, is more desirable for applications in biosensing devices as more outer CNFs surfaces are made available for conjugation with biomolecules which can easily be immobilized on capture substrates.

2.5.3 Surface Functionalization Results

The fabrication process used in CNF growth results in the deposition of varying amounts of oxidized carbonaceous fragments. Coupled with the inert nature of the sidewalls of the CNFs, a combination of acidic and basic solvents were used in the functionalization of the CNF. The schematic modification of the CNF using HNO_3 as an example is shown in Figure 2.9. Acidic oxidation most often results in the oxidation of the carbonaceous fragments and this was avoided by washing with NaOH before oxidizing again with the dilute form of the acid used in oxidation.

SEM micrographs of the three oxidation methods used are shown in Figure 2.7 (a) – (d) while the combination of acidic effect and the several washing resulting in the fracturing and peeling off of the CNFs from the MBs are shown in Figure 2.7 (d).

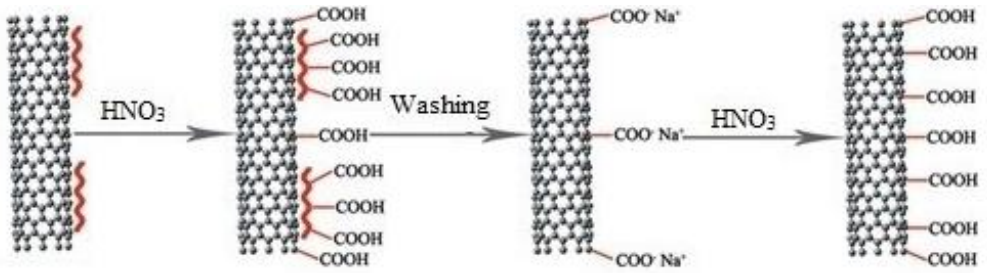

Figure 2.9 The modification process of CNFs by HNO_3 treatment. Carbonaceous fragments are represented by red wavy lines. Similar processes are found elsewhere [88].

The acid oxidation is a more selective technique that removes amorphous carbons and contaminant metals; however, its effect can be seen in the SEM micrographs. The concentrated nature of these acids resulted in the shortening of the CNFs on the MBs and increase number of surface defects with the HNO_3/H_2SO_4 combination having the most pronounced effect. This is consistent with findings by several researchers [48, 86-88, 109]. The interaction between the graphene layers of the CNFs and these concentrated acids have been investigated by Collins [110]. His findings indicate that these highly oxidative acids do not continuously etch the graphene's sidewalls due to their inert nature but instead covalently add to its edges and basal planes resulting in adduct defects which continuously etch off these planes with time. This is responsible for the loss of structure in the acidic functionalization with the stronger HNO_3/H_2SO_4 combination having a more adverse effect, Figure 2.10.

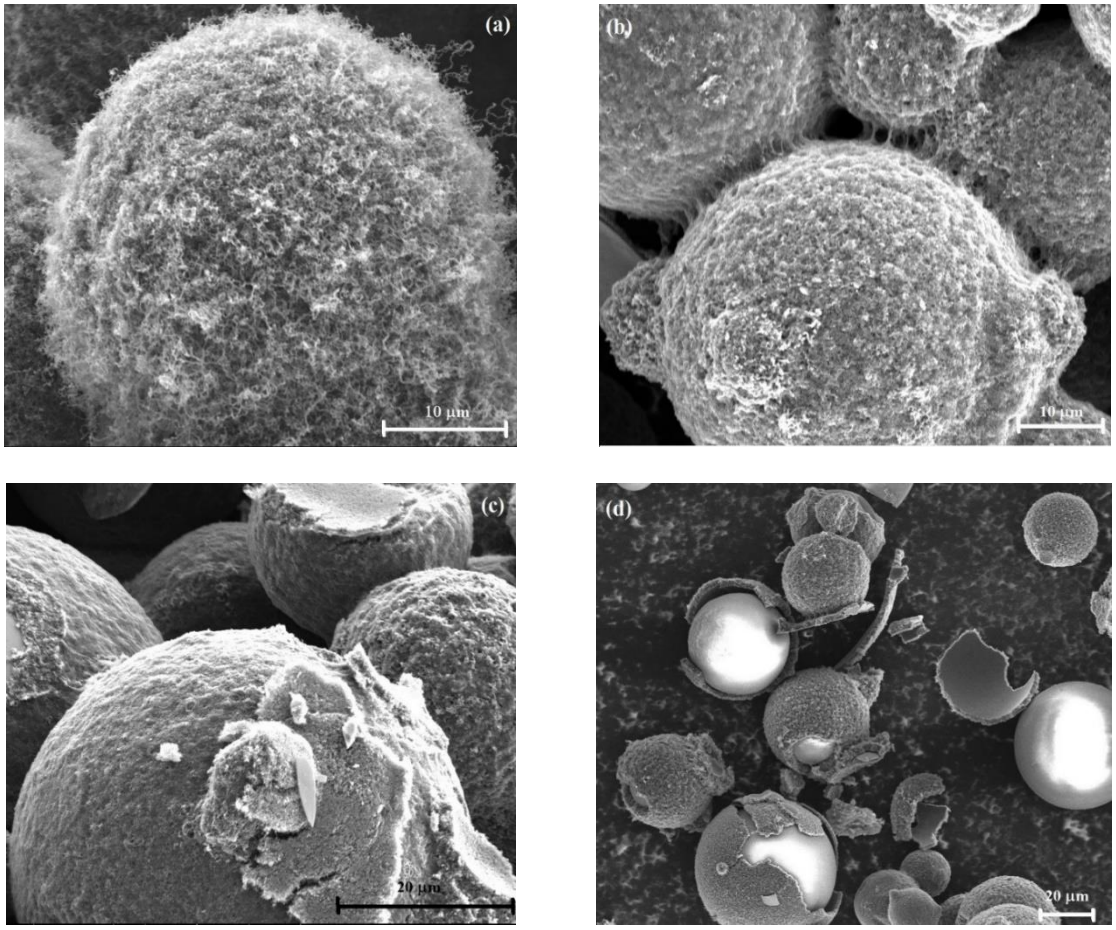

Figure 2.10 SEM micrographs of (a) air oxidized, (b) HNO_3 oxidized, (c) HNO_3/H_2SO_4, and (d) fractured and peeled off CNFs from acidic oxidization of MBs.

Oxidation in air tends to have a harsher purification scheme at temperatures between 400 °C and 750 °C. At the low end of this temperature range, amorphous carbon has been reported to rapidly convert to CO_2 through cooperative reactions with oxygen and water vapor [110]. The graphitic carbons do burn more slowly, since only the carbon atoms on the edges of the graphene are reactive. Therefore, at 400 °C oxidation temperature, the fraction of graphitic impurities on the CNFs surfaces will oxidize faster along their sidewalls than the edges of the graphene. This is responsible for the better retained structure of the NMBs after oxidation.

Figure 2.11 shows the dispersed states of the three different types of oxidized NMBs in water, at the moment of dispersion and approximately 2 mins and 10 mins thereafter. When a surface is oxidized, ionic charged functional groups are introduction onto its surface. In this study, negatively charged carboxyl and hydroxyl groups are chemically introduce onto the surface. These charged groups initially enables the CNFs to repel each other in the water solution, and hence their initial good dispersion. Suspension stability reduces drastically with time with HNO_3 having the worst stability among the three groups as shown in Figure 2.11 (b) after only 2 minutes of suspension. After 10 minutes, most of the NMBs are seen to settle for both the HNO_3/H_2SO_4 and air oxidized with the air oxidized having the better stability. During settling, a portion of the NMBs were seen to settle at the bottom of the tube with the remaining floating on the water.

The air oxidized had the best stability with HNO_3 oxidized having the worst. However, the long term solubility of all oxidized samples was very poor. The difference in solubility can be attributed to the efficiency in functionalization with HNO_3 having the least number of functionalized groups and air oxidized having the most.

Figure 2.12 shows the FTIR spectra of the as fabricated and the three different oxidized NMBs. The introduction of the infrared radiation onto the samples led to a difference in charge state between the carbon atoms which induced the formation of an electric dipole leading to signal generation. The frequency of adsorption is a function of the stretch and bending functional group. Weak signals were generated due to the weak difference of charge state between the carbon atoms leading to a silent spectrum. All four samples presented similar signals with the exception of the ~2359 cm^{-1} peak in the acidic oxidized samples. This peak is from the characteristic disruption of

the quaternary ammonium ($C=N^+$) formed as a result of the presence of nitrogen in the fabrication environment [111]. The acidic oxidants reacts with this functional group, hence the absence of this peak in the acidic oxidized.

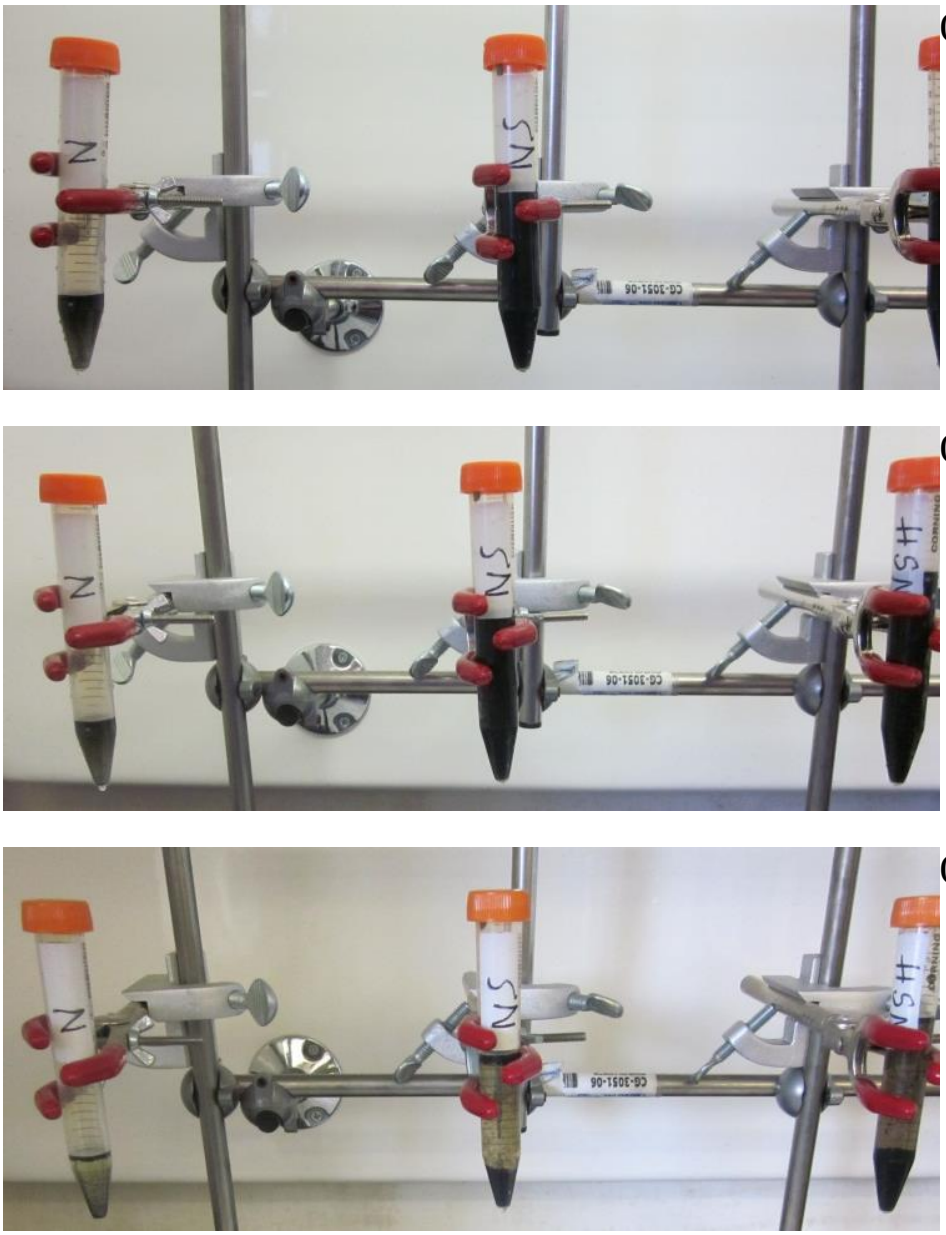

Figure 2.11 Dispersion of NMBs in PBS after modification with HNO_3, HNO_3/H_2SO_4, and air (from left to right). All solutions have 1 mg/ml concentration of NMBs and at times (a) just dispersed, (b) 2 minutes, and (c) 10 minutes.

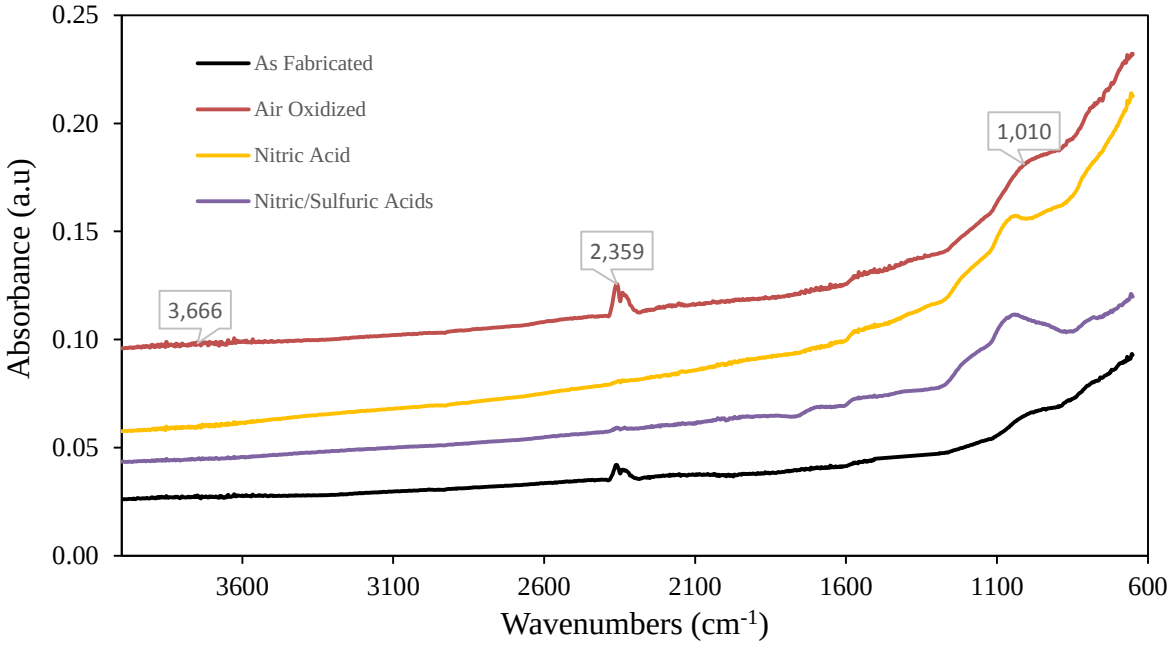

Figure 2.12 FTIR Spectra of as-fabricated and the different types of surface oxidized samples used in the research.

Weak signals were also generated at ~3666 cm^{-1} characteristic of stretching vibrations of O-H bonds preferentially from the hydroxyl groups. The appearance of peaks at ~1000 – 1100 cm^{-1} for all the samples correspond to the C-O stretching indicating the presence of the carboxyl groups. The presence of these functional groups which was confirmed from the FTIR results agrees with the observed stability of these samples in water. These functional groups reduced the van der Waals interactions between the individual NMBs leading to an improvement in their dispersion stability in the aqueous media.

2.6 Summary

In summary, fabrication of CNFs on glass microballoons has been achieved using a classical CVD process. This was made possible by uniformly coating the MBs with nickel using a three stage process: functionalization, activation and deposition techniques. The presence of amorphous

carbonaceous fragments requires further purification techniques. These techniques result in the production of cleaner materials as well as the introduction of functional groups making it easier for further processing of the CNFs. FTIR studies showed the presence of the hydroxyl and carboxyl functional groups on the as fabricated CNFs. The three different purification methods employed in this study also showed the presence of the hydroxyl and carboxyl functional groups. However, the acid modified surfaces resulted in the substantial loss of CNF structure while the air oxidized NMBs maintained its CNF structure. The other major drawback in the use of the acidic oxidants is their effect on downstream processes. These chemicals are not environmentally friendly and may affect applications in biosensing and other acid sensitive uses. The air oxidized CNFs therefore stands out as the ideal surface treatment method for attaching the hydroxyl and carboxyl functional groups needed for biosensing applications.

CHAPTER 3
IMMUNOASSAY ON GLASS SLIDE USING CARBON NANOFIBERS GROWN ON GLASS MICROBALLOONS (NMBs)

3.1 Introduction

Disease diagnostics continues to play a major role in the healthcare sector. It is regarded as an attempt at classifying an individual's condition into separate and distinct categories that allow medical decisions about treatment and prognosis to be made. Several methods have been used in diagnostics. These methods include clinical, laboratory, radiology, retrospective, and immunoassay diagnoses. Technological advances have led to rapid improvements in most of these techniques with immunoassays being no exception.

Immunoassays provide quick and accurate tests that are widely used for on-site and laboratory diagnosis of various diseases. It is a valuable analytical technique based on molecular recognition between antibodies and antigens that allows for detection with high sensitivity and specificity. They have been widely used for the identification and quantification of target molecules in applications such as clinical diagnostics, proteomics, pharmaceutical research, environmental analysis and basic biological investigations [112, 113]. The high specificity of the antibody/antigen interaction enables the relevant analyte to be isolated from complex mixtures with minimal sample preparation while being relatively inexpensive and providing exceptionally low detection limits [113].

The high specificity of the antibody/antigen interaction makes their immobilization on any support a vital process. The ideal support should robustly attach all the chosen biological species in an appropriate orientation without altering their conformation. Attachment has been a challenge on

different substrates due to the variety in the polarities, hydrophobicities, charges, sizes, and structures of different biological species while repelling nonspecific binding. Successful immobilizations have however been achieved on substrate materials such as those made from silicon, glass, and polymers [12, 114-119]. The need for less sample/reagent consumption, a reduced risk of contamination, enhanced sensitivity, low unit cost, lower power consumption, and a higher reliability led to the use of microfluidic devices for immobilization [113].

Silicon and polymeric materials such as polydimethylsiloxane (PDMS) are materials commonly used for the fabrication of these microfluidic systems. As a result, various protocols have been developed for immobilizing various biological species on these substrates. The presence of bubbles and dead volumes continue to hinder the full scale utilization of silicon in microfluidic devices. With PDMS, hydrophobic surface and nonspecific adsorption of proteins and other molecules have constituted their major limitation [118]. The optically transparency of glass throughout the visible spectrum, the ability to easily functionalize the surface of glass, and the recent low cost of fabricating glass-based microfluidic chips has played a role in its continued use as a substrate in immobilization [119]. An added advantage is their ability to offer higher density arrays and the use of lower sample volumes. New materials such as paper and cotton thread have recently also been introduced as simple and low-cost platforms for immobilizing biological species [112, 120, 121].

Labeling biological species has always been a challenge. Labeling on their antigenic epitopes result in the loss of their interlocking ability with affinity reagents, hence their structure and label location need to be understood. Various labels, including fluorescent substrates, enzymes, redox

molecules, and metal/semiconductor particles, are utilized and these play a key role in signal generation [122]. Other immunosensors do also employ label-free detection where the amount of target antigen is quantified by physical and chemical changes arising from target antigen capture on the sensing surface [123]. Sensitive detection still remains one of the main challenges facing clinical diagnostics in the early stages of disease. Extensive research on the use of other labels, such as CNTs, with better signal detection capabilities is currently ongoing [28-32, 124].

Physical adsorption and chemical modification are the two strategies used in the application of biological species onto various substrates. The physical adsorption (interaction) technique takes advantage of non-covalent interactions such as van der Waals forces, hydrogen bonding, and hydrophobic interactions between the species and the substrates [125]. The adsorbed species are usually randomly oriented, forming a heterogeneous surface, which usually lead to low surface density, reduced activity, may prevent analyte binding, and lead to irreproducibility of results. Adsorption processes do cause some species also to denature and are subsequently inactive upon direct contact with the substrate. Finally, due to the weak attractive forces, attached species may easily be washed away during the numerous washing stages and at the same time while also causing the reversibility of the adsorption process [126].

The covalent attachment protocol relies on the formation of covalent bond between a functional group on the substrate and an exposed group on the species. The substrates may be functionalized with a variety of chemical groups such as NH_2^-, SH^-, $COOH^-$, NHS ester and epoxide groups [127]. Substrates with functional groups such as the amine only adsorb proteins via electrostatic interactions but this can be made to change to the aldehyde surface by exposing it to

glutaraldehyde, a crosslinking agent [128]. The presence of these functional groups on all parts of the antibody as well makes it easier for covalent bonding to be achieved in a random orientation [129].

3.2 Antibodies as Recognition Elements

The extraordinary properties of carbon nanomaterials have led to increasing research into their possible use in various applications. Investigation into their use in the detection of biomolecules and other medical related applications continues to attract a lot more interest [24, 31, 74, 86, 120, 130]. CNFs in this study are used as labels with the detection mechanism mainly based on the antigen-antibody interaction. Since the mid-1990s, antibodies have become an important class of drugs, with more than 28 antibodies approved for therapeutic and diagnostic use in the US and Europe [131]. Initially, the approved antibodies were based on mouse (immunoglobulin G) IgG or chimeric IgG with those based on humanized or fully human IgG sequences entering the market most recently.

Immunoglobulin (Ig), also known as antibodies, are large Y-shaped protein produced by B-cells that are used by the immune system to identify and neutralize foreign objects such as bacteria and viruses. IgG is a major effector molecule and accounts for about 75% of the total Ig in plasma of healthy animals including humans. IgM, IgA, IgD and IgE accounts for the remaining 25% with each of them having a characteristic property and function. Human IgG has a molecular weight of ~150 kDa and is secreted by specialized B lymphocytes known as plasma cells. Antibodies display an extraordinary specificity and binding affinity for antigens in nature. Each antibody has a unique structure recognized by a corresponding antigen in a lock-and-key mechanism. This mechanism

makes them useful as analytical reagents in diagnostics, in environmental and food tests, and in many other uses [132].

IgG has a structure made up of three protein domains as shown in Figure 3.1. Two identical domains make up the arms of the Y-shape structure and are known as “Fab”, fragment, domains in which each arm contains a site that can bind to an antigen, making IgG bivalent molecules. The third domain forms the base of the Y-shape and it is known as “Fc”, fragment that crystallizes. The Fab segments are linked to the Fc by the hinge region, which varies in length and flexibility in the different antibody classes and isotypes [133]. This segment allows lateral and rotational movement of the two antigen binding domains. The two heavy-chain polypeptides in the Y structure are identical of about 50 kDa, and the carboxyl-terminal regions of the two chain fold together to make the Fc domain. The two light chains are also identical with a molecular weight of about 25 kDa. All, polypeptide chains are held together by disulfide bridges and non-covalent bonds [133]. The presence of several different functional groups on all parts of the antibody makes it easier for covalent bonding to be achieved in a random orientation with other substances [129].

Two groups of antibodies, polyclonal and monoclonal, have been classified based on their specificity against a given antigen. Polyclonal antibodies are produced by immunizing animals such as chicken, mouse or rabbit with an antigen and adjuvant preparation. The animal’s immune system is stimulated to produce B cells which secrete antibody that is specific for the antigen. These are extracted from the animal antiserum and purified to the desired level. Polyclonal antibody are prepared usually by mixing antibodies of different specificities making them bind with different strengths to different epitopes on the same antigen. The production process is

relatively inexpensive, universal and large quantities of an antibody can be isolated from a single extraction. They are able to withstand greater variation in temperature and pH and are used to confer passive immunity to certain diseases [134].

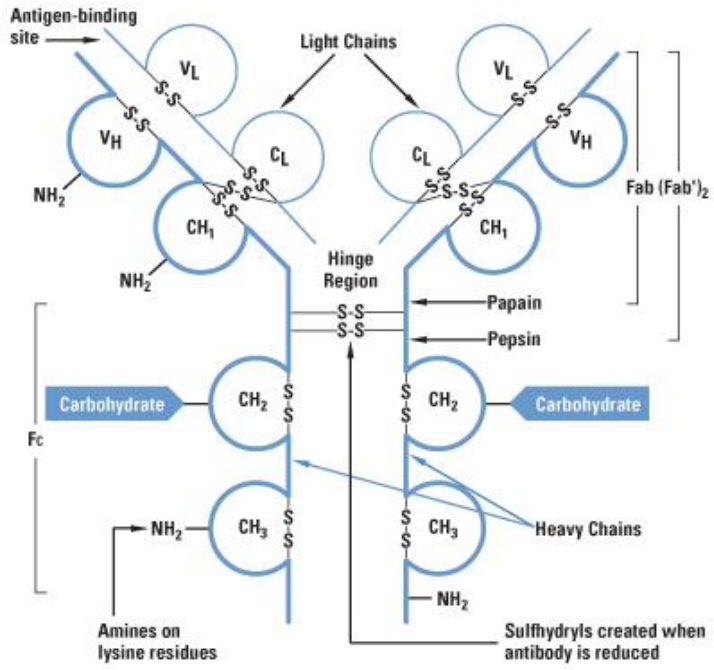

Figure 3.1 Schematic structure of IgG [135].

Monoclonal antibodies are identical because they are produced by specialized cells which have been cloned. Currently, this type of antibodies is only produced in mice. They are obtained by collecting cells from the spleen of a mouse exposed to an antigen. These cells are cultured with cells from a myeloma, a cancer of the plasma cells, to create a hybridoma which will endlessly replicate itself. Tested cells from the hybridoma with the desired antibodies are cloned and used to develop a large store of monoclonal antibodies. These antibodies are pure, making them superior to polyclonal antibodies. A powerful feature of monoclonal antibodies is that the immortal nature of the hybridoma allows for its continual reculturing, thus providing a constant source of

monoclonal antibodies. Monoclonal antibodies bind to only one epitope of a given antigen, being more specific than polyclonal antibodies [136].

3.3 Binding of Antibodies to Carbon Nanofibers

In order to fully recognize the potential of using CNFs as labels in biosensing devices, it is essential to be able to attach biomolecules on to their surfaces. The two most used methods of attachment of biological species to CNFs are the adsorption and covalent attachment methods. Physical adsorption is the simplest method of binding in which biomolecules are mechanically attached on to the surface with the help of van der Waals forces. It involves applying a buffer solution containing the biological molecule on to the CNF. Due to the high aspect ratio and the hydrophobicity nature of the CNF, the applied biological molecule is easily adsorbed to the CNF. Protein surfaces with high degree of hydrophobicity display a stronger affinity to the CNF surface. Suresh et al. [137] have reported a high amount of ricin adsorption on MWCNT compared to graphite paste electrodes using physical adsorption.

Covalent attachment involves the formation of covalent chemical bonds between the biomolecules and the CNFs. The best stability, accessibility and selectivity can be achieved through this type of bonding due to its capability of controlling the location of the biomolecules. Chemical bond formation requires the reaction between functional groups on the surfaces of both the CNFs and the biomolecules. Functionalization of the CNFs is always performed prior to immobilization. The carboxyl acid group is often the best choice because it can undergo a variety of reactions and is easily formed on carbon nanotubes via oxidizing treatments. The control of reactants and/or

reaction conditions may control the locations and density of the carboxyl groups on the nanotubes which can be used for controlled attachment of biomolecules.

The presence of large amounts of both amine and carboxyl acid groups on their surface of proteins can lead to undesirable side reactions of intermolecular conjugation of proteins and CNFs [138]. This intermolecular connection can be avoided by using a two-step process where the carboxyl acid groups on the CNFs are first reacted with the water soluble 1-ethyl-3-(3-dimethylaminopropyl) carbodiimide hydrochloride (EDC). This converts it to active esters surface functionalities and the addition of Nhydroxysulfosuccinimide (sulfo-NHS), another water soluble compound, increases the solubility and stability of the intermediate. The resulting product reacts with the primary amine functional group on the surfaces of the biomolecules to form very strong amide bonds as shown in Figure 3.2 [127]. Thus, the process can guarantee homogenous attachment of proteins onto carbon nanotubes.

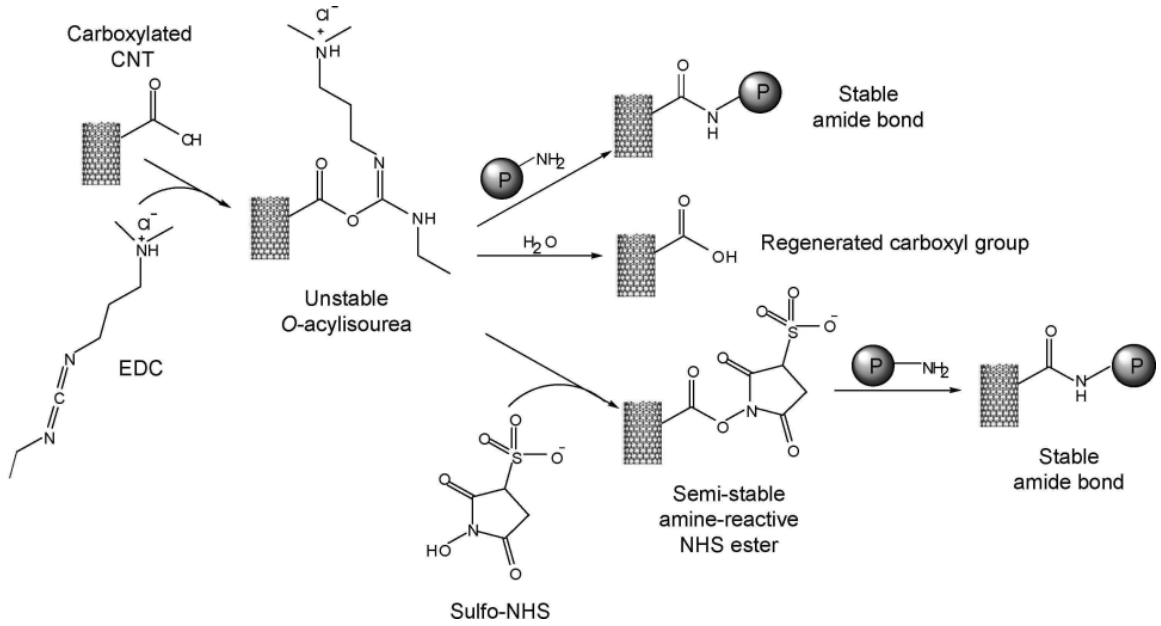

Figure 3.2 Reaction of the carboxylate functional group with a primary amine containing molecule, in the presence of EDC and sulfo-NHS [139].

Abera and Choi have reported the covalent immobilization of the protein molecules on MWCNT via the two-step EDC and sulfo-NHS coupling chemistry [140]. They chemically bonded human IgG to carboxyl acid functionalized MWCNT through the two step coupling chemistry [141]. Their process avoided the intermolecular conjugation of proteins, and guaranteed the uniform attachment of the IgG on the MWCNT. Lerner et al. have also been able to use the two –step approach to treat SWCNT and used the treated CNTs to rapidly detect very low concentrations of Lyme disease antigens [142]. Covalent attachments, however, do provide good stability between the antibodies and the CNFs and also better binding selectivity due to their ability to directly control the location of the antibody [143]. However, their electronic and mechanical properties are negatively affected.

3.4 Blocking as a Means of Preventing Non-Specific Binding

Biological samples are complex in nature containing numerous types of proteins and other molecules. Non-specific binding (NSB) of undesired molecules from a sample is a major obstacle in the development of biosensors. NSB becomes a major issue when incorporating carbon nanomaterials into biosensors. CNFs have a high chemical affinity for biomolecules and end up binding with unwanted molecules as well. As a result, the generated signal are not proportional to the analyte concentration. NSB can therefore increase detection limits and degrade sensitivity. Minimizing protein NSB have been achieved by using specific molecular receptors. The receptors cover the gaps on the CNFs wall left unprotected by the immobilized protein with specific blocking agents [141, 144, 145].

NSB, mainly by the spontaneous adsorption of the protein, to the nanostructure surface is usually attributed to hydrophobic interactions between the protein and the nanotube surface. Various

surfactants including polyvinylpyrrolidone (PVP), Tween 20 and polyethylene glycol (PEG) have been used in reducing this type of NSB. All these three surfactants display protein-resistant properties. Successful modification of the surface of MWCNTs has been achieved with PVP enabling the uniform dispersion of the MWCNTs in aqueous solutions [141]. Hasan et al. have also reported the dramatic improvement in the stability of SWCNT in N-methyl-2-pyrrolidone solution by PVP. In addition, their SWCNTs spontaneously debundled some nanotube aggregates, increasing the isolated SWCNT population without any further ultrasonic treatment [146]. The improvement in the dispersion was attributed to the wrapping and twisting of the PVP polymer around the CNT centers through their flexible or semi-flexible backbones [147].

Tween 20 contains a long alkyl chain of twelve carbons with twenty ethylene glycol and three terminal hydroxyl groups. It has been reported that a Tween 20 coated semiconducting nanotube device did not show any changes in conductance upon exposure to various types and concentrations of protein solutions. The surfactant was found to strongly adsorb onto the CNT surface forming a nearly uniform layer by favorable hydrophobic interactions which imparted a high protein resistance [148]. PEG has also been adsorbed onto the surface of CNTs where it acts as an effective barrier against nonspecific protein adsorption by forming a highly hydrophilic, neutrally charged, sterically hindering layer at the surface.

Shim et al. (40) found the coadsorption of Triton and PEG on SWCNTs to be highly effective in preventing nonspecific adsorption of streptavidin to nanotubes [149]. The adsorption of PEG on the surface of MWCNTs has also been reported to improve the dispersion of MWCNTs in aqueous solutions [141]. In the case of PEG, the adsorption mechanism of NSB onto the surface of the CNT

is less understood. However, a brush-induced steric repulsion preventing contact between proteins and the underlying surface, and the hydration shells around the PEG moieties, has been proposed as the dominant mechanism for their adsorption [150].

3.5 Detection Principle

3.5.1 Biomolecule – NMBs Conjugation

The use of both competitive and sandwich protocol in disease detection has been studied. Sandwich immunoassay format is preferred in RDTs devices because samples do not have to be purified before analysis. The schematic of the fluorescence studies for the sandwich format is shown in Figure 3.3. CNFs are grown on glass microballoons (NMBs) and initially conjugated to the primary antibodies. The NMBs are further immersed in a solution containing the desired antigens. The antigens are interlocked by the primary antibodies after which the NMBs are then immersed in a solution containing secondary antibodies coupled to fluorescein isothiocyanate isomer I (FITC). Further interlocking between the antigens and the secondary antibodies occur leading to the formation of a strong bond between the NMBs and the biomolecules.

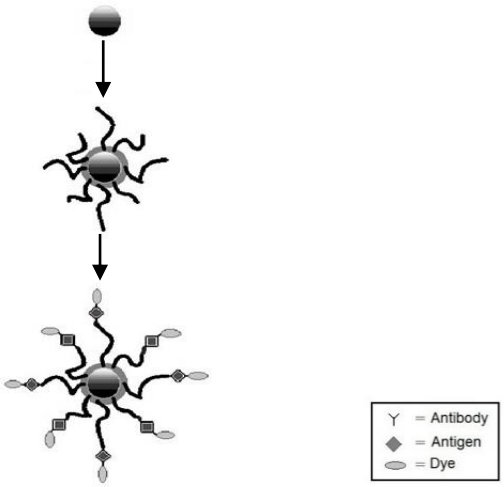

Figure 3.3 Schematic of the processing stages of a sandwich immunoassay protocol.

3.5.2 NMBs Immobilization on Glass Slide

The schematic of the NMBs immobilization process on glass substrate using the sandwich immunoassay protocol is demonstrated in Figure 3.4. The sandwich protocol is used in RDTs due to its high specificity resulting from the use of two antibodies [151]. This sandwich protocol is also suitable for analyzing complex samples and provides high flexibility and sensitivity. All antibodies are designated as Y in Figure 3.4. NMBs {shown in Figure 3.4 (a)} are initially conjugated with secondary antibodies {Figure 3.4 (b)}. Primary antibodies, however, are immobilized on the capture zone of the glass slide as shown in Figure 3.4 (c). Antigens are locked by the immobilized primary antibodies when PBS/antigen suspension was passed through the capture zone {Figure 3.4 (d)}. NMBs in Figure 3.4 (b) were then flowed through the capture zone in Figure 3.4 (d) with captured antigens interlocking with the secondary antibodies on the NMBs as shown in Figure 3.4 (e).

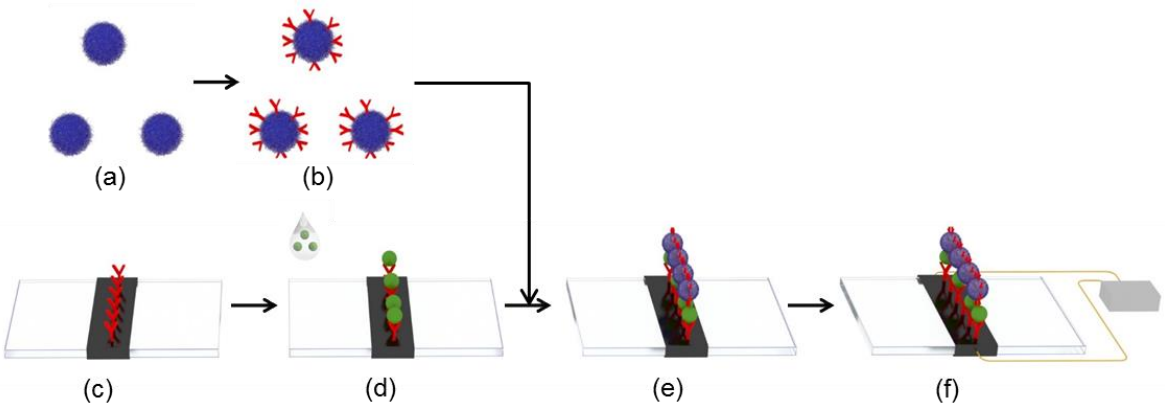

Figure 3.4 Schematic of the capture procedure of NMBs on glass slide. (a) NMBs, (b) secondary anti-IgG conjugated NMBs, (c) primary IgG immobilized on glass slide, (d) anti-IgG locked by immobilized primary IgG, (e) immobilized NMBs on slide, and (f) signal detection setup.

The binding of primary and secondary antibodies with antigens gives a visibly dark signal at the capture zone. Electrical resistivity measurements can be conducted at the capture zone {Figure 3.4

(f)} and the generated electrical signal will vary with the antigen concentration. Increasing the antigen concentrations will result in increasing density of NMBs being immobilized at the capture zone as depicted in Figure 3.5. As a result, the capture zone becomes darker while the resistivity of the zone reduces accordingly.

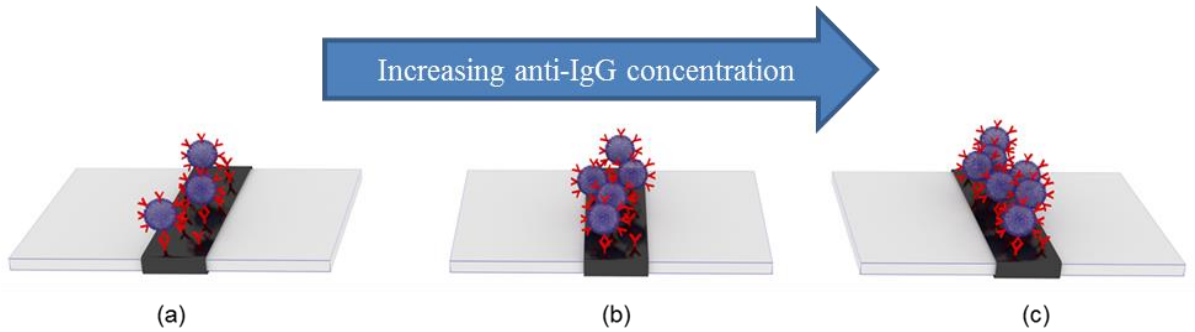

Figure 3.5 Schematic of increasing anti-IgG concentrations on NMBs network at the capture zone.

3.6 Experimental Procedures

Air oxidized NMBs samples were used for all tests. 4-morpholinoeethanesulfonic acid (MES) and polyethylene glycol solution (PEG) (MW 8000) purchased from Sigma-Aldrich, GA, USA and phosphate buffered saline 1X solution (PBS), 1-ethyl-3-(3-dimethylaminopropyl) carbodiimide hydrochloride (EDC) and N-hydroxysulfosuccinimide (Sulfo-NHS) obtained from Thermo Fisher Scientific, IL, USA were used in the immobilization process. Fluorescein isothiocyanate isomer I (FITC), purified immunoglobulin G (IgG, 4.7 mg/ml) from human serum, anti-human IgG (10.2 mg/ml) antibody produced in goat, anti-goat IgG-FITC (15.4 mg/ml) produced in rabbit, and sodium borohydride were obtained from Sigma-Aldrich, MO, USA. All biomolecule contained samples were obtained in a solution of 0.01 M PBS, pH 7.4 and containing 15 mM of sodium azide. A marathon 8K centrifuge was used.

3.6.1 Blocking

PEG was used as the surfactant for non-covalent functionalization of the NMBs in this study. Its use has been reported to prevent NSB [140]. For all blocking procedures, 2 mg of NMBs was dissolved in 5 ml of PEG and 5 ml of PBS. The suspension was mildly swirled for 6 hours. Dilution with PBS, centrifugation at 2000 rpm for 3 minutes and subsequent filtration were performed to obtain the PEG covered NMBs filtrate. Further washing with PBS was done to completely remove all unbound PEG. The PEG coating prevents nonspecific binding (NSB) of unwanted proteins to the NMBs.

3.6.2 Functionalization of NMBs with EDC/Sulfo-NHS

The covalent immobilization of the biomolecules to the carboxyl groups of the NMBs was performed using a modified EDC/Sulfo-NHS chemistry [141]. 5 ml, pH 6.0 solution of 0.2 M EDC and 0.1 M Sulfo-NHS was prepared in MES solution. 2 mg of NMBs were suspended in the prepared solution. The suspension was mildly agitated for 2 hours at room temperature. The carboxylated CNFs on the microballoons reacted with the EDC/Sulfo-NHS solution forming a semi-stable amine-reactive Sulfo-NHS ester. The reaction process is shown in Figure 3.2. The NMBs were recovered by centrifuging at 2000 rpm for 3 minutes followed by filtration. MES was added and the centrifugation and filtration process repeated three times. This completely removes excess EDC/Sulfo-NHS from the NMBs.

3.6.3 Biomolecule – NMBs Conjugation

Various protocols were studied using the fluorescence test. Firstly, the binding of both antigens and antibodies tagged with FITC to NMBs were performed. Secondly, non-covalent

functionalization with PEG was performed before the conjugation of NMBs to antibodies. Thirdly, NSB was studied by conjugating excess anti-IgG to PEG treated NMBs. The filtrate was treated further with anti-IgG-FITC. Competitive assay format was also tested. IgG conjugated to NMBs was treated with anti-IgG-FITC. Finally, sandwich assay format was performed by treating IgG conjugated to NMBs with anti-IgG.

The sandwich conjugation of antigens to the EDC/Sulfo-NHS treated NMBs samples was achieved by adding a solution containing 1 ml of PBS and 100 µl of anti-IgG. The mixture was incubated at room temperature and mildly agitated for 24 hours. Excess reactants were removed by washing with PBS as described earlier. This conjugates primary IgG to the NMBs. PBS (1 ml) and anti-IgG (100 µl of 1 ng/ml) was added to the NMBs that contains immobilized primary IgG and incubated for 24 hours at room temperature to bind the anti-IgG with the IgG. Thorough washing with PBS was performed to remove all unbound anti-IgG. The filtrate was again dissolved in 1 ml PBS and 100 µl of secondary IgG-FITC. The solution was incubated at room temperature and mildly swirled for 24 hours. Unbound IgG-FITC was removed by washing with PBS. The sandwich interlocking of the IgG with anti-IgG was confirmed from fluorescence studies.

The effect of IgG concentration on its conjugation with NMBs was studied using four different IgG concentrations. 1.6 mg of EDC/Sulfo-NHS treated NMBs dissolved in 5 ml of PBS was prepared. To each solution, 20 µl of 0.001 ng/ml, 0.01 ng/ml, 1 ng/ml, and 10 ng/ml of IgG-FITC was added. The solutions were left to stand for 24 hours after which they were centrifuged and filtered. Three separate washings were performed on these samples using PBS and the obtained filtrates used for fluorescence studies. Similar test was carried out using anti-IgG-FITC.

3.6.4 Preparation of Immunosensor

Micro-glass slides used for the fabrication of the immunosensor were obtained from Corning, NY, USA. Tween-20 purchased from Amresco, OH, USA, NaOH and H_2O_2 from Macron Chemicals, PA, USA, and H_2SO_4 from Fisher Scientific, USA were used in the cleaning process. Anhydrous toluene solution from Macron Chemicals, PA, USA, glutaraldehyde obtained from Sigma-Aldrich, MO, USA, and 3-aminopropyltriethoxysilane (APTES) from Alfa Aesar Chemicals, MA, USA were used in the amino functionalization of the glass slides.

Glass preparation and cleanliness are of critical importance in antibody immobilization. Glass slides were cut into rectangular shapes (1 cm × 2.5 cm) and capture zones marked within the mid portion of the slides. The slides were ultrasonicated in deionized water containing 2% Tween-20 by volume for an hour. The washed slides were thoroughly flushed in deionized water and ultrasonicated again for an hour.

Surface modification of the glass with APTES reported by Tang et al. [115] and Tsutsumi et al [116] were modified to suit our process. Slides were initially soaked in 1 M NaOH for 30 mins and then rinsed with deionized water. Washed slides were soaked in piranha solution, 30% H_2O_2 and 70% H_2SO_4, at 80 °C for 2 hours. They were thoroughly washed with deionized water, followed by ethanol and acetone and dried for an hour at 110 °C. The piranha solution roughens the surface of the slides for subsequent immobilization procedures. Modification by immersing slides in 5% APTES in anhydrous toluene solution for 10 mins proceeded immediately resulting in the formation of amino groups on the surface of the glass slides. The slides were thoroughly

rinsed with toluene and acetone before drying at 110 °C for an hour. This removed completely excess APTES and toluene solution.

Activation of the amino functionalized slide surfaces was achieved by immersing the slides in a 3% glutaraldehyde in PBS solution for an hour. The slides were thoroughly rinsed with ethanol and deionized water to completely remove unreacted glutaraldehyde. Nitrogen gas was used to dry the slides. Two treated slides were used for the immobilization processes. A solution made up of 50 µl of 1 mg/ml human IgG and 20 µl of glycerol was prepared and spotted on the capture zones of both slides. The slides were left to incubate for an hour after which they were thoroughly washed with PBS to remove unbound IgG. The slides were incubated in a 2% BSA and 0.05% Tween-20 in PBS solution for an hour. This blocks all sites from nonspecific binding. Slides were thoroughly washed with 0.05% Tween-20 in PBS.

50 µl of 0.01 ng/ml of anti-IgG in PBS was applied onto the capture zone of the first slide. The anti-IgG is expected to be captured by the immobilized human IgG on the slides. The slide was allowed to incubate for 30 seconds after which it was thoroughly rinsed in PBS solution. 1 mg of IgG conjugated NMBs were then suspended in 5 ml PBS solution. Both slides were dipped in the NMBs/PBS solution for 30 seconds. The slides were carefully rinsed with PBS solution. Immobilization of NMBs using anti-IgG concentrations of 0.1, 0.5, 1, 5, 10 and 50 ng/ml were also studied. The presence of visible NMBs at the capture zones of the slides indicates the successful detection of anti-IgG. Electrical resistance measurements were also performed on the slides.

Same treatment procedure was used for the immobilization of the NMBs on the glass slides.

3.6.5 Imaging

Scanning electron microscope (SEM) micrographs were obtained using an FEI Quanta 3D FEG Dual Beam FIB/SEM and its xT Microscope Control Software.

Fluorescence studies was performed on samples using a Leica DM RXA2 fluorescence microscope fitted with a 100× objective lens with a 1.4 N.A. Slidebook version 4.1 was used for image acquisition from a Cooke SensiCam QE camera attached to the microscope. The FITC used in the study incorporate excitation filters in the green (530 to 565 nm) spectral regions allowing the detection of green emissions.

Optical images were obtained from an Axiovert 40 CFL inverted microscope fitted with a 20× objective with a 1.0 N.A. AxioVision 4.6.1.0 was used for image acquisition from an AxioCam MRc camera attached to the microscope.

Percentage area occupied by the NMBs on the glass slides were obtained using ImageJ 1.46r software.

3.6.6 Electrical Measurements

A Lucas Labs Pro-4 four point resistivity system was used in obtaining resistivity measurements. The system is made up of a Keithley 2400, a Pro4 and a notebook with a Pro4 V1.2.4 software installed. The system uses the dual configuration test method of ASTM standard F84-99 to

compensate for errors in probe spacing and errors caused by proximity to the edge of the conducting layer. A V/I measurement was taken and recorded and the subsequent resistivity computed.

3.7 Results and Discussion

3.7.1 EDC/Sulfo-NHS Functionalized NMBs

The use of EDC reagent acts as a crosslinker for the terminal –COOH groups on the ends of the CNFs on the NMBs. This forms an inefficient amine reactive O-acylisourea intermediate that dissociates rapidly regeneration of the carboxyl group. This makes it unstable and short-lived in aqueous solutions. The addition of sulfo-NHS, in a two-step crosslinking procedure, results in the formation of the semi-stable amine-reactive sulfo-NHS ester. This intermediate has sufficient stability and bonds with the amine groups on proteins to form a very strong and stable amide bond [152]. This reaction allows the carboxyl groups on proteins to remain unaltered [153].

The FTIR spectrum from the EDC/Sulfo NHIS treated NMBs show three additional peaks compared to that of the as-fabricated. The spectra are shown in Figure 3.6. There was a weak signal from the O-H stretching at ~2104 cm^{-1}. A broader peak was created at 3100 – 3600 cm^{-1} and this is attributed to vibrations of the hydroxyl (O=C-OH and C-OH) group [104]. The third peak observed between 1470 – 1735 cm^{-1} is associated with the two amide bands of the semi-stable intermediate. The amide band I is located at 1650 cm^{-1} (80% C=O stretch), the amide band II at 1550 cm^{-1} (60% N-H bend and 40% C-N stretch [103, 154]. The appearance of the amide bands I and II indicates the successful functionalization of the carboxylated CNFs with the semi-stable amine-reactive NHS ester.

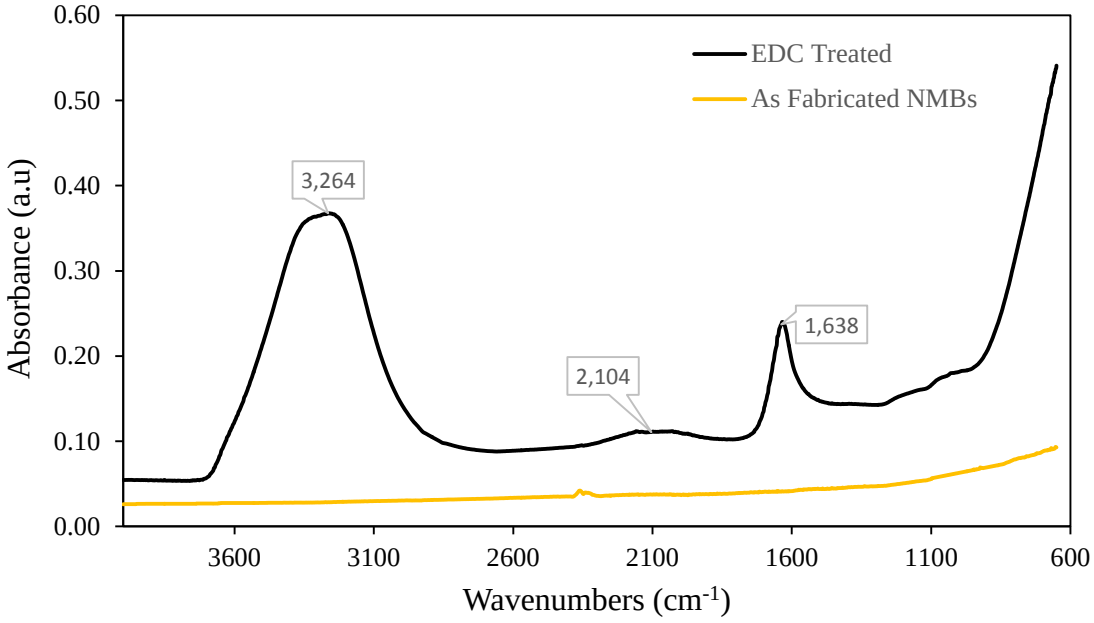

Figure 3.6 FTIR spectra of EDC/Sulfo NHS treated NMBs.

3.7.2 Non-Specific Binding

Proteins are made up of 20 amino acids groups that are either hydrophilic or hydrophobic, acidic or basic in nature. This gives proteins a broader diversity in properties with each protein having different individual functionalities [155]. As a result, proteins are physically and chemically heterogeneous making them possess a three-dimensional structure that is critical to their function. Proteins lose activity when they bound to solid surfaces and have been reported to absorb nonspecifically to each other, to substrate materials, and to other proteins [156]. The variety of polarities, hydrophobicities, charges, sizes, and structures, of proteins poses a challenge when attaching different types of proteins to various substrates. This makes it difficult to achieve both low nonspecific binding and high protein attachment.

The stability of CNFs in buffer solutions and the elimination of NSB are critical prerequisites for their use in biosensing applications. Results from this study show that a coating of PEG on the NMBs reduces the duration for the particles to cluster {Figure 3.7} compared to that for the air oxidized NMBs samples shown in Figure 2.11. The PEG chain completely wraps around the CNF surface leading to its hydrophilic chaining extending into the aqueous phase, imparting water solubility and biocompatibility. The presence of the hollow glass microballoons are responsible for the eventual coalescence of the NMBs with time. Treatment with PEG also led to the saturation of the free binding sites on the CNFs which resulted in the reduction of non-specific binding in our study.

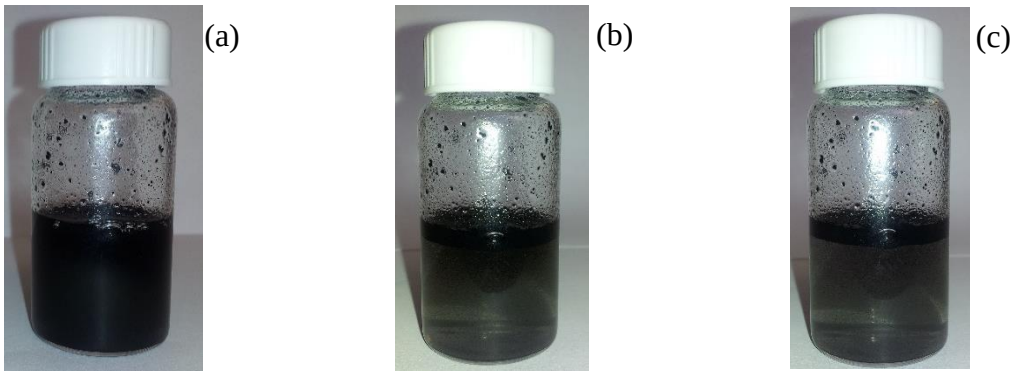

Figure 3.7 Dispersion of NMBs in PEG solution at times (a) just dispersed, (b) 10 minutes, and (c) 20 minutes.

Figure 3.8 shows fluorescence micrographs of anti-IgG-FITC bound to NMBs (a) without PEG and (b) with PEG. The covalent binding between the CNFs and proteins allowed for high stringent binding conditions allowing weakly bound proteins to be washed away during subsequent processes. Observance of fluorescence showed the successful conjugation of both IgG and anti-IgG to the NMBs.

PEG treated NMBs initially bound to excess anti-IgG and further conjugation with anti-IgG-FITC showed no fluorescence { Figure 3.8 (c)}. This shows the achievement of complete passivation in the use of PEG. Treating our NMBs with PEG will eliminate NSB in our conjugation process. The use of lower molecular weight PEG (below 5000 Da) have been reported not to efficiently prevent non-specific protein adsorption, while longer linear PEG (molecular weights greater than 5000 Da) or branched PEG (molecular weight ~ 8000 Da) do prevent most interactions [157].

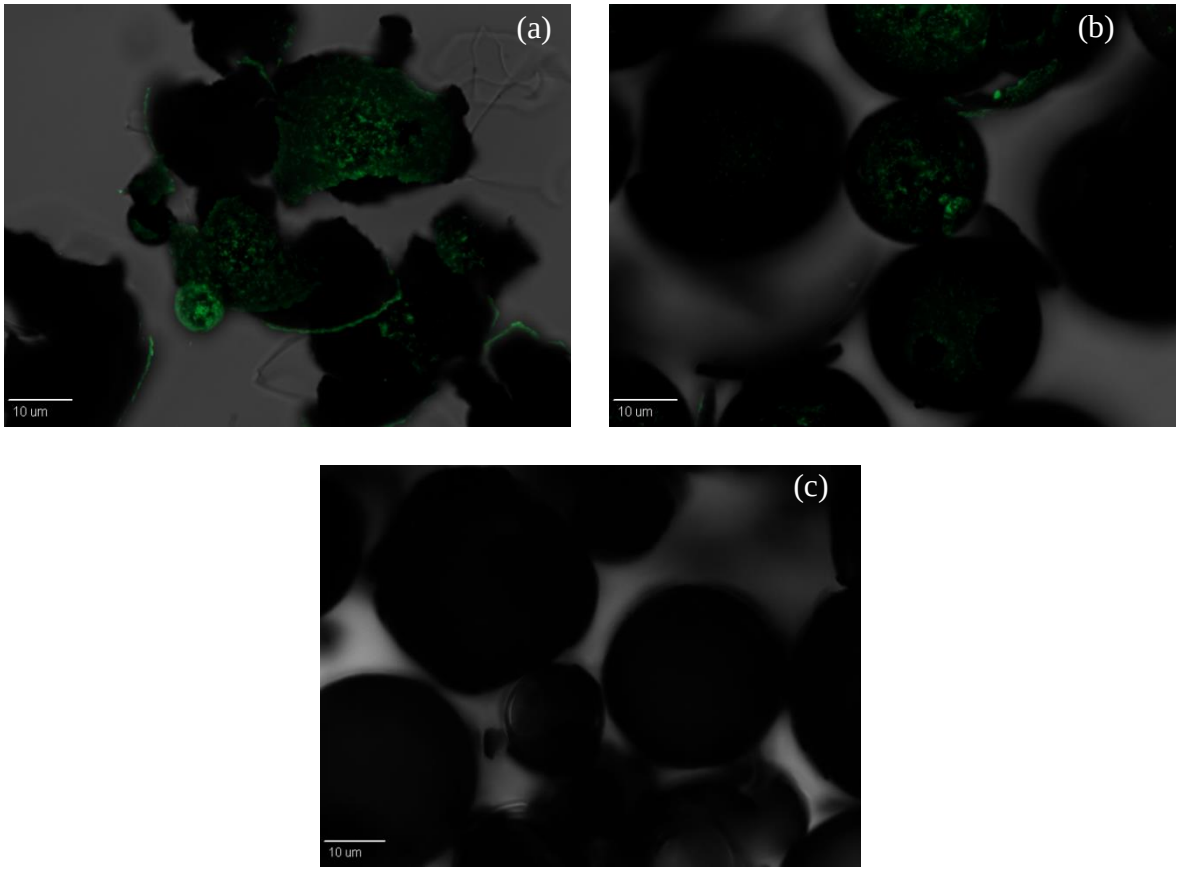

Figure 3.8 Fluorescence micrographs of anti-IgG-FITC bound to NMBs (a) without PEG and (b) with PEG. (c) Fluorescence micrograph of PEG treated NMBs initially conjugated with excess anti-IgG followed by treatment with anti-IgG-FITC.

The FTIR spectra of the NMBs coated PEG is shown in Figure 3.9. The spectra has similar peaks to those observed after EDC/Sulfo-NHS treatment of the NMBs as shown in Figure 3.6. An extra

broader peak is observed from 870 to 1130 cm^{-1} after the PEG treatment. Within this wavelength region, strong C-O and Si-O stretching vibrations have been reported between 1000 to 1200 cm^{-1} [103, 158]. This region comprises of the typical vibration band of –Si-O-Si– at 1110 cm^{-1} and the absorption band at 1115 cm^{-1} attributed to the characteristic –C-O-C– stretching vibration of the repeated -O-CH_2-CH_2- units of the PEG backbone. Characteristic bands of the crystalline phase of PEG have also been reported to be centered at 963 and 843 cm^{-1} [158]. The presence of this peak indicating the functional groups associated with PEG further confirms the successful functionalization of the NMBs with the NMBs.

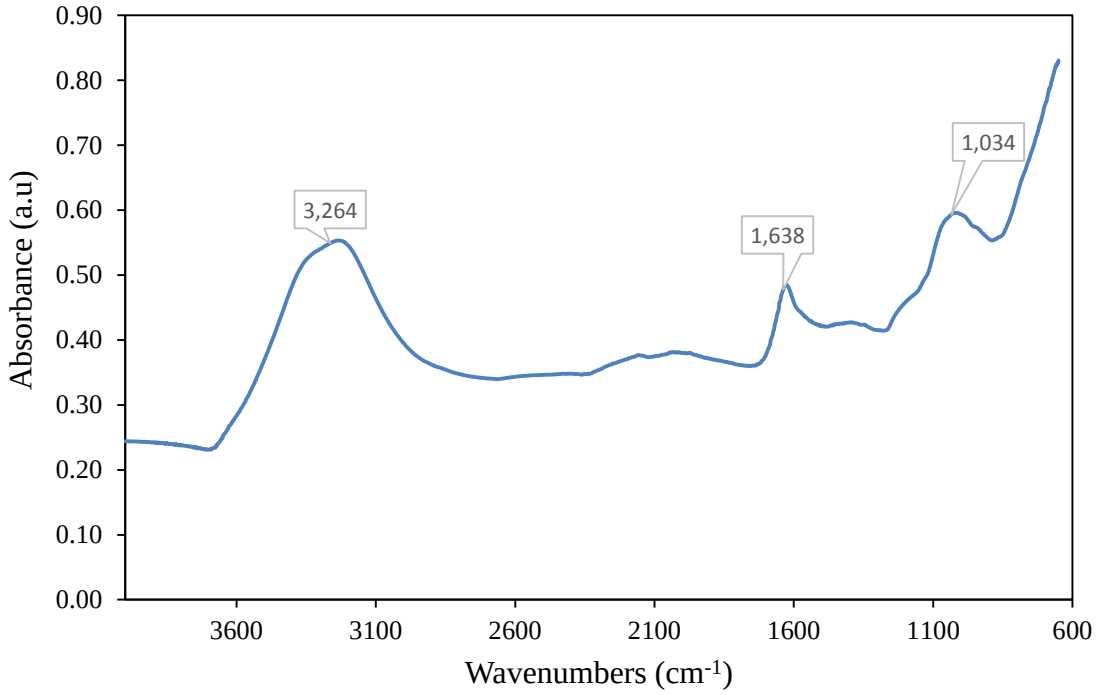

Figure 3.9 FTIR spectra of PEG modified EDC/Sulfo NHS treated NMBs.

3.7.3 Conjugation of Biomolecules to NMBs

Immunoassay is a laboratory technique that uses antibodies to capture molecules of the antigen present in samples. Competitive immunoassay protocol is preferred in the detection of minute

antigen concentrations in solution. Antigens that undergo this protocol usually have smaller sizes. The small molecules have insufficient binding sites and are therefore unable to bind to two separate antibodies. No secondary antibodies are used. Instead, a capture antibody is attached beforehand to the surfaces of the immobilization material. Antigen (analyte) and a separate antigen molecules conjugated to a label compete for the available antibody sites. The material is washed to remove all unbound analyte and conjugate and substrate added. For enzyme labels, bound enzyme present reacts with the substrate yielding color which inversely proportional to the concentration of the analyte in the sample.

Other competitive assay formats have been used where antigen is initially immobilized on solid material and antibody conjugated with label material introduced. For enzymatic labels, substrates are added and captured conjugates yield color which are linearly proportional to the concentration of the captured conjugates.

The use of NMBs as label in a competitive immunoassay protocol was performed. IgG was first immobilized on NMBs. Treatment of the NMBs with varying concentrations of anti-IgG-FITC was studied with the fluorescence microscope. Fluorescence was not observed in the sample treated with 2 pg/ml of anti-IgG-FITC. The interlocking of the IgG with anti-IgG for the remaining three samples was confirmed with fluorescence images being generated for those samples {Figure 3.10}. Similar studies was performed on NMBs conjugated with anti-IgG treated with varying concentration of IgG-FITC. Fluorescence imaging indicated successful interlocking of IgG with anti-IgG for concentrations of 0.01 ng/ml of IgG-FITC and greater as shown in Figure 3.11.

The competitive interlocking of anti-IgG and anti-IgG-FITC with IgG was also studied. Varying the anti-IgG concentrations led to fluorescence being observed on samples treated with 0.01 ng/ml and 1 ng/ml of anti-IgG {shown in Figure 3.12 (a) and (b)}. No fluorescence was observed on the NMBs sample treated with 50 ng/ml of anti-IgG. Low concentrations of the anti-IgG led to fewer interlocking with the primary IgG. Free IgG were therefore still available for binding. Addition of the anti-IgG-FITC resulted in their equivalent number being able to bind with the available free IgG. As the concentration of the anti-IgG increases, the number of free IgG reduces to a point were all free IgG get consumed. Absence of free IgG leads to the washing off of anti-IgG-FITC, which indicates no bonding and hence the absence in the fluorescence imaging for higher concentrations (as shown in Figure 3.12 (c)).

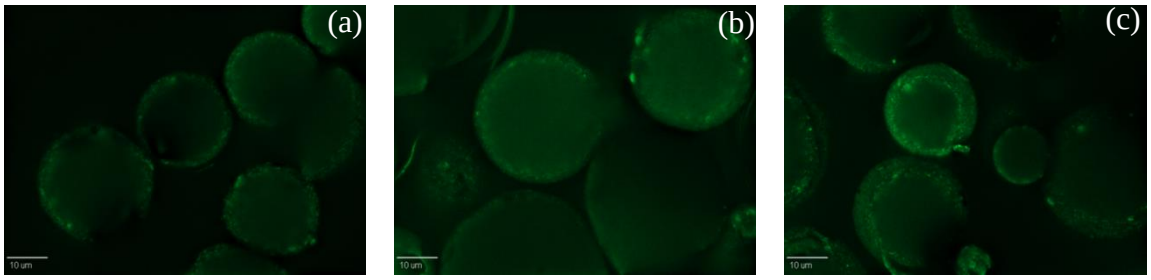

Figure 3.10 Fluorescence micrographs of NMBs conjugated with IgG and further treated with (a) 0.01 ng/ml, (b) 1 ng/ml, and (c) 10 ng/ml of anti-IgG-FITC.

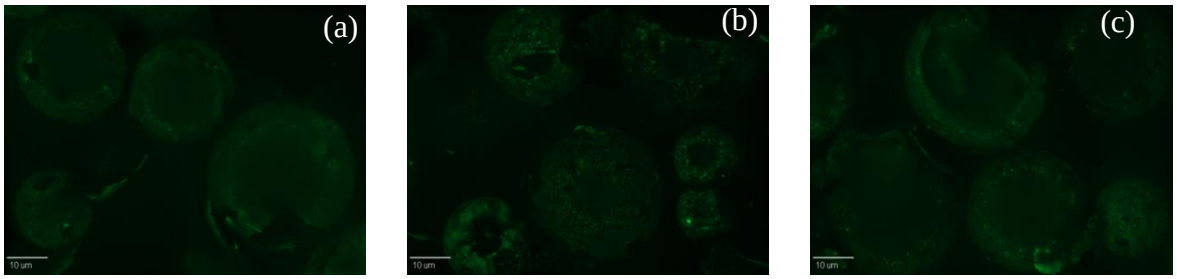

Figure 3.11 Fluorescence micrographs of NMBs conjugated with anti-IgG and further treated with (a) 0.01 ng/ml, (b) 1 ng/ml, and (c) 10 ng/ml of IgG-FITC.

The sandwich protocol is a more efficient method of sample antigen detection. Samples do not have to be purified before analysis while providing relatively higher sensitivity in comparison with the competitive format. This method quantifies antigens between two layers of antibodies (i.e. capture and detection antibody). The antigen must contain at least two antigenic epitope capable of binding to antibody. Either monoclonal or polyclonal antibodies are used. The monoclonal antibodies recognize a single epitope and allows fine detection and quantification of small differences in antigen. Polyclonal, on the other hand, is used as the capture antibody to pull down as much of the antigen as possible.

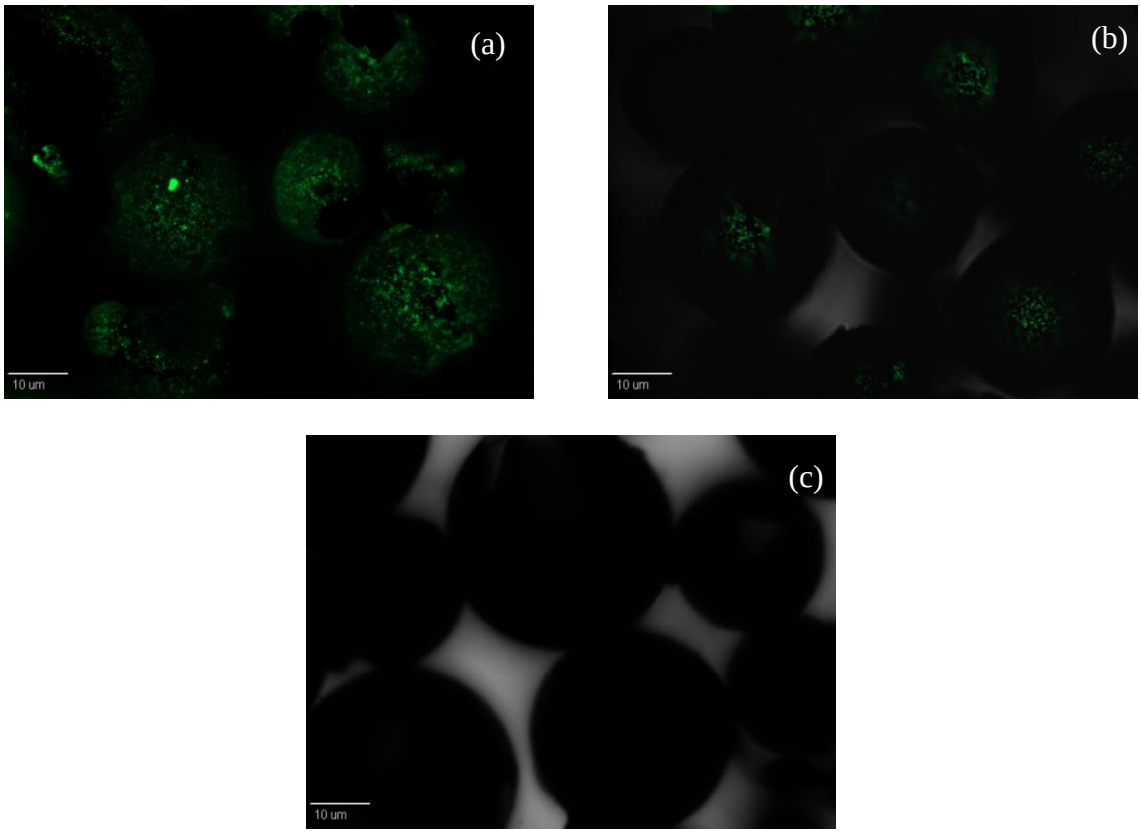

Figure 3.12 Fluorescence micrographs of NMBs conjugated with IgG. The NMBs were then treated with varying anti-IgG concentrations followed by anti-IgG-FITC (a) 0.01 ng/ml, (b) 1 ng/ml, and (c) 50 ng/ml of anti-IgG.

The use of NMBs as label in a sandwich immunoassay protocol was performed. Monoclonal and polyclonal IgG and anti-IgG were used. Successful interlocking of the biomolecules was observed from the fluorescence imaging as shown in Figure 3.13.

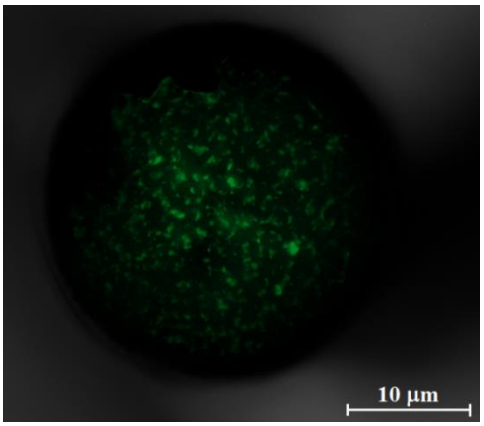

Figure 3.13. Fluorescence micrograph showing sandwich conjugation of IgG/anti-IgG/IgG-FITC on NMBs.

3.7.4 Immunosensor

Various sensing mechanisms are being used in immunosensors. The use of CNTs/CNFs allow sensing to be achieved through optical and/or electrical means with several demonstrations been reported [30-32, 78, 138, 141, 142, 159, 160]. The electrochemical methods are highly attractive due to their simplicity and relative ease of calibration while allowing quantification to be made [159]. Currently, optical sensing is the only method being used in RDTs. This study demonstrates the use of both optical and electrical sensing in RDTS.

Plain glass slides have been reported to exhibit a high degree of protein immobilization [161]. The cleaning and roughening of the glass slides prior to any biological immobilization process is a necessary step in getting rid of all residual organic contaminants which would otherwise interfere

with the subsequent silanization procedure. The use of piranha solution in the cleaning process, in our case, has been reported to introduce hydrophilicity to the surface of the glass slides as well as maximizing the number of carboxyl groups [162].

Biomolecules are very diverse in nature possessing several carboxyl and amine groups. The use of competitive immunoassays techniques in immobilizing biomolecules onto glass substrates poses a great challenge. This technique permits signal amplification, however, recognition antigens that are in low abundance must compete with more abundant proteins for immobilization on the glass substrates. The sandwich format differs by being highly specific while permitting cross reactivity of the antigens with two different antibodies. This makes them ideal formats for detecting disease causing antigens and has therefore been adopted for use in RDTs devices.

Sandwich immobilization of NMBs on glass slide was achieved by using primary IgG, secondary IgG labeled with NMBs and varying concentrations of 0.002, 0.004, 0.006, 0.008, 0.01, 0.1, 0.5, 1, 5, 10 and 50 ng/ml of anti-IgG. Successful detection of anti-IgG on the capture zones of the glass slides were achieved within one minute. This was detected by observing visible network of NMBs on the capture zone {Figure 3.14}. Increasing the anti-IgG concentration increased the density of the NMBs as depicted in the optical micrographs shown in Figure 3.15 for some anti-IgG concentrations. A linear relationship between the number of immobilized NMBs and anti-IgG concentrations was observed as shown in Figure 3.16.

Figure 3.14 NMBs immobilized on glass substrate using the sandwich format for IgG and anti-IgG biomolecules.

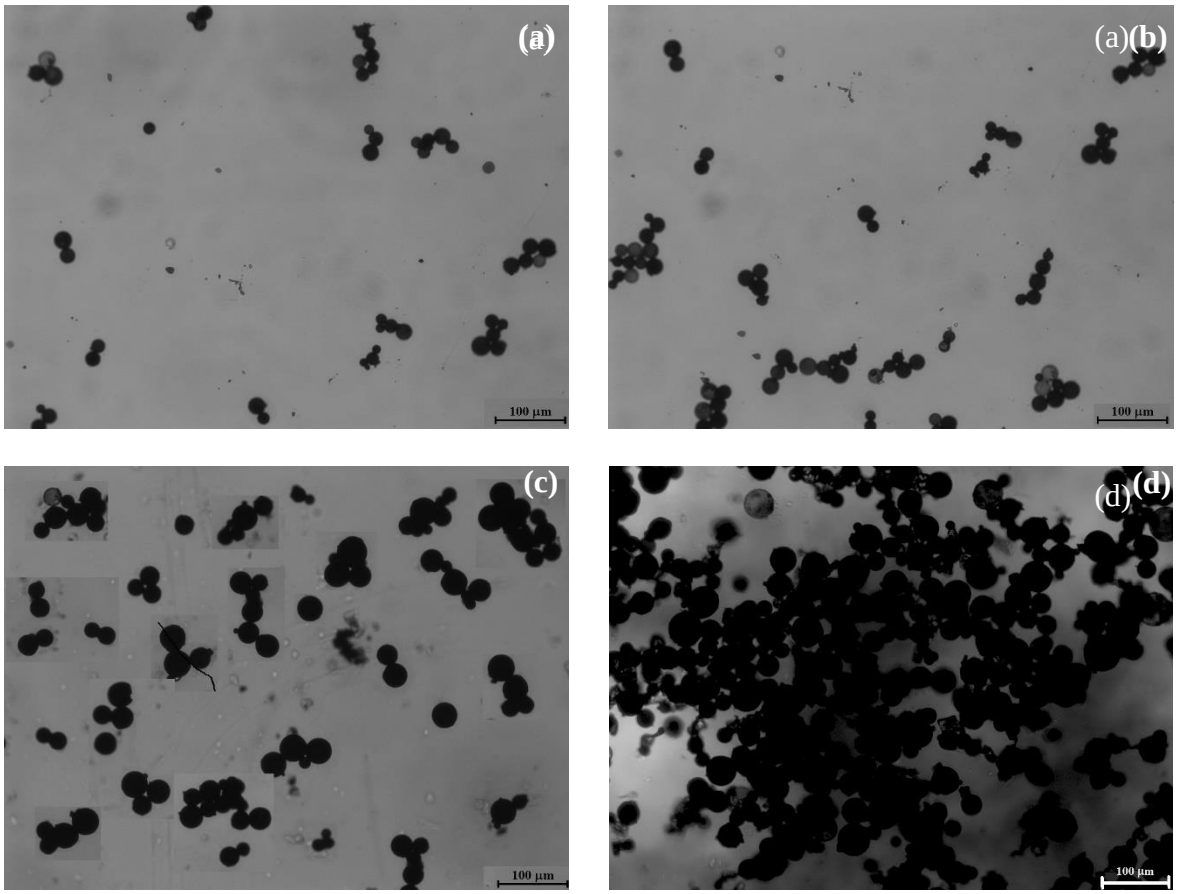

Figure 3.15 Optical micrographs showing NMBs captured on glass slides in a sandwich assay format with (a) 1, (b) 5, (c) 10, and (d) 50 ng/ml of anti-IgG concentrations.

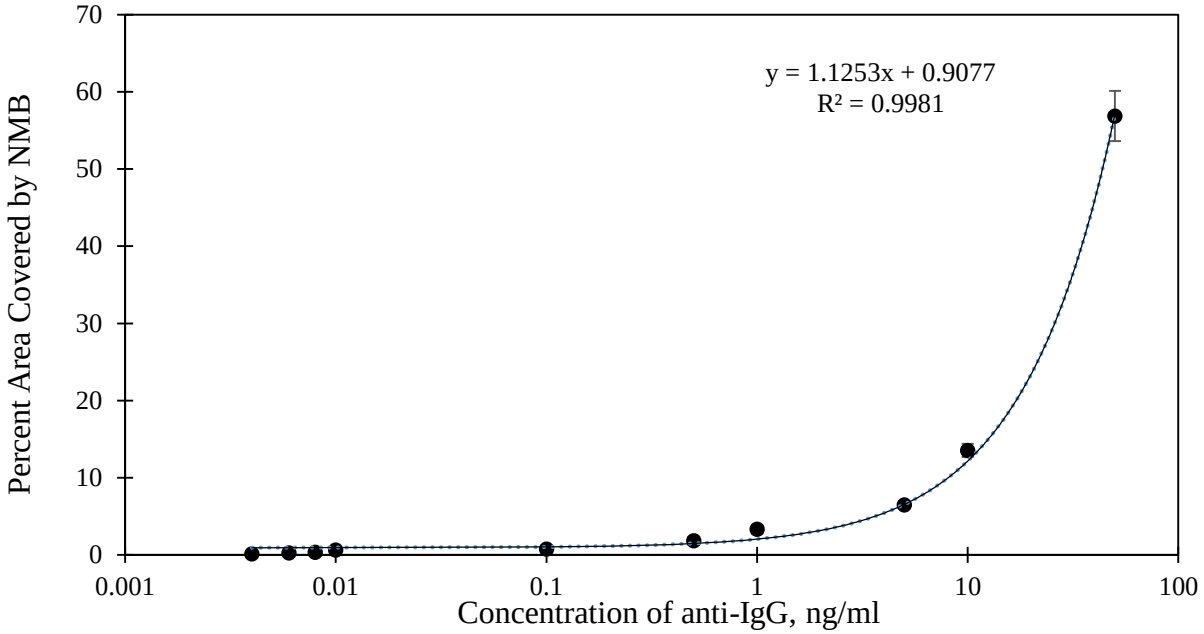

Figure 3.16 Variation of percent area of the capture zone covered with NMBs against anti-IgG concentrations.

The use of the four-point probe method for electrical measurements helps in eliminating the impedance contribution of the wiring and contact resistances. In this study, the use of CNTs as label in the detection of anti-IgG was also performed. That allowed comparison to be made between CNTs and NMBs labels under same conditions. The resistance measurements of immobilized CNTs and NMBs as separate labels at the capture zone was performed. A plot of the resistance measurements obtained against concentration of anti-IgG is shown in Figure 3.17. As can be observed in Figure 3.17, continuous decline in the resistance within the capture zone was observed when the zone was exposed to an increasing anti-IgG concentrations. This pattern was observed for both CNT and NMBs labels and was attributed to the formation of interconnecting conducting pathway due to the capture of more CNTs/CNFs. The network of NMBs formed were more visible even at low anti-IgG concentrations compared to those formed by the CNTs. Electrical resistance of the capture zone also reduced drastically as shown in Figure 3.17.

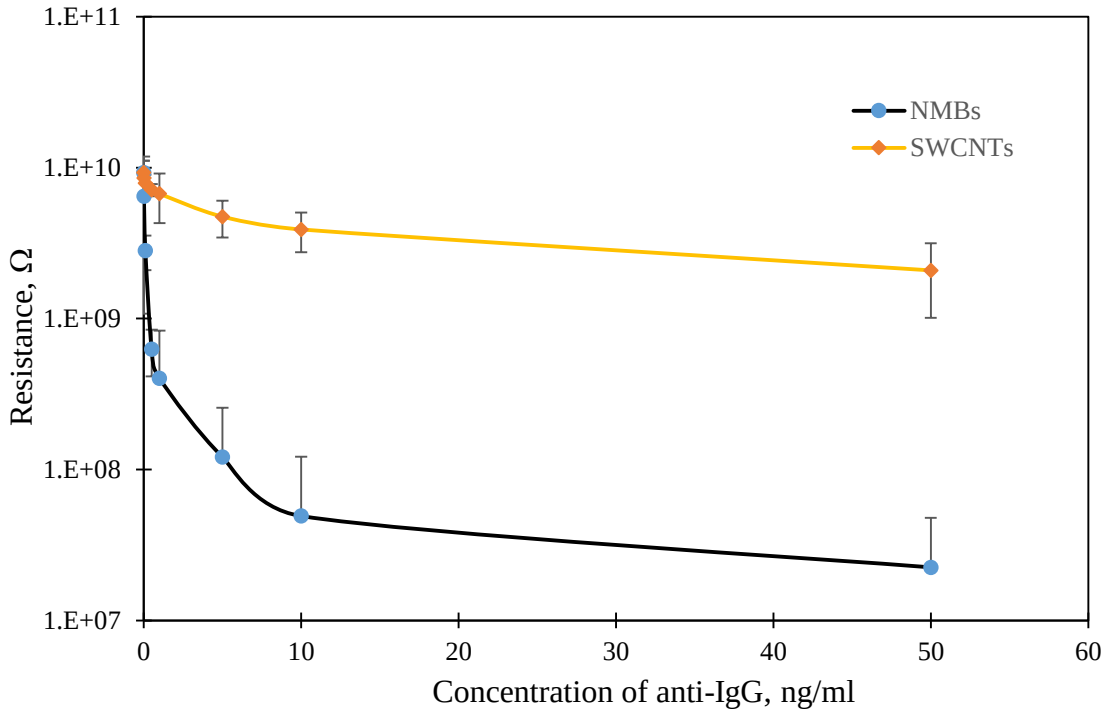

Figure 3.17 Variation of the resistance of the capture zone with anti-IgG concentration for immobilized NMBs and CNTs.

At anti-IgG concentration of 0.002 ng/ml, the resistivity obtained was the same as that of the plain glass. Change in resistivity was first observed when a concentration of 0.004 ng/ml anti-IgG was used for NMBs immobilization. This set a detection limit for our immunosensor. At anti-IgG concentrations above 5 ng/ml resistivity gradually started to reach a plateau. At higher concentrations, (> 10 ng/ml) saturation occurred. Hence, further increases in the number of captured NMBs did not result in any significant changes in the resistivity. These measurements formed the basis for the quantification of our immunosensor.

As shown in Figure 3.17, the change in measured resistivity was amplified when NMBs were used as labels compared to CNTs. This makes NMBs very sensitive to detection of the slightest changes in concentration of antigens. A detection limit of 0.01 ng/ml IgG concentration was obtained for

the CNTs. Below this limit, all measurements were approximately equal to the that of the untreated glass slides. Hence, NMBs have a far lower detection limit compare with that of CNTs. This comparable low detection limit was attributed to the several millions of CNFs on a glass microballoon. This gives NMBs better control, larger surface area and higher probability of capture of biomolecules.

The NSB of NMBs to the capture zone was also tested to check for the possibility of false alarm. No NMBs were observed on the capture zone in the absence of anti-IgG. The resistance measurement of the NSB test was obtained to be 8.74×10^{10} Ω-cm which is comparable to the 9.30×10^{10} Ω-cm obtained for the glass slide. Resistance changes can therefore be attributed to the change in concentration of anti-IgG. The successful elimination of NSB reduces the generation of false positives and hence minimization of false alarms of the sensor.

3.8 Summary

The successful immobilization of biomolecules on NMBs fabricated in the laboratory was demonstrated in this study. This was achieved through the use of competitive and sandwich immunoassay protocols and the results confirmed through fluorescence studies. The fluorescence results paved the way for studies into the potential use of NMBs as ultra-low detection labels in RDTs. Using glass slide as a substrate and antibody conjugated NMBs as labels, various concentrations of anti-IgG have been immobilized. The density of the immobilized NMBs network formed varies with the concentration of anti-IgG detected. This network generates both colorimetric and conductimetric signaling which relates to the amount of anti-IgG detected. Both signals generated are inexpensive, simple, and dependable.

Substituting NMBs with CNTs for the anti-IgG detection generated weaker signals. This can be attributed to signals being generated from fewer CNTs compared to the several millions of CNFs found on each glass microballoons. Therefore NMBs provide better ease of handling while offering a higher sensitivity of detection compared to the CNTs.

NMBs can therefore be utilized to achieve ultra-low detection limit in RDTs. Integration of millions of carbon nanofibers arranged on such micro-particles provided a higher probability of detecting minute concentrations of antigen in analyte. The NMBs also offered significantly higher level of sensitivity, as well as, simple and fast visual and/or electrical identification as labels in RDTs. It also has an added advantaged of eliminating false-alarms while reducing the incubation period required for detection.

CHAPTER 4
ULTRA-LOW IMMUNOASSAY DETECTION OF MALARIA AND PREGNANCY IN HUMANS

4.1 Introduction

Rapid immunoassay test configuration use antibodies (Ab) to react with antigens and have been developed using a monoclonal – polyclonal (MoAb-PoAb) sandwich assay format. This format is well suited for use in malaria and pregnancy test kits. The primary MoAb is bound to solid substrates. Positive samples are introduced and react with immobilized MoAb. The flow rate of the excess fluids are controlled and channeled to a non-reactive part of the substrate. Secondary PoAb and labeling conjugate are then reacted and results obtained a few minutes thereafter [163]. This flow through mode of testing utilizes a disposable plastic cassette or strip. This type of test requires little sample processing, is cheaper, and generates a yes/no answer without the use of an instrument. However, they are not as sensitive as chemical chromatographic methods [164].

Sensitivity is a measure of the reproducibility of sample data from various measurements. This is affected by both the uniformity of the test and the analyst's technique. It is measured by conducting several analyses of a sample or a control sample and calculating the relative standard deviation [165]. As with all bioassays, the inherent variability between replicate measurements makes it necessary to validate most immunoassays tests against their gold-standards. This validation eliminates the possibility of presenting both false positive and false negative results [164]. Control tests are incorporated to validate the accuracy of the immunoassay tests. Malaria and pregnancy test kits integrate both the test and control runs in the same setup.

Malaria is the most significant tropical disease known to man. It is estimated that 3.3 billion people (living in 107 countries), almost half of the world's population (as shown in Figure 4.1), live in areas where malaria transmission occurs [166]. Approximately 300 to 500 million cases of clinical malaria occur each year with about 90% of all malaria deaths occurring in sub-Saharan Africa [166, 167]. Malaria is spreading as a result of environmental degradation, civil disturbances, misplaced populations, increasing travel and drug resistance [168]. Children have been the most affected due to their vulnerability to infection. One in every 5 infant deaths is attributed to malaria [169]. The disease is preventable and curable. As such, various organizations continue to invest resources in its management.

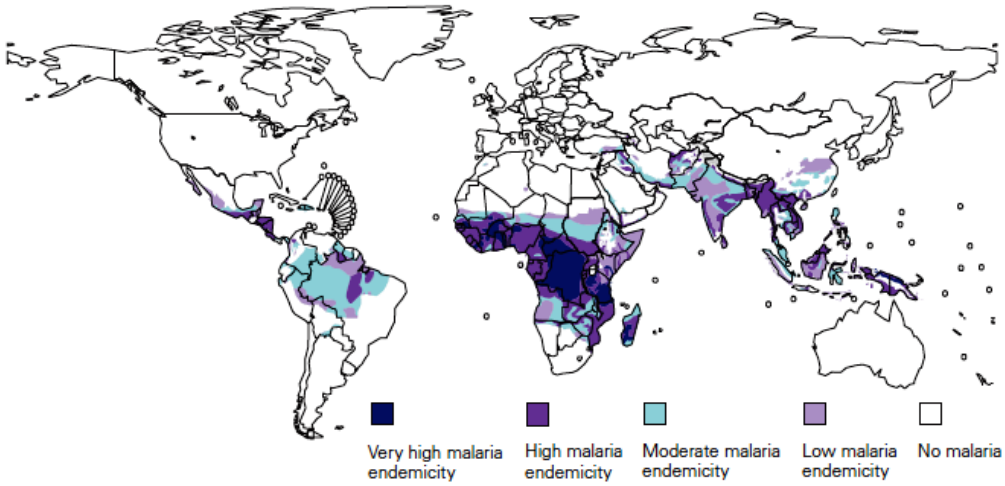

Figure 4.1 Global distribution of malaria endemicity [170].

Rapid and accurate malaria diagnosis is therefore essential to the management of the infection in the affected communities [169]. The gold-standard for malaria treatment still remains the microscopic examination of blood; thick and thin stains [171]. Research into antigen detection and molecular detection assays are also on the rise. These methods are used as alternatives to the traditional microscopy method. Subjective diagnosis have also been used in low resource settings

for early treatment of malaria. However, malaria rapid diagnostic test kits (MRDTs) have a much greater potential of reaching most affected population due to their low cost, simplicity, rapid, ultra sensitivity and selectivity of identifying *Plasmodium* species.

Pregnancy on another hand is a clinical condition that involves the fertilization and development of an embryo in a woman's uterus [172]. On average, a pregnancy with a single embryo lasts 40 weeks from the first day of the last menstrual period. Most women are anxious to know the start of their pregnancy, whereas it may provide a health risk for others and as such needs an early diagnosis. Pregnancy diagnosis requires a multifaceted approach using three tools. These approaches involve the history and physical examination, ultrasonography, and laboratory evaluation [173]. The woman's menstrual pattern gives healthcare providers an idea of an early pregnancy. Physical examination are then carried out to determine enlarged uterus, breast changes, and softening and enlargement of the cervix to confirm or dispel the pregnancy diagnosis [174]. Ultrasound-based diagnostic imaging technique is also used to confirm a normal pregnancy and the age of a baby. It is usually done 12 weeks after the first day of the last menstrual period.

Laboratory diagnostic involves the measuring and monitoring of the quantity of human chorionic gonadotropin (hCG). The hCG levels increases significantly after fertilization. The four assays used for hCG determination are the radioimmunoassay, immunoaradiometric assay, enzyme-linked immunosorbent assay and fluoroimmunoassay. These assays are highly specific for hCG with antibodies directed against 2 or more isotopes on the intact hCG molecule. Blood and urine samples are used for analyses. Urine devices are formulated to detect hyperglycosylated hCG, the key molecule in early pregnancy [173].

4.2 Malaria

Malaria infection is caused by the *Plasmodium* parasites. *Plasmodium* is a one-cell organism which spread in humans through infected mosquito bites and during blood transfusion. The female Anopheles mosquito bite is responsible for the spread. The bite is necessary to support the nurturing of her eggs [166]. More than 100 different species of *Plasmodium* exist and have been reported to produce malaria in many types of animals and birds, as well as in humans [167]. Four of the *Plasmodium* species that commonly affect humans are the *P. falciparium*, *P. vivax*, *P. ovale*, and *P. malariae* [169].

The bite of the female Anopheles mosquitoes leads to the feeding of malaria causing parasite (called sporozoites) into the blood stream of humans. The four different species of *Plasmodium* have similar life cycle with minor variation. The general life cycle is shown in Figure 4.2. The sporozoites travel to the liver and invade the liver cells. They grow, divide, and produce tens of thousands of a different form of sporozoites called the merozoites in each liver. Majority of the merozoites then exit the liver cells into the bloodstream infecting the red blood cells (RBCs) in the process. The minority of merozoites remain dormant in the liver causing relapses weeks or month later. The merozoites multiply inside the RBCs, break open within 1 – 3 days, and infect more RBCs. This results in several thousands of parasite-infected RBCs in the bloodstream [167].

Malaria symptoms occur a few days after an infective mosquito bite. This period, known as incubation period, varies between 7 to 30 days. The variation of the incubation periods depends on the type of *Plasmodium* parasite. *P. falciparum* symptoms occurs early with the less deadly *P.*

malariae symptoms occurring after longer incubation periods [169]. Symptoms occur in cycles of 48 to 72 hours coinciding with the bursting of infected RBCs [167].

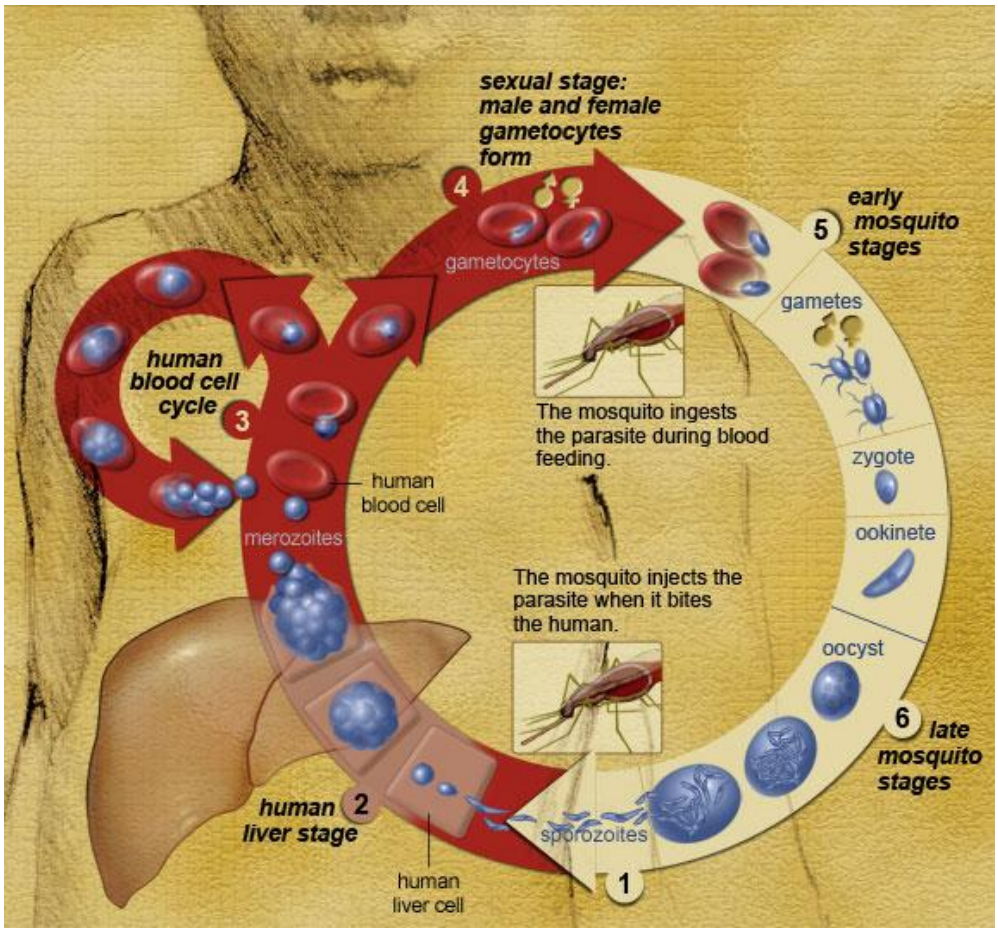

Figure 4.2 The life cycle of the malaria parasite [167].

The initial malaria attack lasts for 6 – 10 hours. It consists of a cold stage (sensation of cold and shivering), a hot stage (fever, headaches, vomiting, and seizures in young children), and a sweating stage (sweats, return to normal temperature, and tiredness) [169]. In malaria prone regions, residents often recognize these initial signs. They begin treatment with on-the-shelf medications without seeking diagnostic confirmation of the type of *Plasmodium* species.

The type of *Plasmodium* species infection determines the extent of the malaria attack. Symptoms from *P. malariae* are hardly observed due to the low level of parasitemia produced. *P. vivax* and *P. ovale* infections only show symptoms between attacks. The paroxysms subside within a few weeks even without treatment. *P. vivax* and *P. ovale* are able to infect only young RBCs. Hence the number of parasites in the blood does not reach the same high levels as observed for the *P. falciparum* infection. The body is able to develop antibodies over time subsiding the infection even without treatment. *P. falciparum* infected individuals may feel miserable even between attacks and may lead to death if treatment is delayed. The severity of this attack is due to the ability of the *P. falciparum* parasites to infect RBCs in all stages of their development. Very high levels of parasitemia are present in the blood resulting in severe symptoms only after a few days [169].

P. falciparum parasites are mainly found in tropical parts of Africa and are responsible for the severe complications reported. Serious complications observed include cerebral malaria (abnormal behavior, impairment of consciousness, seizures, coma, or neurologic abnormalities), severe anemia due to hemolysis (destruction of RBCs), hemoglobinuria (hemoglobin in the urine), rupture of the spleen, acute respiratory distress syndrome (ARDS) (an inflammatory reaction in the lungs that inhibits oxygen exchange), abnormalities in blood coagulation, low blood pressure caused by cardiovascular collapse, acute kidney failure, and hypoglycemia (low blood glucose) [169, 170].

4.3 Diagnosis of Malaria

Rapid and precise diagnosis of malaria is integral to the appropriate treatment of affected individuals. This also prevents the further spread of infection in the community. In low resource settings, clinical features of malaria are not specific and presumptive diagnosis is generally used.

Healthcare professions use symptoms and physical findings at examination to predict the presence of the disease. This presumptive diagnosis is not reliable. The designs of more reliable clinical algorithms have helped to accurately diagnose malaria. The designs include microscopy, immunology, molecular, and serology [169].

4.3.1 Microscopy

Microscopy is an established and relatively simple technique that is familiar to most laboratory technicians. This approach remains the gold standard for laboratory confirmation of malaria because of its sensitivity, specificity, and ability to quantify the parasitemia level [175-177]. However, it is labor intensive and time consuming [178]. The limitation of this method arises when mixed infections are present at low parasitemia levels. Highly trained personnel are also required in the use of the microscopes as well as in sample preparation. There are two main types of sample preparation for the microscopy test: thin and thick films malaria smear methods. Sensitivity and selectivity are adequately accommodated using the thick and thin films malaria smears, respectively.

In thick film smear, the RBCs are approximately 6 – 20 layers thick resulting in a larger volume of blood being used and ability to detect very low parasitemia. As few as 5 parasites/µl of blood can be determined [179]. Thick film is used to determine the presence of parasites. In examining the thick blood films, the RBCs are lysed (destroyed) making it difficult to differentiate between the various *Plasmodium species*. In thin films, the RBCs are fixed so the morphology of the parasitized cells is easily seen. Species identification is clearly made based on the size and shape

of the various stages of growth of the parasites. The presence of stippling (bright red dots) and fimbriation (ragged ends) are also clearly seen [180].

4.3.2 Molecular

The use of molecular methods has been reported to yield higher sensitivity, detect mixed infections, and to accurately identify *Plasmodium* species [177, 178, 181]. However, all the methods that rely on this method are relatively expensive and require a specialized laboratory setup. The results are also not available quickly enough to be of value in establishing the diagnosis of a malaria infection. Therefore, molecular tests are used as complementary tools for the diagnosis of malaria in some reference laboratories to accurately diagnosis low parasitemia infected patients [177]. While this methodology is unlikely to be useful at the peripheral level of healthcare, it may have a place as a research tool to monitor malaria control programs.

The molecular diagnostic tests include polymerase chain reaction (PCR), loop-mediated isothermal amplification (LAMP), mass spectrometry (MS), and flow cytometric (FCM) assay techniques. PCR-based techniques are used extensively to confirm malaria infection, follow-up therapeutic response, and identify drug resistance [182]. High cost has limited its use in low-resource settings. The LAMP method is relatively easier, sensitive, quick, and cheaper than PCR. However, its reagents require cold storage, and further trails are needed to validate its feasibility and clinical utility [183]. MS has been reported to be rapid, high throughput, and can be automated [184]. FCM has the advantage of diagnosing clinically unsuspected malaria. The disadvantages of the MS and FCM techniques are their costly diagnostic equipment, labor intensive, and the need for trained technicians [184]

4.3.3 Serology

The diagnosis of malaria using the serological methods is mostly based on the detection of antibodies against the macrogametocytes and microgametocytes malaria parasites. The main use of this method is for retrospective studies, particularly for epidemiological purposes and for tracing asymptomatic infections in blood donors. The various serological tests include immunofluorescence antibody test (IFA), enzyme-linked immunosorbent assay (ELISA), radioimmunoassays, latex agglutination, indirect haemagglutination, and solid-phase dipstick and membrane dot-blot.

The IFA test is the main method for routine serology testing. It is relatively easy to setup and highly sensitive and specific [185]. This serological method is not widely used for malaria diagnosis because it is time consuming and cannot be automated limiting the number of sera that can be studied daily. IFA requires the use of a fluorescence microscope and trained technicians. Readings obtained from testing are subjective based on the level of training of the technician. Finally, the method is highly labor-intensive limiting its application to specialized centers [184].

4.3.4 Antigen Detection

Malaria antigen detection tests assist in the diagnosis of infection by providing evidence of the presence of malaria parasites in human blood. They are commercially available and allow the rapid diagnosis by individuals who are not otherwise skilled in traditional laboratory techniques. Antigen-based malaria rapid diagnostic tests (MRDTs) are also cost effective, accurate and find widespread use in low resource settings where traditional equipment are not available [184]. Currently, over 100 commercially available MRDTS have been approved by the World Health

Organization [186]. These MRDTs are based on a lateral flow 'immunochromatographic' (dipstick), cassette, or card formats [169]. Although MRDTs are supposed to be rapid, it takes at least 15 minutes for results to be displayed. BinaxNow has been reported as the fastest MRDT on the market with an incubation period of 15 minutes [187, 188].

MRDTs are all based on the same principle: capturing of *P. falciparum* on a first band, all other *Plasmodium* species on a second band, and a control on a third band of a nitrocellulose strip. A lyzing agent is used for rapturing the RBCs. This makes available all merozoites available for conjugation with immobilized antibodies.

MRDT performance for diagnosis has been reported to be excellent in several publications [182, 184, 186, 189-193]. However, several issues remain to be addressed. These include improving their accuracy; lowering their cost; improving their detection time and ensuring their adequate performance under adverse field conditions. The MRDTs may also not able to detect some infections with lower numbers of malaria parasites circulating in the patient's bloodstream. MRDTs are also not able to differentiate between *P. vivax, P. malariae* and *P. ovale*. The use of dyes as labels have also been reported to negatively impact on MRDTs [194]. These dyes readily or continually undergoes chemical, physical, or biological breakdown and may not be available for the reaction when needed. Researches into the use of other diagnostic methods are ongoing to aid in the best management of the disease.

4.4 Pregnancy

Pregnancy is a clinical condition that occurs between the conception and birth of a baby. Human chorionic gonadotropin (hCG) is a critical hormone whose presence in humans can be used as a marker for various aspects of human health. It is used as a biomarker for pregnancy detection, gestational trophoblastic disease (GTD), germ cell tumors and some non-trophoblastic gynecological cancers and common epithelial tumors [195-197]. Detection and quantification of this hormone are essential during pregnancy as it gives valuable information concerning the progress of a pregnancy.

hCG is a 37 kDa glycoprotein hormone composed of two dissimilar subunits joined non-covalently [198]. These subunits are termed alpha and beta. Common hCG-related molecules in serum samples include the regular hCG, hyperglycosylated hCG, nickel hCG, hCG missing the beta-subunit C-terminal extension, free alpha-subunit, free beta-subunit (hCGβ), free beta-subunit missing the C-terminal extension, hyperglycosylated free beta-subunit (hCGβcf) and nickel free beta-subunit [196]. The same molecules and the beta-core fragment are present in urine samples.

During the early stage of conception, hCG hormone has the crucial role of maintaining the essential steroid production ensuring that the pregnancy progresses unabated. An increase in the concentration of hCG and its subunits becomes pronounced when the fertilized egg attaches to the wall of the uterus. This occurrence takes a minimum of six days after fertilization [199]. These initial concentrations are difficult to detect. However, the amount of this hormone doubles every two or three days increasing the probability of its detection with increasing length of the pregnancy.

Hence, most commercially available RDTs are able to correctly detect its presence only after high concentrations of the hormone are produced.

4.5 Diagnosis of Pregnancy

hCG is found in both serum and urine of all humans with only a slight concentrations difference observed with age and sex. The upper reference limit in serum for men has been reported as 2.1 pmol/l and in non-pregnant women as 8.6 pmol/l [200]. The upper limit of hCG in the urine of men below 50 years is 2.9 pmol/l and 8.4 pmol/l for those older than 50 years. The corresponding values for non-pregnant women are 8.8 and 11.5 pmol/l, respectively.

The increase in hCG and its subunits is nearly exponential during the first 5 weeks after ovulation [201]. hCGβcf can be detected in serum during pregnancy in quantities corresponding to 0.03% of the hCG content. The concentration in urine is about 4000 times more than found in serum [202]. hCGβcf is the major form of hCG immunoreactivity in pregnancy urine except during the first month of pregnancy, when hCG predominates [203]. The concentrations of hCG immunoreactivity in paired serum and urine samples are similar and correlate strongly [204]. Total hCG immunoreactivity is higher in urine and apparently attributable to hCGβcf [200].

Specific measurement of hCG and its directives in serum became possible with the development of ultrasensitive immunometric assays that were based on monoclonal antibodies [205]. RDTs are also designed to detect hCG in urine.

4.6 Experimental Procedures

4.6.1 Reagents and Materials

As-grown and functionalized NMBs were used for the study. *Plasmodium falciparum* histidine rich protein-2 (*Pf*HRP-2) antigen, *Plasmodium vivax* merozoites surface protein-1 (*Pv*MSP-1) antigen, mouse monoclonal to *Pv*MSP1 antibody (Ms-MAbv), rabbit polyclonal to *Pv*MSP1 antibody (Rb-PAbv), mouse monoclonal to *Pf*HRP-2 antibody (Ms-MAbf), and rabbit polyclonal to *Pf*HRP-2 antibody (Rb-PAbf) were obtained from MyBioSource Inc., USA. hCG, mouse monoclonal to hCG (Ms-hCG), and rabbit polyclonal to hCG (Rb-hCG) were also purchased from Abcam, USA. All biological samples were obtained in a PBS solution, pH 7.4, and containing 0.1% of sodium azide.

4.6.2 NMB-*Plasmodium* Species Conjugation

CNFs have very high chemical affinity for biospecies [206]. A two-step reaction approach described in Section 3.6.3 was used in preparing the NMBs for covalent conjugation with Rb-PAbf, Rb-PAbv, and Rb-hCG. This reaction forms an ester intermediate on the NMBs that aids the amidation reaction. The amidation reaction involves the reaction of the intermediate with the primary amine group on the surfaces of Rb-PAbf. Same procedure was followed for the covalent conjugation of NMBs with Rb-PAbv, and Rb-hCG. Very strong amide bonds were formed in each of the processes [127]. PEG was then applied forming a polyethylene oxide coating on NMBs. This coating prevents NSB of unwanted proteins to the NMBs.

4.6.3 Preparation of Glass Substrate

Single and double capture zones marked on several slides were used for the study. Slides were thoroughly cleaned, modified, and activated with amino functional groups as described previously. All capture zones were treated to prevent NSB with unwanted proteins. Details of immobilization Ms-MAbf, Ms-MAbv, and Ms-hCG on glass slides to capture *Pf*HRP-2, *Pv*MSP-1, and hCG respectively based on sandwich immunoassay protocol is described in Section 3.6.4.

First, Ms-MAbf was immobilized on glass slides with single capture zone marks. The capture zone was used for sandwich immunoassay investigation of *Pf*HRP-2 with concentrations in the linear range of 0.01 ng/ml and 10 ng/ml. Similarly, Ms-hCG immobilized on other single marked capture zone slides was used to investigate the capture of hCG in the linear range of 0.025 ng/ml and 10 ng/ml. The visual and electrical detection limits of the *Pf*HRP-2 and hCG were determined within their specific ranges.

Second, for the glass slides with double capture zones, Ms-MAbf were immobilized on the first capture zone and Ms-MAbv on the second capture zone. Same immunoassay procedure was then executed. For performance evaluation, *Pf*HRP-2 was caught at the first capture zone. Experiment was repeated using *Pv*MSP-1 sample in PBS with concentrations ranging from 0.01 ng/ml to 10 ng/ml. *Pv*MSP-1 was caught at the second capture zone and the detection limits of *Pv*MSP-1 in PBS solution was obtained.

Third, solutions made up of equal amounts of *Pf*HRP-2 and *Pv*MSP-1 samples were also prepared. Concentrations in the range of 0.01 ng/ml and 10 ng/ml for both antigens were used for the study.

Similarly, it was observed that *Pf*HRP-2 was caught at the first capture zone and *Pv*MSP-1 at the second capture zone. This allows the identification of both antigens from the same mixed sample. Scanning electron microscopy (SEM), optical microscopy, and electrical resistivity characterization were performed. The procedure and equipment for the characterization was reported in the previous chapter.

4.6.4 Characterization

The morphology of the *Plasmodium* species was studied using an Olympus CH Binocular microscope fitted with a 100× objective with a 1.25 N.A.

4.7 Results and Discussion

4.7.1 Principle of Disease Detection

Most MRDTs currently employ the immunochromatographic strip assay technique. This technique allows for separation and identification of soluble antigens in solution using complementary antibodies. The technique allows for mass production of kits, which in turn allows lower manufacturing and distribution cost, and a simplified supply chain. The strip assay technique also allows for easy training of users, standardization of result interpretation, and ease of use in countries or regions where multiple languages are spoken [207].

Similarly, the NMBs detection technique is based on the immunochromatography sandwich approach. As a result of specific binding between the capture antibody and antigen, visible signal is generated from the NMBs conjugated with secondary antibody. The optical signal is assessed

using the naked eye and quantified using a reading device. Immobilized NMBs on the capture zone can also be quantified using the change in electrical resistivity of that capture zone.

The success of the sandwich immunoassay test requires the use of an antigen large enough to contain at least two epitopes [165]. *Pf*HRP-2, which satisfies this requirement, has two epitopes specific to Ms-MAbf and Rb-PAbf. The primary monoclonal antibody, Ms-MAbf, was immobilized on the capture zone of the glass slide as shown in Figure 4.3 (a). *Pf*HRP-2 in PBS was applied to the sample pad of the strip. Extra PBS was introduced and acts as a lysing agent to improve the sample flow to the absorption pad. The sample mixture migrated across the membrane to the capture zone, where Ms-MAbf immobilized on the strip surface captured most of the *Pf*HRP-2 present in the mixture. The absorption pad regulated the flow and collected all excess fluid. A second liquid specimen of the secondary polyclonal antibodies, Rb-PAbf, coupled to NMBs in PBS was applied to the sample pad. The Rb-PAbf and NMBs conjugate bind to different epitopes on the captured *Pf*HRP-2 antigens. As a result, the Rb-PAbf and NMBs conjugate captured by the *Pf*HRP-2 generated a dark line at the capture zone, giving a positive test result shown in Figure 4.3 (b). Electrical resistivity of the capture zone can also be obtained {Figure 4.3(b)}.

4.7.2 Detection Limit of *Pf*HRP-2 Assay

Successful immobilization of NMBs on the capture zone of the glass slide was achieved within one minute. NMBs were observed to form an interconnecting network at the capture zone as shown in Figure 4.4. This network confirmed the detection of *Pf*HRP-2 by the sandwich immunochromatography method. Increasing *Pf*HRP-2 concentration increased the density of the

immobilized NMB network at the capture zone. This is depicted in Figure 4.4 for four different concentrations of *Pf*HRP-2 studied.

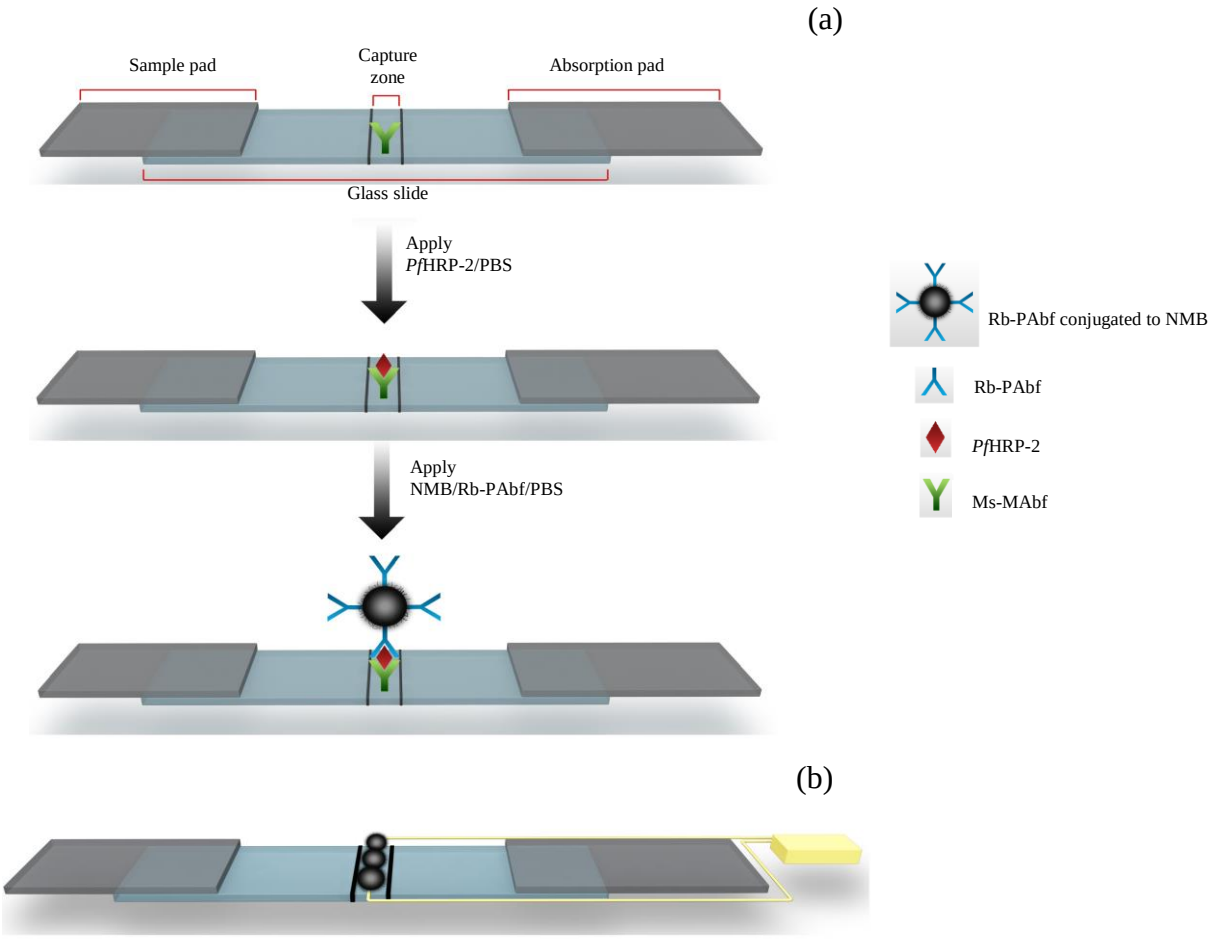

Figure 4.3 (a) Schematic illustration of the sandwich immunochromatographic set-up used to detect *Pf*HRP-2 and (b) Illustration of the two different types of signal generation from the immunosensor. The yellow cable is used for electrical measurements.

The network of immobilized NMBs at the capture zone for the various *Pf*HRP-2 concentrations were characterized. A linear relationship between the percentage area covered by the NMBs (A_{pct}) at the capture zone and the concentration of *Pf*HRP-2 in the range of 0.01 ng/ml to 10 ng/ml was attained {shown in Table 4.1 and Figure 4.5 (a)}. The correlation equation, $A_{pct} = 0.7212 + 1.286x$ ($R^2 = 0.9968$) was used, where x is the concentration of *Pf*HRP-2. With high coefficient

of determination, this equation can be used to estimate the concentration of *Plasmodium falciparum* in any sample tested. The visual detection limit of the assay was obtained to be 0.025 ng/ml. This is the lowest concentration at which the NMB network was observed with the unaided human eye.

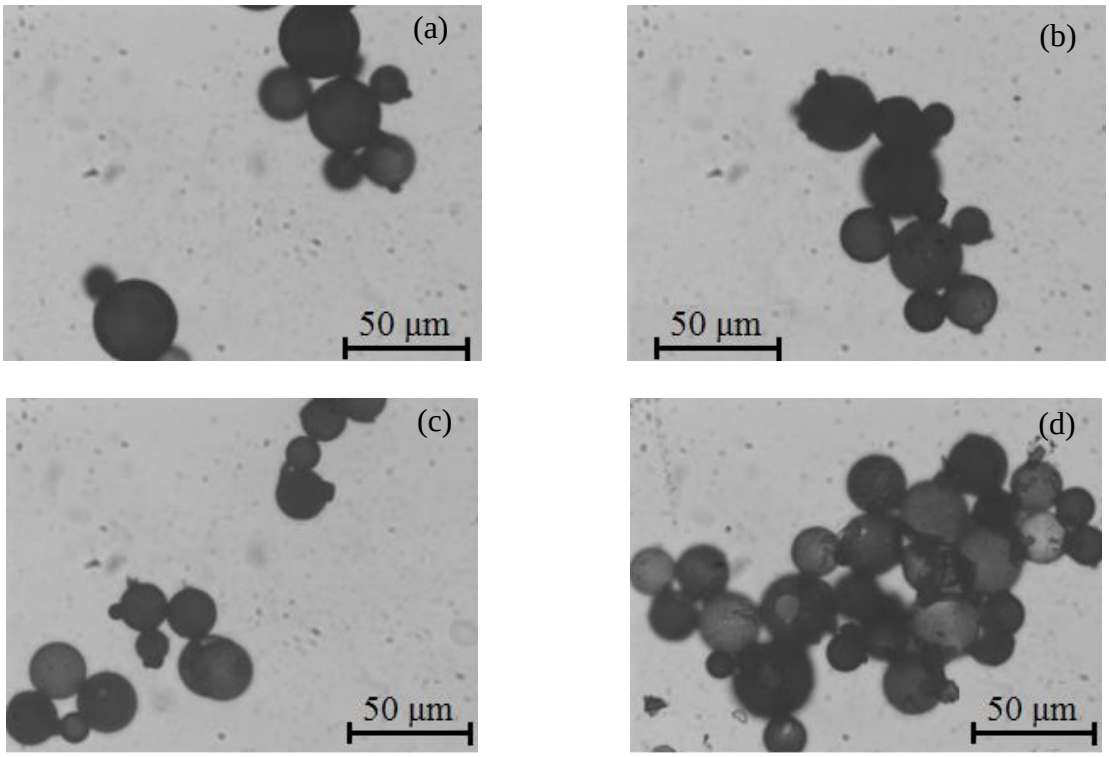

Figure 4.4 Optical micrographs showing NMBs captured on glass slides in a sandwich assay format with (a) 0.025, (b) 0.1, (c) 1, and (d) 10 ng/ml concentrations of *Pf*HRP-2.

Table 4.1 Summary of the percent area of the capture zone covered with NMBs for varying *Pf*HRP-2 concentrations.

Concentration (ng/ml)	Percent Area Covered by NMBs	Standard Deviation
0.025	0.52	0.13
0.05	0.62	0.33
0.1	0.75	0.43
1.0	2.56	0.37
10.0	13.53	0.84

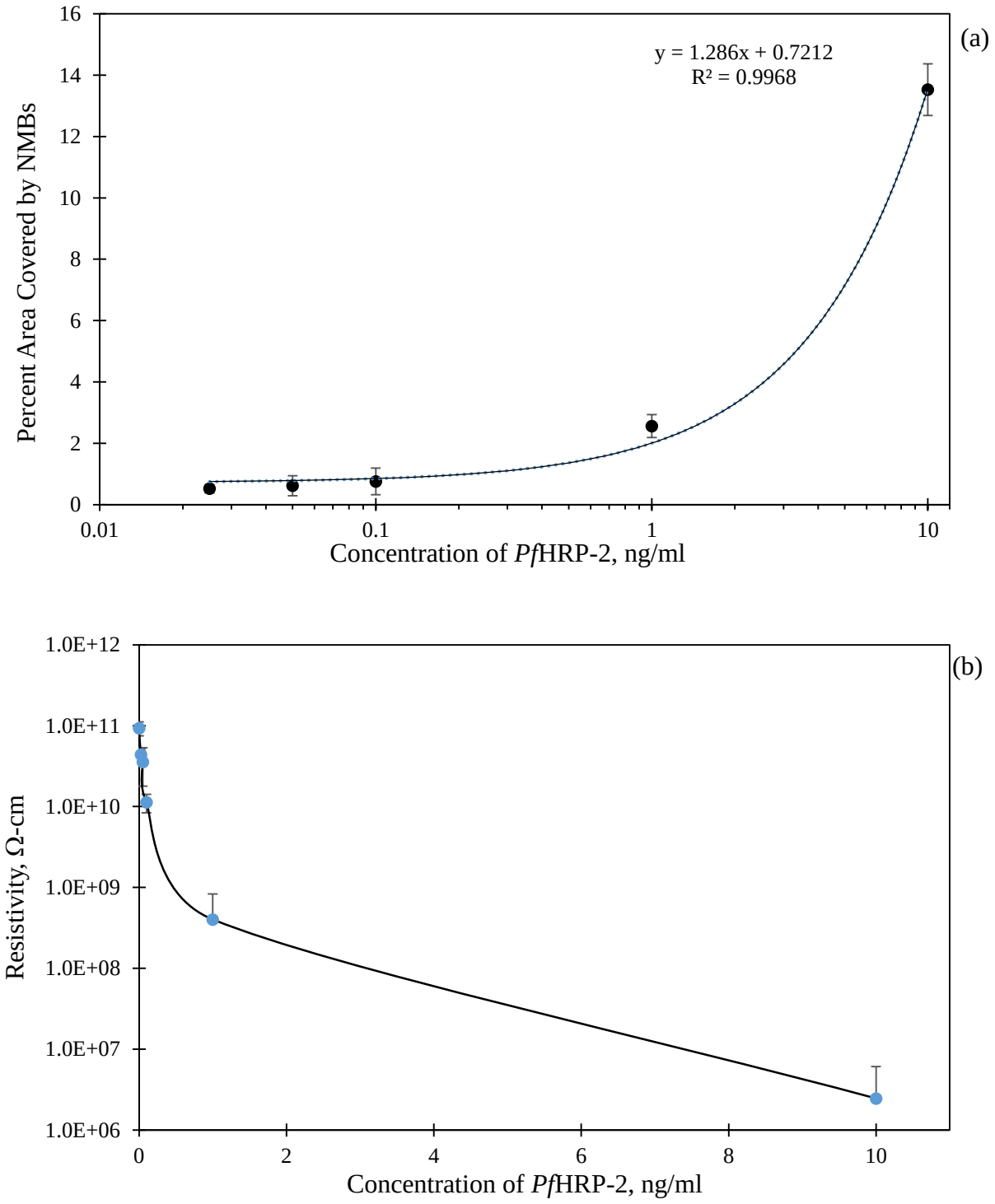

Figure 4.5 (a) Variation of percent area of the capture zone covered with NMBs against *Pf*HRP-2 concentrations and (b) Variation of the resistivity of the capture zone with immobilized *Pf*HRP-2 concentration. The error bars in both graphs each shows the variation of five concentration points.

The lowest detection limit of *Pf*HRP-2 reported in the literature to date using immunoassay technique has been 0.36 ng/ml [208]. The ultra-low visual detection limit of 0.025 ng/ml obtained from this study is attributed to the following. First, the high aspect ratio of CNFs makes available several binding sites for covalent bonding with Rb-MAbf. The high aspect ratio arises from the construction of the CNFs giving them length-to-diameter ratio of up to 132,000,000:1. This high ratio gives CNFs extensive area on their length for several of the nanosized antigens to be immobilized. Second, the exploitation of the high chemical reactivity of CNFs with antibodies of *Pf*HRP-2 and organic surfactants make it possible for CNFs to be highly selective and specific in aqueous environment. Third, large effective surface area remains available on each microstructured NMB allowing it to be treated with several millions of *Pf*HRP-2 antibodies. Finally, the microstructure of the NMBs allows visual signal amplification and hence easier quantification.

Signal detection and quantification of this immunosensor can also be achieved using electrical measurement. The high conducting nature of CNFs [59] provides the flexibility to perform resistivity changes on the capture zone of the immunosensor in addition to the visual characterization. The interconnected pathway formed by the immobilized NMBs at the capture zone allowed for an effective electron transfer to be established with the electrode. The resistivity of the capture zone was measured at different *Pf*HRP-2 concentrations as shown in Figure 4.5(b) and Table 4.2. The higher the concentration of *Pf*HRP-2, the higher was the density of the immobilized NMBs and hence the more the CNFs available for conduction. Resistivity of the plain glass slide used for the study was obtained as 9.30×10^{10} Ω-cm. Resistivity measurement was also conducted in NSB case and it was measured as 8.99×10^{10} Ω-cm. Appreciable change/reduction

in resistivity was only observed for concentrations of *Pf*HRP-2 0.01 ng/ml and greater. This set a limit of detection for *Pf*HRP-2 as 0.01 ng/ml, which is considered very low.

Table 4.2 Summary of the measured resistance values of the capture zone for varying *Pf*HRP-2 concentrations.

Concentration (ng/ml)	Resistivity (Ωcm)	Standard Deviation
0.025	4.39E+10	7.50E+09
0.05	3.57E+10	1.78E+10
0.1	1.13E+10	2.89E+09
1.0	4.02E+08	4.31E+08
10.0	2.46E+06	3.63E+06

4.7.3 Selectivity of the *Pf*HRP-2 Detection Assay

The selectivity performance of the proposed method was also established. In order to determine this capability, two capture zones were identified on the immunosensor. On the first capture zone, primary antibodies specific to *Pf*HRP-2 were immobilized. Antibodies specific to *Pv*MSP-1 were immobilized on the second capture zone. Using the same method as described earlier, the technique was able to capture different densities of NMB networks on the first zone when varying concentrations of *Pf*HRP-2 in PBS solution was applied on the sample pad. Figure 4.6 (a) shows the immunosensor for the detection of 10 ng/ml of *Pf*HRP-2 in PBS solution. Quantification of the percent area covered by captured NMBs showed similar pattern to the graph displayed in Figure 4.5 (a). During the tests with various concentrations of *Pf*HRP-2, no NMBs were observed at the second capture zone.


(a)


(b)


(c)

Figure 4.6 Glass slides showing (a) visual signal obtained at the first capture zone from the detection of *Pf*HRP-2 in PBS solution, (b) signal observed at the second capture zone from the detection of *Pv*MSP-1 in solution, and (c) signals obtained at the *Pf*HRP-2 and *Pv*MSP-1 capture zones from a mixed *Pf*HRP-2 and *Pv*MSP-1 solution.

The assays with varying concentration of *Pv*MSP-1 in PBS showed a colored signal only at the second capture zone. Figure 4.6 (b) shows the immunosensor for the detection of 10 ng/ml of *Pv*MSP-1 in PBS solution. Both optical and electrical characterizations were performed on the captured NMB network at the second capture zone. Similar to the microscopic characterization of *Pf*HRP-2, a linear relationship between A_{pct} at the capture zone and concentrations of *Pv*MSP-1 was obtained {shown in Figure 4.7 (a) and Table 4.3}. The correlation equation was $A_{pct} = 0.6133 + 2.1059x$ $(R^2 = 0.9902)$. Likewise, R^2 has a good correlation and can be used to estimate the concentration of *Plasmodium vivax* in any sample tested. The visual detection limit of the assay was obtained to be 0.025 ng/ml. The lowest detection limit of *Pv*MSP-1 reported in the literature using immunoassay technique is 6.3 ng/ml [209]. The limit of detection using electrical measurements for the detection of *Pv*MSP-1 was obtained at 0.02 ng/ml {Figure 4.7 (b) and Table 4.4}.

In another set of tests, a solution containing equal concentrations of *Pf*HRP-2 and *Pv*MSP-1 in PBS was prepared. The concentration of both antigens used for the study ranged from 0.025 ng/ml to 10 ng/ml. In all the tests performed, NMBs were observed to be captured selectively on both capture zones. Figure 4.6(c) shows the immunosensor with specific NMBs at both capture zones.

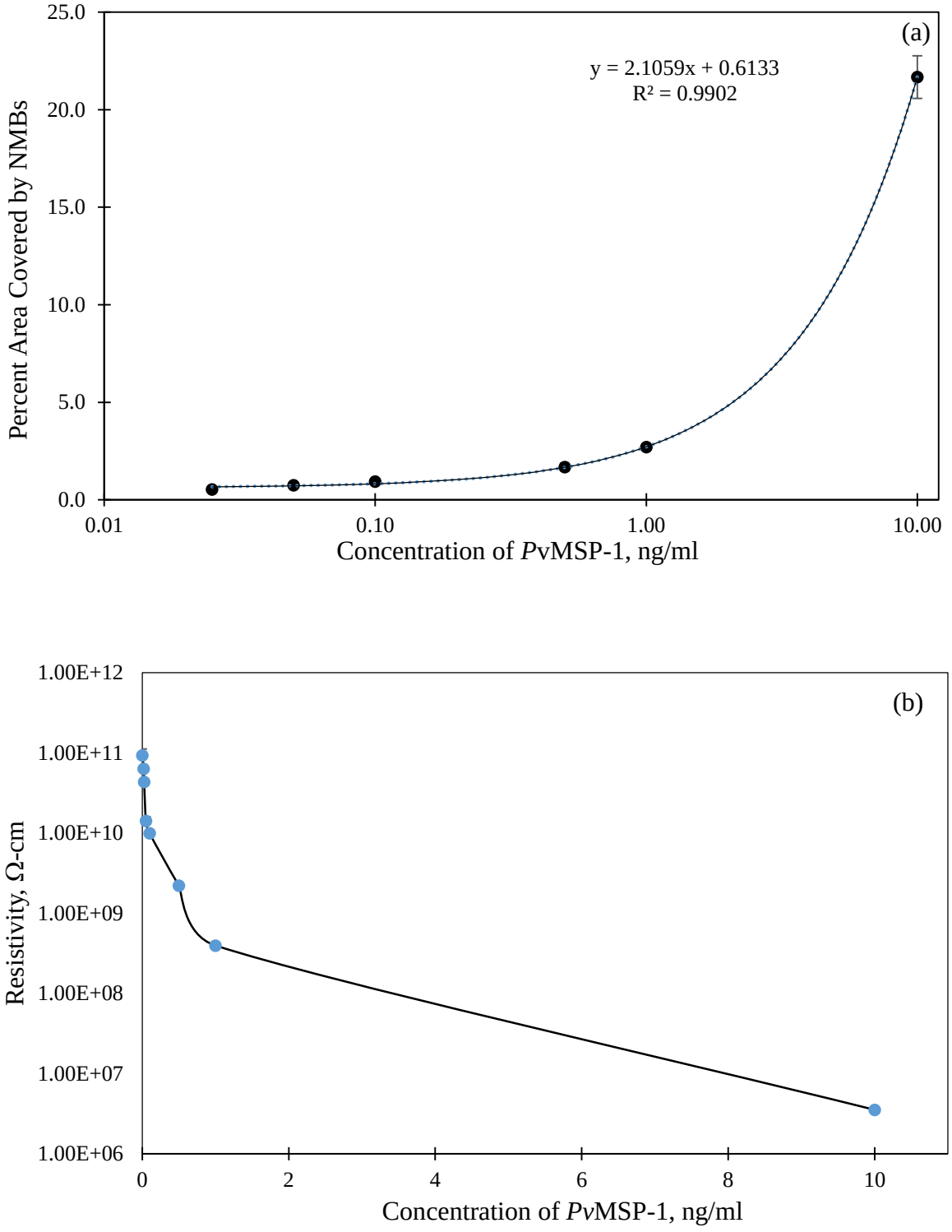

Figure 4.7 (a) Variation of percent area of the capture zone covered with NMBs against *Pv*MSP-1 concentrations and (b) Variation of the resistivity of the capture zone with immobilized *Pv*MSP-1 concentration.

Table 4.3 Summary of the percent area of the capture zone covered with NMBs for varying *Pv*MSP-1 concentrations.

Concentration (ng/ml)	Percent Area Covered by NMBs	Standard Deviation
0.025	0.53	0.11
0.05	0.75	0.11
0.1	0.93	0.13
1.0	2.70	0.19
10.0	21.67	1.09

Table 4.4 Summary of the measured resistivity values of the capture zone for varying *Pv*MSP-1 concentrations.

Concentration (ng/ml)	Resistivity (Ωcm)	Standard Deviation
0.02	6.30E+10	1.82E+10
0.025	4.32E+10	3.22E+09
0.05	1.41E+10	4.28E+09
0.1	9.91E+09	1.80E+09
0.5	2.20E+09	8.29E+08
1.0	3.95E+08	3.40E+07

4.7.4 Selectivity of the hCG Detection Assay

hCG, the clinical condition responsible for the diagnosis of pregnancy, was also tested using the immunochromatographic approach as described previously. Ms-hCG was initially immobilized on the glass substrates with Rb-hCG conjugated to the NMBs. Varying the concentration of hCG in PBS, different densities of NMB networks were immobilized on the capture zone. The correlation equation of $A_{pct} = 0.4596 + 1.6452x$ ($R^2 = 0.9838$) was obtained after optical characterization of the NMB networks. This linear relationship is shown in Table 4.5 and Figure 4.8 (a). The visual detection limit of the assay was obtained as 0.05 ng/ml. The lowest detection limit of hCG reported in the literature using immunoassay technique is 0.5 ng/ml [210]. The limit of detection using electrical measurements for hCG capture was also obtained as 0.025 ng/ml {Figure 4.8 (b) and Table 4.6}.

Table 4.5 Summary of the percent area of the capture zone covered with NMBs for varying hCG concentrations.

Concentration (ng/ml)	Percent Area Covered by NMBs	Standard Deviation
0.05	0.43	0.15
0.10	0.72	0.14
0.50	1.33	0.18
1.00	2.08	0.18

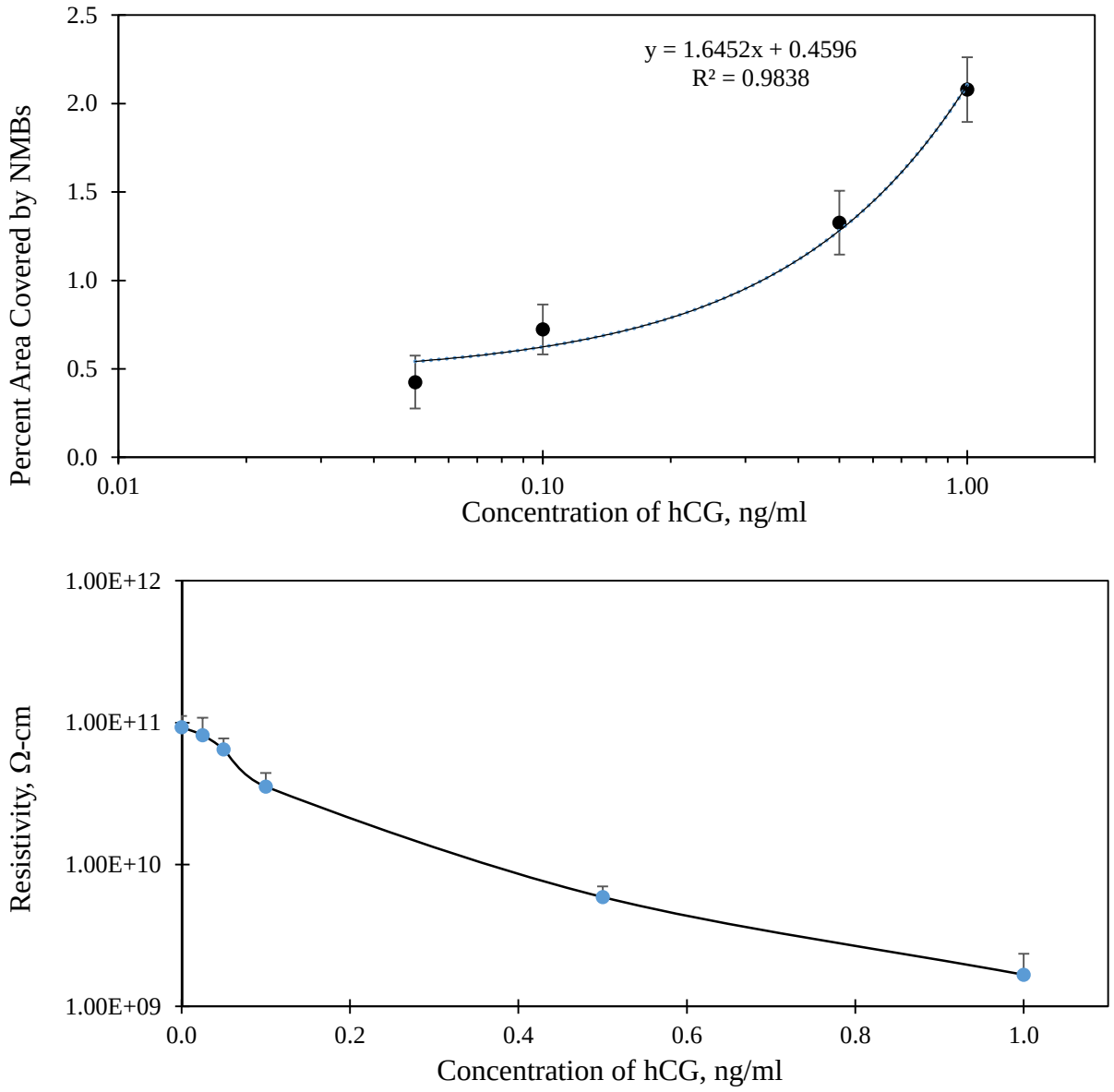

Figure 4.8 (a) Variation of percent area of the capture zone covered with NMBs against hCG concentrations and (b) Variation of the resistivity of the capture zone with immobilized hCG concentration.

Table 4.6 Summary of the measured resistance values of the capture zone for varying hCG concentrations.

Concentration (ng/ml)	Resistivity (Ωcm)	Standard Deviation
0.025	6.17E+10	2.29E+10
0.05	6.50E+10	1.26E+10
0.1	3.55E+10	8.77E+09
0.5	5.90E+09	1.11E+09
1.0	1.67E+09	6.75E+08

4.8 Summary

The higher probability of capture available to biological species on the novel NMB particles made it possible for the immunochromatographic sandwich approach to be used in diagnosing various clinical conditions. hCG, the hormone used in the detection of pregnancy was tested. *P. falciparium* and *P. vivax*, the two most deadly parasites responsible for the majority of severe malaria cases were also detected in this study. Ultra-low visual detection limits were obtained for all three clinical conditions studied. The method was rapid with detection being achieved within one minute of testing. The approach was also able to selectively capture the required antigen at different capture zones within the immunosensor.

This unbeatable simplicity, speed of the technique, specific, and ultrasensitive approach makes the process very selective with a potential for establishing a visual quantitative relationship for varying antigens concentration. Further validation and quantification of results were achieved by measuring the change in resistivity within the capture zone. Compared with RDTs which required the addition of dyes and enzymatic substrates to the detection solution, the immunochromatographic sensor proposed in this work avoided the limitations resulting from the requirement of these substrates. The immunosensor exhibited a reliable accuracy and proved to be

practical and convenient. This method highlights the potential strategy that can be substituted in RDTs in general. This will usher in, a highly effective RDTs to improve the overall global healthcare system.

CHAPTER 5
CONCLUSIONS AND FUTURE WORK

5.1 Conclusions

5.1.1 Surface Functionalization of NMBs

Carbon nanofibers (CNFs) were grown on nickel coated glass microballoons (NMBs) using the dual zone chemical vapor deposition (CVD) technique. The growth process deposited residual amorphous carbonaceous fragments on the NMBs. The amorphous carbon was removed through surface functionalization. The surface functionalization resulted in the production of cleaner NMBs and also the formation of carboxyl and hydroxyl functional groups on the surface of the NMBS. Functionalization was carried out in nitric acid, nitric/sulfuric acid, and air oxidized environments. The acidic modified NMBs led to substantial loss of CNF structure while the air oxidized process maintained the CNF structure. Acidic treated NMBs were also found to negatively impact on biological species and hence not suitable for use in biosensors. Air oxidized NMBs therefore stands out as the ideal surface treatment approach.

The air oxidized NMBs preserved their structure and were able to maintain good dispersion in water for two minutes. Suspension stability was observed to reduce drastically with nitric acid having the weakest stability and air oxidized the best among the nitric, nitric/sulfuric acid and air oxidized methods. Reduction in suspension stability occurs by dispersed NMBs coalescing at the bottom of the containers while the remaining NMBs float on the water surface. The floating NMBs were due to the hollow nature of the microballoons. Air oxidation also introduces carboxyl and hydroxyl functional groups to the surface of the NMBs. FTIR studies confirmed the presence of the carboxyl and hydroxyl groups. These functional groups are needed for conjugation with

biological species in biosensors. Hence, NMBs with the potential of improving the performance of rapid diagnostics test kits (RDTs) was successfully fabricated and functionalized.

5.1.2 Conjugation of Biological Species to NMBs

The integration of millions of CNFs arranged on such micro-particle provided a higher probability of attaching several millions of biological species to the NMBs. The ability of CNFs to form countless combination and derivatives was exploited to develop next generation sensors. Biological species were covalently bonded to the CNFs through an amidation process by taking advantage of the EDC/Sulfo-NHS activation method. Non-covalent bonding of PEG to the NMBs was also accomplished. The PEG organic molecules covered the sidewalls of the CNFs providing a nano-scale coating that led to the prevention of non-specific binding during the sensing application.

Competitive and sandwich immunoassay formats were demonstrated using IgG and anti-IgG and the results confirmed through fluorescence studies. The fluorescence results paved the way for studies into the potential use of NMBs as ultra-low detection labels in RDTs. Using glass slide as a substrate and antibody conjugated NMBs as labels, various concentrations of anti-IgG were immobilized. The density of the immobilized NMBs network formed varies with the concentration of anti-IgG detected. Electrical resistivity measurements of the test zone showed the potential for establishing a quantitative relationship for the antigen concentration. Ultra-low detection limit of 4 pg/ml was obtained from electrical signaling. Visual detection was also achieved due to the dark nature of the NMBs at the capture zone. As low as 0.1 ng/ml of anti-IgG were observed with the unaided eye at the test zone. The NMBs offered significantly higher level of sensitivity, as well as,

simple and fast visual and/or electrical identification of IgG/anti-IgG on the test glass slides. This novel approach holds the promise for early detection of various diseases, as well as providing healthcare professionals with information regarding the stage of infection. Utilizing this type of label could also lead to the elimination of false-alarms while reducing the incubation period required for detection in currently used RDTs.

5.1.3 Pathogen Detection on Immunochromatographic Device

The methodology developed for fabricating, functionalizing and conjugating of NMBs with biological species was applied in detecting two major clinical conditions. *P. falciparium* and *P. vivax*, the two most deadly parasites responsible for the majority of severe malaria cases, were detected in this study using the immunochromatographic sandwich approach. *P. falciparum* histidine rich protein-2 (*Pf*HRP-2) and *P. vivax* merozoites surface protein-1 (*Pv*MSP-1) antigens were tested over their linear range of 0.01 – 10 ng/ml. The approach was ultrasensitive and highly selective with visual detection limit of 0.025 ng/ml obtained for both *Pf*HRP-2 and *Pv*MSP-1 in PBS at two different test zones on the same glass slide achieving multiple disease detection. Electrical detection limits were measured as 0.01 ng/ml for *Pf*HRP-2 and 0.02 ng/ml for *Pv*MSP-1. hCG, the clinical condition responsible for the diagnosis of pregnancy, was also tested at a linear range of 0.025 – 10 ng/ml. Visual detection limit of 0.05 ng/ml and an electrical detection limit of 0.025 ng/ml were obtained. The ultra-low limits obtained for both visual and electrical detection for the two clinical conditions have never been achieved using RDTs in the field nor in the lab as provided in the literature.

The use of WAG RDTs avoided the limitations commonly encountered from the use of dyes and enzymatic substrates in RDTs. This detection process is reliably accurate, practical and convenient. Thus, the highly reactive, rapid, selective and signal amplification capabilities of NMBs is a promising tool for use in MRDTs and pregnancy test kits for the early diagnosis of these clinical conditions.

5.2 Future Work

5.2.1 Pathogen Detection in Microfluidic Device

The developed immunochromatographic device (WAG RDT) in this study was able to effectively detect ultra-low concentrations of antigen within a minute of analysis. However, all the reagents integral to the process are expensive and therefore miniaturization will reduce the cost and efficiency drastically. Miniaturization can be achieved by using a microfluidic immunosensing device. Microfluidic devices consist of microchannels for transporting fluids, with part or all of the necessary components of the immunoassay procedure integrated in the device [211]. A microfluidic device reduce diffusional distances limiting analysis time and enabling more rapid, POC diagnostics that significantly enhances the speed of the process. Microfluidic devices are passive requiring no external power input, but instead relying on diffusion and/or capillary action to control the assay [212, 213]. Precision is drastically improved in microfluidic devices by using software linked to pumps, valves, mixers, etc., to control the movement of fluids.

Successful immobilization of antibodies on interdigitated array (IDA) microelectrodes fabricated on a glass substrate and incorporated within microfluidic immunosensing device has been achieved [140]. Similarly, a microfluidic device suitable for the conjugate used in this study need to be

designed. Studies on optimizing the detection process in the microfluidic device must be carried out.

5.2.2 Design and Optimization of Microfluidic Device

Microfluidic immunosensing has been demonstrated using CNT matrix [140]. Human serum albumin (HSA) protein in a sandwich assay format and polydimethylsiloxane (PDMS) microfluidic system were used. The microfluidic system allowed passive sample transport to the test zone by capillary action. The test zone had an IDA microelectrode on which primary anti-HSA was immobilized. Secondary anti-HSA conjugated with CNTs formed a conducting matrix across the IDA which generated electrical signal equivalent to the amount of captured HSA.

The CNT microfluidic immunosensor can be redesigned to use microsized particles of the NMBs in place of the nanosized CNTs. The flow system within the microfluidic system will be optimized by using a combination of a capillary pump and an absorbent pad. An optimum condition within the system can be obtained by manipulating the dimensions of the pump, channel, test zone, and IDA. Incorporating the conjugate solution within the system can also eliminate the application of multiple reagents which can lead to the overall improvement in the sensitivity of the device. Therefore further studies need to be performed in designing and optimizing the detection process in a microfluidic device. Simulating the process will also lead to a better understanding of the influence of the different parameters involved in the microfluidic system.

5.2.3 Clinical Trials using Microfluidic Device

The successful diagnostic of malaria and pregnancy clinical conditions using the immunochromatographic assay format has been demonstrated. The purified protein derivative of the antigens of the clinical conditions were used. In RDTs, in vivo tests of antigens are rather conducted. Hence, for completely successful use of WAG RDTs, tests on the whole genome antigens have to be conducted. The whole genome antigen has many other components which do interfere with in vivo immunoassay tests. Such components include polysaccharides, lipids, and other proteins.

Detection of whole genome antigens in the microfluidic system also need to be carried out. The statistical prediction of the confidence interval of the device from a clinical study will be performed to determine the sensitivity and specificity of the microfluidic device. The sensitivity gives an indication of how the device correctly identifies tested patients with the disease while the specificity of the device provides the ability to accurately identify tested patients without the disease [214]. Results obtained from testing a sample on the device and testing same sample using the ‘gold standard test’ are used as basis. True positive and true negative results obtained are used for the sensitivity and specificity calculations.

REFERENCES

1. Tsang, S. C., Davis, J. J., Green, M. L. H., Hill, H. A. O., Leung, Y. C., and Sadler, P. J., "Immobilization of small proteins in carbon nanotubes: High-resolution transmission electron microscopy study and catalytic activity". Journal of the Chemical Society, Chemical Communications, 1995(17): 1803-1804.

2. Chen, B. X., Wilson, S. R., Das, M., Coughlin, D. J., and Erlanger, B. F., "Antigenicity of fullerenes: Antibodies specific for fullerenes and their characteristics". Proceedings of the National Academy of Sciences, 1998. **95**: 10809-10813.

3. Naguib, N. N., Mueller, Y. M., Bojczuk, P. M., Rossi, M. P., Katsikis, P. D., and Gogotsi, Y., "Effect of carbon nanofibre structure on the binding of antibodies". Nanotechnology, 2005. **16**(4): 567-571.

4. Wermuth, C.-G., Ganellin, C. R., Lindberg, P., and Mitscher, L. A., "Glossary of Terms Used in Medicinal Chemistry (IUPAC Recommendations 1997)". Annual Reports in Medicinal Chemistry, 1998. **33**: 385-395.

5. Zhang, D. W., Liu, J. X., Nie, J., Zhou, Y. L., and Zhang, X. X., "Micropipette tip-based miniaturized electrochemical device combined with ultramicroelectrode and its application in immobilization-free enzyme biosensor". Analytical Chemistry, 2013.

6. Chen, G., "Fluorescence biosensor for H5N1 antibody based on metal-organic framework platform". Journal of Materials Chemistry B, 2013. **1**: 1812-1817.

7. Po-Yueh, W. and Lu, M. S. C., "CMOS thermal sensor arrays for enzymatic glucose detection". Sensors Journal, IEEE, 2011. **11**(12): 3469-3475.

8. Rayana, R. R.-A., Hugo Javier, S.-P., María Liliana, M.-G., Bernardo, A. F.-U., and Abel, M., "Chemical biosensors based on proteins involved in biomineralization processes". 2011. 589-600.

9. Lu, Y., Peng, S., Luo, D., and Lal, A., "Low-concentration mechanical biosensor based on a photonic crystal nanowire array". Nat Commun, 2011. **2**: 578.

10. Hua, W., Yan, C., Hassibi, A., Scherer, A., and Hajimiri, A. "A frequency-shift CMOS magnetic biosensor array with single-bead sensitivity and no external magnet". in Solid-State Circuits Conference - Digest of Technical Papers, 2009. ISSCC 2009. IEEE International. 2009.

11. Gong, J. L., Sarkar, T., Badhulika, S., and Mulchandani, A., "Label-free chemiresistive biosensor for mercury (II) based on single-walled carbon nanotubes and structure-switching DNA". Applied Physics Letters, 2013. **102**(1): 013701-013701-3.

12. Struss, A., Pasini, P., Ensor, C. M., Raut, N., and Daunert, S., "Paper strip whole cell biosensors: a portable test for the semiquantitative detection of bacterial quorum signaling molecules". Analytical Chemistry, 2010. **82**(11): 4457-4463.

13. Kaman, W. E., Andrinopoulou, E., and Hays, J., "Perceptions of point-of-care infectious disease testing among European medical personnel, point-of-care test kit manufacturers, and the general public". Patient Preference and Adherence, 2013. **7**: 559-577.

14. Lazcka, O., Campo, F. J. D., and Muñoz, F. X., "Pathogen detection: A perspective of traditional methods and biosensors". Biosensors and Bioelectronics, 2007. **22**(7): 1205-1217.

15. Clearblue, Accessed on August 14, 2013 from: http://www.clearblueeasy.com/pregnancy-test.php.

16. Rapid Diagnostic Testing, Accessed on July 5, 2013 from: http://www.rapiddiagnostictesting.com/.

17. Hughes, T. V. and Chambers, C. R., "Manufacture of carbon filaments", in Patent 405480, P. Office, Editor 1889: United States. 1-3.

18. Thompson, E. P., "Manufacture of carbon filaments". US Patent 401606, 1889: 1-4.

19. Kroto, H. W., Heath, J. R., O'Brien, S. C., Curl, R. F., and Smalley, R. E., "C60-Buckminsterfullerene". Nature, 1985. **318**: 162-163.

20. Iijima, S., "Helical microtubules of graphitic carbon". Nature, 1991. **354**(6348): 56-56.

21. Itoh, S., Ihara, S., and Kitakami, J.-i., "Toroidal form of carbon C360". Physical Review B, 1993. **47**(3): 1703-1704.

22. Ge, M. and Sattler, K., "Observation of fullerene cones". Chemical Physics Letters, 1994. **220**: 192-196.

23. Amerlinckx, S., Bernaerts, D., Ivanov, V., Nagy, J. B., Zhang, X. B., and Zhang, X. F., "A formation mechanism for catalytically grown helix-shaped graphite nanotubes". Science, 1994. **265**: 635-639.

24. Mendes, R. G., Bachmatiuk, A., Büchner, B., Cuniberti, G., and Rümmeli, M. H., "Carbon nanostructures as multi-functional drug delivery platforms". Journal of Materials Chemistry B, 2013. **1**(4): 401.

25. Teo, K. B. K., Singh, C., Chhowalla, M., and Milne, W. I., "Catalytic synthesis of carbon nanotubes and nanofibers.pdf". Encyclipedia of Nanoscience and Nanotechnology, 2003. **X**: 1-22.

26. Price, R. L., Waid, M. C., Haberstroh, K. M., and Webster, T. J., "Selective bone cell adhesion on formulations containing carbon nanofibers". Biomaterials, 2003. **24**(11): 1877-1887.

27. Karousis, N., Tagmatarchis, N., and Tasis, D., "Current progress on the chemical modification of carbon nanotubes". Chemical Reviews, 2010. **110**(9): 5366-5397.

28. Lahiff, E., Lynam, C., Gilmartin, N., O'Kennedy, R., and Diamond, D., "The increasing importance of carbon nanotubes and nanostructured conducting polymers in biosensors". Analytical and Bioanalytical Chemistry, 2010. **398**(4): 1575-1589.

29. Justino, C. I. L., Rocha-Santos, T. A. P., Duarte, A. C., and Rocha-Santos, T. A. P., "Advances in point-of-care technologies with biosensors based on carbon nanotubes". TrAC Trends in Analytical Chemistry, 2013. **45**(0): 24-36.

30. De Volder, M. F. L., Tawfick, S. H., Baughman, R. H., and Hart, A. J., "Carbon nanotubes: Present and future commercial applications". Science, 2013. **339**(6119): 535-539.

31. Sritongkham, P., Wisitsoraat, A., Tuantranont, A., and Somasundrum, M., "Integration of CNT-based chemical sensors and biosensors in microfluidic systems". 2012, Springer Berlin Heidelberg. 1-43.

32. Kim, J., Lee, J.-Y., Jin, J.-H., Park, C., Lee, C., and Min, N., "A fully microfabricated carbon nanotube three-electrode system on glass substrate for miniaturized electrochemical biosensors". Biomedical Microdevices, 2012. **14**(3): 613-624.

33. Meyyappan, M., "Carbon nanotubes: science and applications". 2004: CRC press.

34. Sano, M., Kamino, A., Okamura, J., and Shinkai, S., "Ring closure of carbon nanotubes". Science, 2001. **293**(5533): 1299-1301.

35. Wei, B. Q., Vajtai, R., Jung, Y., Ward, J., Zhang, R., Ramanath, G., and Ajayan, P. M., "Microfabrication technology: Organized assembly of carbon nanotubes". Nature, 2002. **416**(6880): 495-496.

36. Hou, H. and Reneker, D. H., "Carbon nanotubes on carbon nanofibers: A novel structure based on electrospun polymer nanofibers". Advanced Materials, 2004. **16**(1): 69-73.

37. Han, M., Zhang, W., Gao, C., Liang, Y., Xu, Z., Zhu, J., and He, J., "Hollow nickel microspheres covered with oriented carbon nanotubes and its magnetic property". Carbon, 2006. **44**(2): 211-215.

38. Kim, D. Y., Sugime, H., Hasegawa, K., Osawa, T., and Noda, S., "Sub-millimeter-long carbon nanotubes repeatedly grown on and separated from ceramic beads in a single fluidized bed reactor". Carbon, 2011. **49**(6): 1972-1979.

39. He, D., Bozlar, M., Genestoux, M., and Bai, J., "Diameter- and length-dependent self-organizations of multi-walled carbon nanotubes on spherical alumina microparticles". Carbon, 2010. **48**(4): 1159-1170.

40. Martin-Gullon, I., Vera, J., Conesa, J. A., González, J. L., and Merino, C., "Differences between carbon nanofibers produced using Fe and Ni catalysts in a floating catalyst reactor". Carbon, 2006. **44**(8): 1572-1580.

41. Kang, I., Heung, Y. Y., Kim, J. H., Lee, J. W., Gollapudi, R., Subramaniam, S., Narasimhadevara, S., Hurd, D., Kirikera, G. R., Shanov, V., Schulz, M. J., Shi, D., Boerio, J., Mall, S., and Ruggles-Wren, M., "Introduction to carbon nanotube and nanofiber smart materials". Composites Part B: Engineering, 2006. **37**(6): 382-394.

42. Pyrograf Products, Accessed on February 12, 2014 from: http://pyrografproducts.com/carbon-nanotubes.html.

43. Inno-X, Accessed on June 29, 2013 from: http://www.inno-x.ch/en/153/Nano-Materials.htm.

44. Merkulov, V. I., Hensley, D. K., Melechko, A. V., Guillorn, M. A., Lowndes, D. H., and Simpson, M. L., "Control mechanisms for the growth of isolated vertically aligned carbon nanofibers". The Journal of Physical Chemistry B, 2002. **106**(41): 10570-10577.

45. Ahmad, B., Ahmad, M., Akhter, J. I., and Ahmad, N., "Formation of diamond-like carbon balls, self aligned and nonaligned nanotubes at the tip of the cathode during the synthesis of fullerenes in the DC arc discharge experiment". Materials Letters, 2005. **59**(12): 1585-1588.

46. Ren, Z., Lan, Y., and Wang, Y., "Growth techniques of carbon nanotubes", in Aligned Carbon Nanotubes. 2013, Springer Berlin Heidelberg. 45-66.

47. Kim, Y. A., Muramatsu, H., Hayashi, T., and Endo, M., "Catalytic metal-free formation of multi-walled carbon nanotubes in atmospheric arc discharge". Carbon, 2012. **50**(12): 4588-4595.

48. Liu, C. and Cheng, H.-M., "Carbon nanotubes: controlled growth and application". Materials Today, 2013. **16**(1–2): 19-28.

49. Zhang, Q., Huang, J.-Q., Zhao, M.-Q., Qian, W.-Z., Wang, Y., and Wei, F., "Radial growth of vertically aligned carbon nanotube arrays from ethylene on ceramic spheres". Carbon, 2008. **46**(8): 1152-1158.

50. Xiang, R., Luo, G. H., Qian, W. Z., Wang, Y., Wei, F., and Li, Q., "Large area growth of aligned CNT arrays on spheres: Towards large scale and continuous production". Chemical Vapor Deposition, 2007. **13**(10): 533-536.

51. Rodriguez, N. M., Chambers, A., and Baker, R. T. K., "Catalytic engineering of carbon nanostructures". Langmuir, 1995. **11**(10): 3862-3866.

52. Tracz, E., Scholz, R., and Borowiecki, T., "High-resolution electron microscopy study of the carbon deposit morphology on nickel catalysts". Applied Catalysis, 1990. **66**(1): 133-147.

53. Boellaard, E., de Bokx, P. K., Kock, A. J. H. M., and Geus, J. W., "The formation of filamentous carbon on iron and nickel catalysts: III. Morphology". Journal of Catalysis, 1985. **96**(2): 481-490.

54. Krishnankutty, N., Rodriguez, N. M., and Baker, R. T. K., "Effect of Copper on the Decomposition of Ethylene over an Iron Catalyst". Journal of Catalysis, 1996. **158**(1): 217-227.

55. Chambers, A. and Baker, R. T. K., "Influence of chlorine on the decomposition of ethylene over iron and cobalt particles". The Journal of Physical Chemistry B, 1997. **101**(9): 1621-1630.

56. Nolan, P. E., Lynch, D. C., and Cutler, A. H., "Carbon deposition and hydrocarbon formation on group VIII metal catalysts". The Journal of Physical Chemistry B, 1998. **102**(21): 4165-4175.

57. Huang, S., "Growing carbon nanotubes on patterned submicron-size SiO2 spheres". Carbon, 2003. **41**(12): 2347-2352.

58. Zegeye, E. F. and Woldesenbet, E., "Processing and mechanical characterization of carbon nanotube reinforced syntactic foams". Journal of Reinforced Plastics and Composites, 2012. **31**(15): 1045-1052.

59. Zegeye, E., Jin, Y., and Woldesenbet, E., "A paper like structure formed by binding self-assembled glass microballoons using random CNF networks". Materials Letters, 2012. **68**(0): 490-492.

60. Huang, C.-W., Wu, H.-C., Lin, W.-H., and Li, Y.-Y., "Temperature effect on the formation of catalysts for growth of carbon nanofibers". Carbon, 2009. **47**(3): 795-803.

61. Kovalenko, G. A., Rudina, N. A., Chuenko, T. V., Ermakov, D. Y., and Perminova, L. V., "Synthesis of catalytic filamentous carbon by the pyrolysis of alkanes on alumina–silica foam supporting nickel nanoparticles". Carbon, 2009. **47**(2): 428-435.

62. Endo, M., Kim, Y. A., Hayashi, T., Yanagisawa, T., Muramatsu, H., Ezaka, M., Terrones, H., Terrones, M., and Dresselhaus, M. S., "Microstructural changes induced in "stacked cup" carbon nanofibers by heat treatment". Carbon, 2003. **41**(10): 1941-1947.

63. Chuang, C.-C., Liu, W.-L., Chen, W.-J., and Huang, J.-H., "Temperature and substrate dependence of structure and growth mechanism of carbon nanofiber". Applied Surface Science, 2008. **254**(15): 4681-4687.

64. Yang, X., Guillorn, M. A., Austin, D., Melechko, A. V., Cui, H., Meyer, H. M., Merkulov, V. I., Caughman, J. B. O., Lowndes, D. H., and Simpson, M. L., "Fabrication and characterization of carbon nanofiber-based vertically integrated Schottky barrier junction diodes". Nano Letters, 2003. **3**(12): 1751-1755.

65. Kataura, H., Kumazawa, Y., Maniwa, Y., Umezu, I., Suzuki, S., Ohtsuka, Y., and Achiba, Y., "Optical properties of single-wall carbon nanotubes". Synthetic Metals, 1999. **103**(1–3): 2555-2558.

66. Carneiro, O. C., Rodriguez, N. M., and Baker, R. T. K., "Growth of carbon nanofibers from the iron–copper catalyzed decomposition of $CO/C_2H_4/H_2$ mixtures". Carbon, 2005. **43**(11): 2389-2396.

67. Mukhopadhyay, K., Porwal, D., Lal, D., Ram, K., and Mathur, G. N., "Synthesis of coiled/straight carbon nanofibers by catalytic chemical vapor deposition". Carbon, 2004. **42**(15): 3254-3256.

68. Zheng, G.-B., Kouda, K., Sano, H., Uchiyama, Y., Shi, Y.-F., and Quan, H.-J., "A model for the structure and growth of carbon nanofibers synthesized by the CVD method using nickel as a catalyst". Carbon, 2004. **42**(3): 635-640.

69. Helveg, S., Lopez-Cartes, C., Sehested, J., Hansen, P. L., Clausen, B. S., Rostrup-Nielsen, J. R., Abild-Pedersen, F., and Norskov, J. K., "Atomic-scale imaging of carbon nanofibre growth". Nature, 2004. **427**(6973): 426-429.

70. Kim, Y.-A., Hayashi, T., Naokawa, S., Yanagisawa, T., and Endo, M., "Comparative study of herringbone and stacked-cup carbon nanofibers". Carbon, 2005. **43**(14): 3005-3008.

71. Javey, A., Guo, J., Wang, Q., Lundstrom, M., and Dai, H., "Ballistic carbon nanotube field-effect transistors". Nature, 2003. **424**(6949): 654-657.

72. Katsnelson, M. I., "Graphene: carbon in two dimensions". Materials Today, 2007. **10**(1–2): 20-27.

73. Choi, W. and Lee, J., "Graphene: Synthesis and applications". 2012: Taylor & Francis.

74. Yao, J., Sun, Y., Yang, M., and Duan, Y., "Chemistry, physics and biology of graphene-based nanomaterials: new horizons for sensing, imaging and medicine". Journal of Materials Chemistry, 2012. **22**(29): 14313-14329.

75. Tada, K., Furuya, S., and Watanabe, K., "Ab initio study of hydrogen adsorption to single-walled carbon nanotubes". Physical Review B, 2001. **63**(15): 155405.

76. Lee, S., Kim, T.-R., Ogale, A. A., and Kim, M.-S., "Surface and structure modification of carbon nanofibers". Synthetic Metals, 2007. **157**(16–17): 644-650.

77. Olenic, L., Pruneanu, S., Almasan, V., and Biris, A. R., "Electrochemical and adsorption properties of catalytically formed carbon nanofibers". Nanofibers, Edited by: Ashok Kumar, 2010: 227-252.

78. Pujadó, M. P., "Carbon nanotubes as platforms for biosensors with electrochemical and electronic transduction". 2012: Springer.

79. Prato, M., Kostarelos, K., and Bianco, A., "Functionalized carbon nanotubes in drug design and discovery". Accounts of Chemical Research, 2007. **41**(1): 60-68.

80. Vanhorenbeke, B., Vriamont, C., Pennetreau, F., Devillers, M., Riant, O., and Hermans, S., "Radical addition of xanthates on carbon nanotubes as an efficient covalent functionalization method". Chemistry – A European Journal, 2013. **19**(3): 852-856.

81. Touhara, H., Yonemoto, A., Yamamoto, K., Komiyama, S., Kawasaki, S., Okino, F., Yanagisawa, T., and Endo, M., "Fluorination of cup-stacked carbon nanotubes, structures and properties". MRS Online Proceedings Library, 2004. **858**: null-null.

82. Khabashesku, V. N., Billups, W. E., and Margrave, J. L., "Fluorination of single-wall carbon nanotubes and subsequent derivatization reactions". Accounts of Chemical Research, 2002. **35**(12): 1087-1095.

83. Kumar, I., Rana, S., and Cho, J. W., "Cycloaddition reactions: a controlled approach for carbon nanotube functionalization". Chemistry, 2011. **17**(40): 11092-101.

84. Stenehjem, E. D., Ziatdinov, V. R., Stack, T. D. P., and Chidsey, C. E. D., "Gas-phase azide functionalization of carbon". Journal of the American Chemical Society, 2013. **135**(3): 1110-1116.

85. Lavorgna, M., Romeo, V., Martone, A., Zarrelli, M., Giordano, M., Buonocore, G. G., Qu, M. Z., Fei, G. X., and Xia, H. S., "Silanization and silica enrichment of multiwalled carbon nanotubes: Synergistic effects on the thermal-mechanical properties of epoxy nanocomposites". European Polymer Journal, 2013. **49**(2): 428-438.

86. Madani, S. Y., Tan, A., Dwek, M., and Seifalian, A. M., "Functionalization of single-walled carbon nanotubes and their binding to cancer cells". International Journal of Nanomedicine, 2012. **7**: 905-914.

87. Kanbur, Y. and Küçükyavuz, Z., "Surface modification and characterization of multi-walled carbon nanotube". Fullerenes, Nanotubes and Carbon Nanostructures, 2011. **19**(6): 497-504.

88. Liang, X., Zhong, J., Wang, Y., Zhao, T., Yao, P., Chu, W., Ibrahim, K., Qian, H., and Wu, Z., "An XANES study on the modification of single-walled carbon nanotubes by nitric acid". Journal of Synchrotron Radiation, 2009. **16**(3): 428-431.

89. Zhang, N. Y., Me, J., and Varadan, V. K., "Functionalization of carbon nanotubes by potassium permanganate assisted with phase transfer catalyst". Smart Materials & Structures, 2002. **11**(6): 962-965.

90. Ma, R., Yoon, D., Chun, K.-Y., and Baik, S., "The effects of UV/ozone treatments on the electrical transport behavior of single-walled carbon nanotube arrays". Chemical Physics Letters, 2009. **474**(1-3): 158-161.

91. Hussain, S., Amade, R., Jover, E., and Bertran, E., "Functionalization of carbon nanotubes by water plasma". Nanotechnology, 2012. **23**(38): 385604.

92. Jeon, I.-Y., Chang, D. W., Kumar, N. A., and Baek, J.-B., "Functionalization of carbon nanotubes". Carbon Nanotubes - Polymer Nanocomposites. 2011.

93. Harris, P. J. F., "Carbon nanotube science: Synthesis, properties and applications". 2009, UK: Cambridge University Press. 301.

94. Bai, Y., Lin, D., Wu, F., Wang, Z., and Xing, B., "Adsorption of Triton X-series surfactants and its role in stabilizing multi-walled carbon nanotube suspensions". Chemosphere, 2010. **79**(4): 362-367.

95. Chen, R. J., Zhang, Y., Wang, D., and Dai, H., "Noncovalent sidewall functionalization of single-walled carbon nanotubes for protein immobilization". JOURNAL-AMERICAN CHEMICAL SOCIETY, 2001. **123**(16): 3838-3839.

96. Zhang, A., Tang, M., Luan, J., and Li, J., "Noncovalent functionalization of multi-walled carbon nanotubes with amphiphilic polymers containing pyrene pendants". Materials Letters, 2012. **67**(1): 283-285.

97. Zhao, B., Hu, H., Yu, A., Perea, D., and Haddon, R. C., "Synthesis and characterization of water soluble single-walled carbon nanotube graft copolymers". Journal of the American Chemical Society, 2005. **127**(22): 8197-8203.

98. 3M, Accessed on April 08, 2013 from: http://solutions.3m.com/wps/portal/3M/en_US/Energy-Advanced/Materials/Industry_Solutions/Paints-Coatings/Glass_Bubbles/.

99. Gao, J., Tang, F., and Ren, J., "Electroless nickel deposition on amino-functionalized silica spheres". Surface and Coatings Technology, 2005. **200**(7): 2249-2252.

100. Lee, C. J., Son, K. H., Park, J., Yoo, J. E., Huh, Y., and Lee, J. Y., "Low temperature growth of vertically aligned carbon nanotubes by thermal chemical vapor deposition". Chemical physics letters, 2001. **338**(2): 113-117.

101. Osorio, A. G., Silveira, I. C. L., Bueno, V. L., and Bergmann, C. P., "H2SO4/HNO3/HCl—Functionalization and its effect on dispersion of carbon nanotubes in aqueous media". Applied Surface Science, 2008. **255**(5, Part 1): 2485-2489.

102. Zegeye, E. F., "Multifunctional carbon/epoxy glass microballoons nanocomposite", in Mechanical Engineering Department2012, Louisiana State University and Agricultural and Mechanical College.

103. Glagovich, N. "IR absorptions for representative functional groups". Accessed on April 11, 2013 from: http://www.chemistry.ccsu.edu/glagovich/teaching/316/ir/table.html.

104. Davis, W., Erickson, C., Johnston, C., Delfino, J., and Porter, J., "Quantitative Fourier Transform Infrared spectroscopic investigation humic substance functional group composition". Chemosphere, 1999. **38**(12): 2913-2928.

105. Jung, H.-S., Moon, D.-S., and Lee, J.-K., "Quantitative analysis and efficient surface modification of silica nanoparticles". Journal of Nanomaterials, 2012. **2012**: 48.

106. Kowalczyk, D., Slomkowski, S., Chehimi, M. M., and Delamar, M., "Adsorption of aminopropyltriethoxy silane on quartz: an XPS and contact angle measurements study". International journal of adhesion and adhesives, 1996. **16**(4): 227-232.

107. Young Lee, T., Han, J.-H., Hong Choi, S., Yoo, J.-B., Park, C.-Y., Jung, T., Yu, S., Yi, W., Han, I., and Kim, J., "Effects of source gases on the growth of carbon nanotubes". Diamond and related materials, 2003. **12**(3): 851-855.

108. Hata, K., Futaba, D. N., Mizuno, K., Namai, T., Yumura, M., and Iijima, S., "Water-assisted highly efficient synthesis of impurity-free single-walled carbon nanotubes". Science, 2004. **306**(5700): 1362-1364.

109. Kitamura, H., Sekido, M., Takeuchi, H., and Ohno, M., "The method for surface functionalization of single-walled carbon nanotubes with fuming nitric acid". Carbon, 2011. **49**(12): 3851-3856.

110. Collins, P. G., "Defects and disorder in carbon nanotubes", 2010, Oxford University Press: Oxford.

111. LU, M., LIU, Z.-M., WANG, H.-Y., and ZHANG, Y.-Q., "Synthesis and characterization of novel polyether quaternary ammonium salt PECH-QL [J]". Journal of Henan University of Science & Technology (Natural Science), 2008. **3**: 029.

112. Han, K. N., Li, C. A., and Seong, G. H., "Microfluidic Chips for Immunoassays". Annual Review of Analytical Chemistry, 2013. **6**(1): null.

113. Lin, C.-C., Wang, J.-H., Wu, H.-W., and Lee, G.-B., "Microfluidic Immunoassays". Journal of the Association for Laboratory Automation, 2010. **15**(3): 253-274.

114. Nakanishi, K., Sakiyama, T., Kumada, Y., Imamura, K., and Imanaka, H., "Recent advances in controlled immobilization of proteins onto the surface of the solid substrate and its possible application to proteomics". Current Proteomics, 2008. **5**(3): 161-175.

115. Tang, Z. M., Mei, Q., Zhang, C. X., Zhu, Y., and Lu, Z. H. "A comparative study of protein arrays immobilized on different substrates". in Chinese Materials Research Society ed. Advanced Nanomaterials and Nanodevices. Presented at the 8th International Conference on Electronic Materials. Xi'an, China. 2002.

116. Tsutsumi, E., Henares, T. G., Funano, S.-i., Kawamura, K., Endo, T., and Hisamoto, H., "Single-step sandwich immunoreaction in a square glass capillary immobilizing capture and enzyme-linked antibodies for simplified enzyme-linked immunosorbent assay". Analytical Sciences, 2012. **28**(1): 51-56.

117. Yen-Heng, L., Chun-Hong, L., and Gwo-Bin, L., "Droplet formation utilizing controllable moving-wall structures for double-emulsion applications". Microelectromechanical Systems, Journal of, 2008. **17**(3): 573-581.

118. Sung, W.-C., Chang, C.-C., Makamba, H., and Chen, S.-H., "Long-term affinity modification on poly(dimethylsiloxane) substrate and Its application for ELISA analysis". Analytical Chemistry, 2008. **80**(5): 1529-1535.

119. Fu, L.-M., Ju, W.-J., Yang, R.-J., and Wang, Y.-N., "Rapid prototyping of glass-based microfluidic chips utilizing two-pass defocused CO2 laser beam method". Microfluidics and Nanofluidics, 2013. **14**(3-4): 479-487.

120. Wang, J., Yiu, B., Obermeyer, J., Filipe, C. D. M., Brennan, J. D., and Pelton, R., "Effects of temperature and relative humidity on the stability of paper-immobilized antibodies". Biomacromolecules, 2012. **13**(2): 559-564.

121. Yetisen, A. K., Akram, M. S., and Lowe, C. R., "Paper-based microfluidic point-of-care diagnostic devices". Lab Chip, 2013. **13**(12): 2210-51.

122. Henares, T. G., Mizutani, F., and Hisamoto, H., "Current development in microfluidic immunosensing chip". Analytica Chimica Acta, 2008. **611**(1): 17-30.

123. Qavi, A., Washburn, A., Byeon, J.-Y., and Bailey, R., "Label-free technologies for quantitative multiparameter biological analysis". Analytical and Bioanalytical Chemistry, 2009. **394**(1): 121-135.

124. Eduard, G. R., "Carbon nanotubes in new materials". Russian Chemical Reviews, 2013. **82**(1): 27.

125. Kiselyova, O. and Yaminsky, I., "Atomic Force Microscopy of Protein Complexes", in Atomic Force Microscopy, P. Braga and D. Ricci, Editors. 2004, Humana Press. 217-230.

126. Jianhua, W. and Congzhou, W. "Study on methods of protein immobilization for AFM". in Bioinformatics and Biomedical Engineering (iCBBE), 2010 4th International Conference on. 2010.

127. Hermanson, G. T., "Bioconjugate Techniques". Vol. Second Edition. 2008, London: Academic Press. 1323.

128. Rusmini, F., Zhong, Z., and Feijen, J., "Protein immobilization strategies for protein biochips". Biomacromolecules, 2007. **8**(6): 1775-1789.

129. O'Shannessy, D. J. and Quarles, R. H., "Labeling of the oligosaccharide moieties of immunoglobulins". Journal of immunological methods, 1987. **99**(2): 153-161.

130. Scida, K., Stege, P. W., Haby, G., Messina, G. A., and Garcia, C. D., "Recent applications of carbon-based nanomaterials in analytical chemistry: critical review". Analytica Chimica Acta, 2011. **691**: 6-17.

131. Reichert, J. M., "Marketed therapeutic antibodies compendium". mAbs, 2012. **4**(3): 413-415.

132. Riesen, W., "Structure and biological properties of immunoglobulins and gamma-globulin preparations. I. Structure and function of immunoglobulins". Schweiz Med Wochenschr, 1980. **110**(3): 74-9.

133. Vermeer, A. W. P. and Norde, W., "The thermal stability of immunoglobulin: Unfolding and aggregation of a multi-domain protein". Biophysical Journal, 2000. **78**(1): 394-404.

134. wiseGEEK, Accessed on April 05, 2013 from: http://www.wisegeek.com/what-are-polyclonal-antibodies.htm.

135. Thermo-Scientific, Accessed on April 05, 2013 from: http://www.piercenet.com/method/biotinylation.

136. Voet, D., Voet, J. G., and Pratt, C. W., "Principles of Biochemistry". 2012: John Wiley & Sons.

137. Suresh, S., Gupta, A. K., Rao, V. K., Om, k., and Vijayaraghavan, R., "Amperometric immunosensor for ricin by using on graphite and carbon nanotube paste electrodes". Talanta, 2010. **81**(1–2): 703-708.

138. Rao, V. K., Suresh, S., Sharma, M. K., Gupta, A., and Vijayaraghavan, R., "Carbon nanotubes-A potential material for affinity biosensors", 2011, Gwalior, India.

139. Gao, Y. and Kyratzis, I., "Covalent immobilization of proteins on carbon nanotubes using the cross-linker 1-ethyl-3-(3-dimethylaminopropyl) carbodiimide—a critical assessment". Bioconjugate chemistry, 2008. **19**(10): 1945-1950.

140. Abera, A., "Point-of-care immunoassay system using carbon nanotube labels", Dissertation in The Department of Electrical and Computer Engineering 2010, Louisiana State University.

141. Abera, A. and Choi, J.-W., "Quantitative lateral flow immunosensor using carbon nanotubes as label". Analytical Methods, 2010. **2**(11): 1819-1822.

142. Lerner, M. B., Dailey, J., Goldsmith, B. R., Brisson, D., and Charlie Johnson, A. T., "Detecting Lyme disease using antibody-functionalized single-walled carbon nanotube transistors". Biosensors and Bioelectronics, 2013. **45**(0): 163-167.

143. Venturelli, E., Fabbro, C., Chaloin, O., Menard-Moyon, C., Smulski, C. R., Da Ros, T., Kostarelos, K., Prato, M., and Bianco, A., "Antibody covalent immobilization on carbon nanotubes and assessment of antigen binding". Small, 2011. **7**(15): 2179-87.

144. Rusling, J., Munge, B., Sardesai, N., Malhotra, R., and Chikkaveeraiah, B., "Nanoscience-based electrochemical sensors and arrays for detection of cancer biomarker proteins", in Nanobioelectrochemistry, F.N. Crespilho, Editor. 2013, Springer Berlin Heidelberg. 1-26.

145. Veetil, J. V. and Ye, K., "Development of immunosensors using carbon nanotubes". Biotechnology Progress, 2007. **23**(3): 517-531.

146. Hasan, T., Scardaci, V., Tan, P., Rozhin, A. G., Milne, W. I., and Ferrari, A. C., "Stabilization and “debundling” of single-wall carbon nanotube dispersions in N-Methyl-2-pyrrolidone (NMP) by polyvinylpyrrolidone (PVP)". The Journal of Physical Chemistry C, 2007. **111**(34): 12594-12602.

147. Huang, Y. Y. and Terentjev, E. M., "Dispersion of carbon nanotubes: Mixing, sonication, stabilization, and composite properties". Polymers, 2012. **4**(1): 275-295.

148. Lin, Y., Taylor, S., Li, H., Fernando, K. S., Qu, L., Wang, W., Gu, L., Zhou, B., and Sun, Y.-P., "Advances toward bioapplications of carbon nanotubes". Journal of Materials Chemistry, 2004. **14**(4): 527-541.

149. Shim, M., Shi Kam, N. W., Chen, R. J., Li, Y., and Dai, H., "Functionalization of carbon nanotubes for biocompatibility and biomolecular recognition". Nano Letters, 2002. **2**(4): 285-288.

150. Marie, R., Beech, J. P., Vörös, J., Tegenfeldt, J. O., and Höök, F., "Use of PLL-g-PEG in micro-fluidic devices for localizing selective and specific protein binding". Langmuir, 2006. **22**(24): 10103-10108.

151. Kim, J.-H., Lee, J., Sohn, H.-J., Song, H.-O., Kim, J.-Y., Lee, W.-J., Park, H., and Shin, H.-J., "Production of monoclonal antibodies for Plasmodium vivax lactate dehydrogenase and patient sera screening using sandwich ELISA". Parasitology research, 2012. **111**(4): 1645-1650.

152. Zhao, C., Sun, Y.-L., Kirk, R. L., Thoreson, A. R., Jay, G. D., Moran, S. L., An, K.-N., and Amadio, P. C., "Effects of a lubricin-containing compound on the results of flexor tendon repair in a canine model in vivo". The Journal of Bone & Joint Surgery, 2010. **92**(6): 1453-1461.

153. Thermo-Scientific, "NHS and Sulfo-NHS", Accessed on June 06, 2013 from: http://www.piercenet.com/browse.cfm?fldID=02040114.

154. Pelton, J. T. and McLean, L. R., "Spectroscopic methods for analysis of protein secondary structure". Analytical biochemistry, 2000. **277**(2): 167-176.

155. Mann, C. J., Stephens, S. K., and Burke, J. F., "Production of protein microarrays". Protein Microarray Technology, 2004: 165-194.

156. Metzger, S. W., Lochhead, M. J., and Grainger, D. W., "Improving performance in protein-based microarrays". IVD Technology, 2002.

157. Liu, Z., Tabakman, S., Welsher, K., and Dai, H., "Carbon nanotubes in biology and medicine: in vitro and in vivo detection, imaging and drug delivery". Nano research, 2009. **2**(2): 85-120.

158. Wu, J., Ge, Q., and Mather, P. T., "PEG− POSS multiblock polyurethanes: synthesis, characterization, and hydrogel formation". Macromolecules, 2010. **43**(18): 7637-7649.

159. Balasubramanian, K. and Burghard, M., "Biosensors based on carbon nanotubes". Analytical and bioanalytical chemistry, 2006. **385**(3): 452-468.

160. Trilling, A. K., Beekwilder, J., and Zuilhof, H., "Antibody orientation on biosensor surfaces: a minireview". Analyst, 2013. **138**(6): 1619-1627.

161. Bull, H. B., "Adsorption of bovine serum albumin on glass". Biochimica et biophysica acta, 1956. **19**(3): 464-471.

162. Ogi, T., Modesto-Lopez, L. B., Iskandar, F., and Okuyama, K., "Fabrication of a large area monolayer of silica particles on a sapphire substrate by a spin coating method". Colloids and Surfaces A: Physicochemical and Engineering Aspects, 2007. **297**(1): 71-78.

163. ImmunoChemistry, Accessed on February 12, 2014 from: http://www.immunochemistry.com/what-immunoassay.

164. Crowther, J., "The ELISA guidebook, vol. 149". Methods in Molecular Biology, Human Press Totowa, New Jersey, 2001: 49.

165. Koivunen, M. E. and Krogsrud, R. L., "Principles of immunochemical techniques used in clinical laboratories". Lab Medicine, 2006. **37**(8): 490-497.

166. International Medical Corps, Accessed on February 10, 2014 from: http://internationalmedicalcorps.org/page.aspx?pid=501&gclid=CMWCivyHwrwCFZBj7AodWVAAXw#.UvkJY_ldXFk.

167. National Institutue of Allergy and Infectious Diseases, Accessed on October 9, 2013 from: http://www.niaid.nih.gov/topics/malaria/pages/lifecycle.aspx.

168. Greenwood, B., "The epidemiology of malaria". Annals of tropical medicine and parasitology, 1997. **91**(7): 763-770.

169. Centers for Disease Control and Prevention, Accessed on April 13, 2013 from: http://www.cdc.gov/malaria/diagnosis_treatment/diagnosis.html.

170. United Nationals Children Fund, "Malaria & Children: Progress in Intervention Coverage", Accessed on April 13, 2013 from: http://www.unicef.org/health/files/Malaria_Oct6_for_web%281%29.pdf.

171. Krafts, K., Hempelmann, E., and Oleksyn, B., "The color purple: from royalty to laboratory, with apologies to Malachowski". Biotechnic & Histochemistry, 2011. **86**(1): 7-35.

172. The American Congress of Obstreticians and Gynecologists, Accessed on February 2, 2014 from: http://www.acog.org/About_ACOG/News_Room/News_Releases/2013/Ob-Gyns_Redefine_Meaning_of_Term_Pregnancy.

173. Medscape, Accessed on February 21, 2014 from: http://emedicine.medscape.com/article/262591-overview#a1.

174. Paul, M., Schaff, E., and Nichols, M., "The roles of clinical assessment, human chorionic gonadotropin assays, and ultrasonography in medical abortion practice". American journal of obstetrics and gynecology, 2000. **183**(2): S34-S43.

175. Payne, D., "Use and limitations of light microscopy for diagnosing malaria at the primary health care level". Bulletin of the World Health Organization, 1988. **66**(5): 621.

176. Hänscheid, T. and Grobusch, M. P., "How useful is PCR in the diagnosis of malaria?". Trends in parasitology, 2002. **18**(9): 395-398.

177. Fontecha, G. A., Mendoza, M., Banegas, E., Poorak, M., De Oliveira, A. M., Mancero, T., Udhayakumar, V., Lucchi, N. W., and Mejia, R. E., "Comparison of molecular tests for the diagnosis of malaria in Honduras". Malaria journal, 2012. **11**(1): 119.

178. Mens, P., Spieker, N., Omar, S., Heijnen, M., Schallig, H., and Kager, P., "Is molecular biology the best alternative for diagnosis of malaria to microscopy? A comparison between microscopy, antigen detection and molecular tests in rural Kenya and urban Tanzania". Tropical Medicine & International Health, 2007. **12**(2): 238-244.

179. Guerrant, R. L., Walker, D. H., and Weller, P. F., "Tropical infectious diseases: principles, pathogens and practice". 2011: Elsevier Health Sciences.

180. Sanofi, Accessed on February 26, 2014 from: http://www.impact-malaria.com/web/e-learning_malaria.

181. Redd, S. C., Luby, S. P., Hightower, A. W., Kazembe, P. N., Nwanyanwu, O., Ziba, C., Chitsulo, L., Franco, C., Olivar, M., and Wirima, J. J., "Clinical algorithm for treatment of Plasmodium falciparum malaria in children". The Lancet, 1996. **347**(8996): 223-227.

182. Chotivanich, K., Silamut, K., and Day, N. P., "Laboratory diagnosis of malaria infection-A short review of methods". New Zealand Journal of Medical Laboratory Science, 2007. **61**(1): 4.

183. Erdman, L. K. and Kain, K. C., "Molecular diagnostic and surveillance tools for global malaria control". Travel medicine and infectious disease, 2008. **6**(1): 82-99.

184. Tangpukdee, N., Duangdee, C., Wilairatana, P., and Krudsood, S., "Malaria diagnosis: a brief review". The Korean journal of parasitology, 2009. **47**(2): 93-102.

185. Sulzer, A., Wilson, M., and Hall, E. C., "Indirect fluorescent-antibody tests for parasitic diseases V. An evaluation of a thick-smear antigen in the IFA test for malaria antibodies". The American journal of tropical medicine and hygiene, 1969. **18**(2): 199-205.

186. World Health Organization, "Information note on recommended selection criteria for procurement of malaria rapid diagnostic tests (RDTs)", Accessed on February 27, 2014 from: http://www.wpro.who.int/malaria/NR/rdonlyres/3B0EEC88-A85A-4C66-BED8-46F13F47D087/0/RDT_selection_criteria2012.pdf.

187. Alere, Accessed on March 08, 2013 from: http://www.alere.com/us/en/product-details/binaxnow-malaria.html.

188. Murray, C. K. and Bennett, J. W., "Rapid diagnosis of malaria". Interdisciplinary perspectives on infectious diseases, 2009. **2009**.

189. Kyabayinze, D. J., Tibenderana, J. K., Odong, G. W., Rwakimari, J. B., and Counihan, H., "Operational accuracy and comparative persistent antigenicity of HRP2 rapid diagnostic tests for Plasmodium falciparum malaria in a hyperendemic region of Uganda". Malaria journal, 2008. **7**(1): 221.

190. Ratsimbasoa, A., Fanazava, L., Radrianjafy, R., Ramilijaona, J., Rafanomezantsoa, H., and Ménard, D., "Short report: evaluation of two new immunochromatographic assays for diagnosis of malaria". American Journal of Tropical Medicine and Hygiene, 2008. **79**(5): 670.

191. Wilson, M. L., "Malaria rapid diagnostic tests". Clinical infectious diseases, 2012. **54**(11): 1637-1641.

192. Wongsrichanalai, C., Barcus, M. J., Muth, S., Sutamihardja, A., and Wernsdorfer, W. H., "A review of malaria diagnostic tools: microscopy and rapid diagnostic test (RDT)". The American journal of tropical medicine and hygiene, 2007. **77**(6 Suppl): 119-127.

193. Osman, M. M., Nour, B. Y., Sedig, M. F., De Bes, L., Babikir, A. M., Mohamedani, A. A., and Mens, P. F., "Informed decision-making before changing to RDT: a comparison of microscopy, rapid diagnostic test and molecular techniques for the diagnosis and identification of malaria parasites in Kassala, eastern Sudan". Tropical Medicine & International Health, 2010. **15**(12): 1442-1448.

194. Araj, G. F., "Update on laboratory diagnosis of human brucellosis". International Journal of Antimicrobial Agents, 2010. **36, Supplement 1**(0): S12-S17.

195. Panagiotis, K., Ray, K. I., Richard, H. B., and Andreas, D., "Towards the development of an electrochemical biosensor for hCGβ detection". Physiological Measurement, 2008. **29**(6): S241.

196. Cole, L. A. and Sutton, J. M., "Selecting an appropriate hCG test for managing gestational trophoblastic disease and cancer". The Journal of reproductive medicine, 2004. **49**(7): 545-553.

197. Toriola, A. T., Tolockiene, E., Schock, H., Surcel, H.-M., Zeleniuch-Jacquotte, A., Wadell, G., Toniolo, P., Lundin, E., Grankvist, K., and Lukanova, A., "Free β-human chorionic gonadotropin, total human chorionic gonadotropin and maternal risk of breast cancer". Future Oncology, 2014. **10**(3): 377-384.

198. Chetcuti, A. F., Wong, D. K., and Stuart, M. C., "An indirect perfluorosulfonated ionomer-coated electrochemical immunosensor for the detection of the protein human chorionic gonadotrophin". Analytical chemistry, 1999. **71**(18): 4088-4094.

199. Wilcox, A. J., Baird, D. D., and Weinberg, C. R., "Time of implantation of the conceptus and loss of pregnancy". New England Journal of Medicine, 1999. **340**(23): 1796-1799.

200. Stenman, U.-H., Unkila-Kallio, L., Korhonen, J., and Alfthan, H., "Immunoprocedures for detecting human chorionic gonadotropin: clinical aspects and doping control". Clinical chemistry, 1997. **43**(7): 1293-1298.

201. Pittaway, D. E., Reish, R. L., and Wentz, A. C., "Doubling times of human chorionic gonadotropin increase in early viable intrauterine pregnancies". American journal of obstetrics and gynecology, 1985. **152**(3): 299-302.

202. Wehmann, R. E., Blithe, D. L., Akar, A. H., and Nisula, B. C., "Disparity between β-core levels in pregnancy urine and serum: implications for the origin of urinary β-core". The Journal of Clinical Endocrinology & Metabolism, 1990. **70**(2): 371-378.

203. Schroeder, H. and Halter, C. M., "Specificity of human beta-choriogonadotropin assays for the hormone and for an immunoreactive fragment present in urine during normal pregnancy". Clinical chemistry, 1983. **29**(4): 667-671.

204. Norman, R. J., Buck, R. H., Rom, L., and Joubert, S. M., "Blood or urine measurement of human chorionic-gonadotropin for detection of ectopic pregnacy - A comparative study of quantitative and qualitative methods in both fluids". Obstetrics and Gynecology, 1988. **71**(3): 315-318.

205. Stenman, U.-H., Alfthan, H., Ranta, T., Vartiainen, E., Jalkanen, J., and Seppala, M., "Serum levels of human chorionic gonadotropin in nonpregnant women and men are modulated by gonadotropin-releasing hormone and sex steroids*". The Journal of Clinical Endocrinology & Metabolism, 1987. **64**(4): 730-736.

206. Fachin, F., Wardle, B. L., Chen, G., and Toner, M. "Integration of vertically-aligned carbon nanotube forests in microfluidic devices for multiscale isolation of bioparticles". in Sensors, 2010 IEEE. 2010. IEEE.

207. Wilson, M. L., "Laboratory diagnosis of malaria: conventional and rapid diagnostic methods". Archives of Pathology and Laboratory Medicine, 2013. **137**(6): 805-811.

208. de Souza Castilho, M., Laube, T., Yamanaka, H., Alegret, S., and Pividori, M., "Magneto immunoassays for Plasmodium falciparum histidine-rich protein 2 related to malaria based on magnetic nanoparticles". Analytical chemistry, 2011. **83**(14): 5570-5577.

209. Jang, J. W., Cho, C. H., Han, E. T., An, S., and Lim, C. S., "pLDH level of clinically isolated Plasmodium vivax and detection limit of pLDH based malaria rapid diagnostic test". Malar J, 2013. **12**(1): 181.

210. Schneider, B., Dickinson, E., Vach, M., Hoijer, J., and Howard, L., "Optical chip immunoassay for hCG in human whole blood". Biosensors and Bioelectronics, 2000. **15**(11): 597-604.

211. Bange, A., Halsall, H. B., and Heineman, W. R., "Microfluidic immunosensor systems". Biosensors and Bioelectronics, 2005. **20**(12): 2488-2503.

212. King, K. D., Anderson, G. P., Bullock, K. E., Regina, M. J., Saaski, E. W., and Ligler, F. S., "Detecting staphylococcal enterotoxin B using an automated fiber optic biosensor". Biosensors and Bioelectronics, 1999. **14**(2): 163-170.

213. Juncker, D., Schmid, H., Drechsler, U., Wolf, H., Wolf, M., Michel, B., de Rooij, N., and Delamarche, E., "Autonomous microfluidic capillary system". Analytical chemistry, 2002. **74**(24): 6139-6144.

214. Altman, D. G. and Bland, J. M., "Diagnostic Tests 1: Sensitivity and Specificity". BMJ: British Medical Journal, 1994. **309**(6947): 102.

APPENDIX: PERMISSION TO USE COPYRIGHTED MATERIAL

Fwd: Copyright Permission for Dissertation

Alistair Freeland <freeland@mdpi.com> Mon, Sep 22, 2014 at 1:41 AM
To: egikun2@tigers.lsu.edu

Dear Emmanuel,

This is an open access article distributed under the Creative Commons Attribution License which permits unrestricted use, distribution, and reproduction in any medium, provided the original work is properly cited. Therefore, you may reproduce the above mentioned manuscript in your dissertation as long as the original article in Sensors is cited.

Best regards,

Alistair Freeland

MDPI AG – Multidisciplinary Digital Publishing Institute
www.mdpi.com

Email: freeland@mdpi.com
Postfach, CH-4005 Basel, Switzerland
Office: Klybeckstrasse 64, CH-4057 Basel
Tel. +41 79 572 15 97 (mobile)
Tel. +41 61 683 77 34 (office)
Fax +41 61 302 89 18 (office)

Begin forwarded message:

> -------- Original Message --------
> Subject: Copyright Permission for Dissertation
> Date: Thu, 18 Sep 2014 12:05:04 -0500
> From: Emmanuel Gikunoo <egikun2@tigers.lsu.edu>

> Dear Publisher,
>
> I am Emmanuel Gikunoo, coauthor of 'A Novel Carbon Nanofibers Grown on Glass Microballoons Immunosensor: A Tool for Early Diagnosis of Malaria, Sensors 2014, 14, 14686-14699', and just completed my final PhD exam on 'Utilization of Carbon Nanofibers Grown on Glass Microballoons (NMBs) in Pointof-Care Diagnostic Devices'. My school, Louisiana State

University (LSU), requires a written permission from the Publisher to use a published material in the dissertation.

>

> I am by this email requesting permission to reproduce the above mentioned manuscript in one of the chapters of my dissertation.

>

> Your prompt response would be very much appreciated.

>

> Sincerely,

>

> Emmanuel

VITA

Emmanuel Gikunoo was born in Accra, Ghana. He obtained his Bachelor of Science degree in Metallurgical Engineering from Kwame Nkrumah University of Science and Technology, Ghana (KNUST) in 1999. He was a graduate assistant at the Metallurgical Engineering Department at KNUST for two years. In 2002, he received a scholarship for graduate studies in Canada and obtained the Master of Science degree in Mechanical Engineering from University of Saskatchewan in 2005. He returned to KNUST in 2006 and worked as a lecturer before joining Dr. Woldesenbet's research group at the Mechanical Engineering Department at Louisiana State University in 2010. He is expected to earn the degree of Doctor of Philosophy in Mechanical Engineering in December 2014.